UNIVERSITY OF PADOVA

Department of Chemical Sciences

DOCTORAL SCHOOL IN MOLECULAR SCIENCES

PHARMACEUTICAL SCIENCES CURRICULUM

XXX CYCLE

STAR-LIKE GUANIDYL-OLIGOSACCHARIDIC POLYMER AS A NEW NANOPLATFORM FOR siRNA DELIVERY TOWARDS CANCER CELLS

School Coordinator: Ch.mo Prof. Leonard Jan Prins

Curriculum Coordinator: Ch.mo Prof. Claudia Sissi

Supervisor: Ch.mo Prof. Paolo Caliceti

Ph.D. student : Alessio Malfanti

“Per chi viaggia in direzione ostinata e contraria”

Fabrizio De Andrè

Alla mia famiglia,

Summary

Abbreviations

Acry-Agm	Acryloyl-agmatine
Agm_6-M-COOH	$(agmatinyl)_6$-maltotriosyl-N-acetyl-amino-hexanoic acid
Agm_6-M-PEG	$(agmatinyl)_6$-maltotriosyl-N-acetyl-amino-hexanoate-α-methoxy-poly(ethylene glycol)$_{5kDa}$
Agm_6-M-PEG-FA	$(agmatinyl)_6$-maltotriosyl-N-acetyl-amino-hexanoate-poly(ethylene glycol)$_{6kDa}$-Folate
Agm_6-M-PEG-Cy3	$(agmatinyl)_6$-maltotriosyl-N-acetyl-amino-hexanoate-poly(ethylene glycol)$_{6kDa}$-Cyanine3
ATRP	Atom Transfer Radical Polymerization
Cav-1	Caveolin-1
CCD	Cationic cyclodextrin
$CDCl_3$	Deuterated Chloroform
CHC	Clathrin heavy chain
CO_2	Carbon dioxide
Cy3	Cyanine 3
Cy5	Cyanine 5
Cy5.5	Cyanine 5.5
CuBr	Copper Bromide
Da	Dalton
DAPI	4’,6-diamino-2-phenylindole
DCC	Dicyclohexylcarbodiimide
DC-cholesterol	3β-[N-(N',N'-dimethylaminoethane)-carbamoyl] cholesterol
DCM	Dichlorometane
DCU	Dicyclohexylurea
DDS	Drug delivery system
DLS	Dynamic Light Scattering
DMF	Dimethylformamide
DMEM	Dulbecco’s modified eagle medium
DMSO	Dimethyl sulfoxide

DMRIE	1,2- dimyristyloxy-propyl-3-dimethyl-hydroxy ethyl ammonium
DOGS	dioctadecylamido-glycylspermine
DOSPA	2,3-dioleyloxy-N-[2(sperminecarboxamido)ethyl]-N,N-dimethyl-1-propanaminium
DOTAP	N-(2,3-Dioleoyloxy-1-propyl)trimethylammonium
DOTMA	1,2-di-O-octadecenyl-3-trimethylammonium propane
dsDNA	Double strand DNA
EDC	1-ethyl-3-(3-dimethylaminopropyl)carbodiimide
EDTA	Ethylendiaminetetraacetic acid
EEA-1	Early endosomes antigen-1
EMSA	Electrophoretic mobility gel shift assay
EPR	Enhanced permeability and retention
ESI	Electrospray ionization
Et_2O	Diethyl ether
FA	Folic acid
FBS	Fetal Bovine Serum
FF-DMEM	Folic free Dulbecco's modified eagle medium
FF-RPMI-1640	Folic free Roswell park memorial institute medium
FR	Folate receptor
GPC	Gel permeation chromatography
HCl	Hydrochloric acid
ITC	Isothermal Titration Calorimetry
IU	International Units
LAMP-1	Lysosomal-associated membrane protein-1
M-COOH	Maltotriosyl-N-acetyl-amino-hexanoic acid
M-(Br_6)-COOH	(2-bromoisobutyryl)$_6$-maltotriosyl-N-acetyl-amino-hexanoic acid
MALDI	Matrix-assisted laser desorpton-ionization

MeOH	Methanol
MES	Morpholino-ethan-sulphonic acid buffer
miRNA	MicroRNA
MTT	3-(4,5-dimethylthiazol-2yl)-2,5-diphenyltetrazolium
MW	Molecular weight
MWCO	Molecular weight cut-off
N_2	Nitrogen
NaOH	Sodium Chloride
NaCl	Sodium Chloride
Na_2SO_4	Sodium sulfate
NHS	N-Hydroxysuccinimide
N/P ratio	Nitrogen/Phosphorus ratio
ON	Oligonucleotide
PAMAM	Polyamidoamine
PBS	Phosphate Buffered Saline
PDI	Polydispersivity index
PEI	Polyethilenimine
pDNA	Plasmidic DNA
PGA	Poly-glutamic acid
PLL	Poly-Lysine
PEG	Poly(ethylen)glicole
pKa	Acid dissociation constant
PLGA	Poly(lactic-co-glycolic acid)
RBC	Red Blood Cells
RES	Reticuloendothelial system
ROS	Reactive oxygen species
RP-HPLC	Reverse phase high pressure liquid chromatography
RPMI-1640	Roswell park memorial institute medium
siRNA	Small interfering RNA
siΔH	single injection variation enthalpy
TAE	Tris-Acetate-EDTA
TBE	Tris-Borate-EDTA

TEA	Triethylamine
TFA	Trifluoroacetic acid
TEM	Transmission electron microscopy
TEMED	Tetramethylethylenediamine
TNF-α	Tumor necrosis factor-α
TPMA	Tris(2-pyridylmethyl)amine
UV	Ultraviolet
Vis	Visible
VEGF	Vascular endothelial growth factor
^{1}H-NMR	Proton nuclear magnetic resonance
[^{3}H]FA	Tritiated folic acid
ΔH	Variation of enthalpy
ΔS	Variation of entropy

Riassunto

La terapia genica viene definita come il trattamento o la prevenzione di malattie umane attraverso l'introduzione all'interno di cellule specifiche di nuovo materiale genetico quali gli oligonucleotidi terapeutici (siRNA, miRNA etc.)[1]. Negli ultimi decenni, molti ricercatori hanno investito nello sviluppo in sistemi di *delivery* di oligonucleotidi terapeutici (ONs). Tuttavia, la somministrazione di ONs risulta difficile e si osserva una bassa biodisponibilità ed efficacia biologica data la loro natura anionica, l'elevato peso molecolare e le fragilità strutturali. Queste macromolecole, subiscono una rapida degradazione da parte delle nucleasi del siero, possiedono un trascurabile trasporto transmembrana, possono accumularsi in maniera aspecifica e stimolare il sistema immunitario[2]. *Nanocarrier* cationici (ad esempio polimeri e lipidi) rappresentano una delle più promettenti strategie per proteggere e trasportare ONs all'interno di cellule malate. In questo lavoro, è stato disegnato un nuovo un nuovo polimero cationico per la complessazione di siRNA basata su interazioni di tipo colombiano (attrazione di carica). Partendo da un oligosaccaride (il maltotriosio) una molecola dalla struttura a stella è stata sintetizzata (Agm_6-M-COOH) tramite un protocollo multi-step utilizzando una polimerizzazione a trasferimento atomico radicale (ATRP). A questa molecola è stata quindi coniugata una catena di glicole polietilenico (PEG) al fine di aumentare la biocompatibilità del sistema (Agm_6-M-PEG). I complessi, che normalmente vengono chiamati "poliplessi", sono stati preparati per auto assemblaggio tra il polimero cationico e ONs. I poliplessi hanno dimostrato migliorare i parametri farmacocinetici e farmacodinamici degli ON generando un interessante modello per la terapia antitumorale. I saggi elettroforetici sono stati impiegati per valutare la formazione dei poliplessi a diversi rapporti azoto/fosforo (N/P ratio) partendo da 0.5 fino a 5. La completa complessazione del siRNA è stata ottenuta a valori di N/P ratio pari a 3. Le interazioni termodinamiche tra il polimero cationico e ONs sono state esplorate attraverso la calorimetria a titolazione isotermica (*Isothermal Titration Calorimetry*, ITC). I poliplessi sono stati caratterizzati tramite *Dynamic Light Scattering* (DLS) mostrando un dimensione media nel *range* di 50-75 nm e una carica superficiale in un intervallo di valori da -5 mV a +11 mV in funzione del rapporto N/P. Un basso indice di polidispersione è stato osservato, confermando che le formulazioni sono monodisperse. I poliplessi aventi 3 e 5 N/P ratio hanno mostrato possedere le migliori caratteristiche fisico-chimiche e sono stati ulteriormente caratterizzati

e testati *in vitro*. Le analisi morfologiche delle formulazioni sono state effettuate attraverso la microscopia elettronica a trasmissione. Da tale analisi si è osservato che le particelle possiedono una struttura a bastoncello. I poliplessi inoltre hanno evidenziato la capacità di proteggere siRNA dalle nucleasi e una buona stabilità in siero. La forza dell'interazione tra il polimero e il siRNA e la stabilità dei poliplessi è stata ulteriormente confermata via elettroforesi attraverso il test di spiazzamento con eparina. Infatti, il totale spiazzamento di siRNA dal complesso avviene solo a concentrazioni di eparina pari a 2.5 IU/mL, circa 16 volte superiori rispetto a quelle presenti nel torrente ematico (0.15 IU/mL). Studi preliminari in vitro sono stati effettuati su cellule MCF-7 di adenocarcinoma mammario umano, cellule KB di carcinoma della cervice uterina umana e cellule MC3T3-E1 di fibroblasti di embrioni murini e hanno mostrato una buona biocompatibilità e uptake cellulare. Inoltre, è stato osservato come la differente composizione e struttura dei poliplessi influenzi l'*uptake* cellulare: i poliplessi con un *aspect ratio* più piccolo sono internalizzati più efficientemente rispetto ai poliplessi che presentano un *aspect ratio* maggiore. L'attività emolitica dei poliplessi è stata presa in considerazione misurando l'effetto dei poliplessi sui globuli rossi del sangue. Dai test efettuati è emerso un trascurabile effetto emolitico per entrambe le formulazioni in analisi. Al fine di aumentare la sito-selettività del sistema, i poliplessi sono stati successivamente formulati al fine di essere direzionati contro cellule tumorali. Per questa ragione, il polimero cationico è stato funzionalizzato alla fine della catena con acido folico (Agm_6-M-PEG-FA). L'attività di *silencing* dei poliplessi decorati con diverse quantità di acido folico è stata valutata utilizzando siRac1. Dallo studio è emerso che i poliplessi costituiti con il 25% w/w di Agm_6-M-PEG-FA sono risultati i più efficienti nella riduzione dell'espressione di Rac1. In questo contesto, uno studio comparativo tra poliplessi aventi 25%w/w di polimero derivatizzato con acido folico e poliplessi senza acido folico è stato intrapreso. Al fine di individuare il miglior modello *in vitro* e *in vivo*, è stato fatto uno screening di diverse linee cellulari per valutare l'espressione del recettore dell'acido folico e le cellule MDA-MB-231 di adenocarcinoma mammario sono state selezionate come quelle a maggior espressione. Studi di silenziamento e tossicità da parte dei poliplessi sono stati effettuati. Per questo motivo, siRac1 è stato utilizzato come siRNA terapeutico per le sue capacità di inibire la migrazione cellulare, la formazione di metastasi e l'invasione cellulare[3]. I poliplessi con e senza acido folico hanno mostrato un'elevata biocompatibilità (maggiore dell'80% per tutte le concentrazioni testate con il saggio MTT) e una elevata immuno-compatibilità (valutata attraverso stimolazione del sistema immunitario). I poliplessi

direzionati con acido folico hanno mostrato un miglior *gene silencing* di circa due volte superiore rispetto ai poliplessi non direzionati (86% e 53% rispettivamente). L'abilità dei poliplessi di inibire la migrazione cellulare è stata osservata attraverso il saggio di *wound healing*. La chiusura del "taglio" è stata osservata dopo 12 ore e i risultati hanno mostrato un'inibizione del 40% della migrazione cellulare dopo trattamento con una dose equivalente di siRNA pari a 500 nM di poliplessi decorati con acido folico. Al contrario, poliplessi non decorati inibiscono la migrazione solo del 15%. Nonostante la differente attività di silencing e di inibizione della migrazione cellulare, non sono state osservate differenze di internalizzazione tra i poliplessi con e senza acido folico con analisi confocale e Imagestream. Pertanto, studi di *traffiking* intracellulare sono stati eseguiti. Poliplessi portanti acido folico sono stati osservati nel citoplasma e nessuna co-localizzazione con endosomi e lisosomi è stata osservata. Al contrario, poliplessi non portanti acido folico sono stati visualizzati all'interno di entrambi i compartimenti cellulari. I meccanismi di internalizzazione cellulare sono stati valutati attraverso la marcatura di *caveolin-1* e di *clathrin heavy chain* attraverso anticorpi. L'internalizzazione *caveolae*-mediata è stata osservata per i poliplessi con acido folico mentre per i poliplessi senza acido folico un meccanismo di endocitosi mediato da *clatrine* è stato osservato. Questi risultati evidenziano un coinvolgimento dell'acido folico nel processo di *uptake* mediato da *caveolae* che è stato visto incrementare l'attività di silenziamento genico. La tossicità sistemica dei poliplessi con e senza acido folico è stata studiata su femmine di topo *Nu/Nu* usando dosi equivalenti di siRNA nell'intervallo di 1-6 mg/kg. L'obiettivo di questo test è di raggiungere la massima dose tollerata attraverso una crescente somministrazione di siRNA. Tuttavia nessuna tossicità è stata ottenuta per entrambe le formulazioni. Infine, è stato studiato *in vivo* l'accumulo dei poliplessi con acido folico. Da questo studio si è osservato un accumulo di Rac1 rispetto alla soluzione salina o a un siRNA non codificante (siEGFP) di circa 500 e 65 volte rispettivamente. Inoltre è stato possibile individuare una correlazione tra le dimensioni del tumore e l'accumulo dei poliplessi. Studi istologici hanno confermato l'accumulo dei poliplessi nel tessunto tumorale.

Abstract

Gene therapy is defined as the treatment or prevention of human diseases by introduction of new genetic material, such as therapeutic oligonucleotides (e.g. siRNA, miRNA, etc.), into specific cells.[1] In the last few decades the research community has invested substantial resources in the delivery of therapeutic oligonucleotides (ONs). Unfortunately, due to their anionic nature, high molecular weight and structural fragility, ON administration suffers from poor bioavailability and biological efficiency. In fact, these macromolecules may undergo fast degradation by serum nucleases, negligible transmembrane transport, off-target profile and also elicit immunogenic response.[2] So far, cationic nanocarriers (including polymers and lipids) represent the most promising strategies to protect and deliver ONs. In this work, we have designed a novel cationic polymer for ON (i.e. siRNA) complexation driven by coulombic interactions. Starting from an oligosaccharide (maltotriose) we synthesize through a multistep protocol a star-like molecule (Agm_6-M-COOH) using Atom Transfer Radical Polymerization (ATRP) which was then conjugated to polyethylene glycol (PEG) to improve the biocompatibility of the system (Agm_6-M-PEG). Complexes, here referred as polyplexes, were prepared by self-assembly of the cationic polymer with a model ON. The obtained polyplexes have been found to improve the pharmacokinetic and pharmacodynamics parameters of ONs generating a valuable tool for cancer treatment.

Electrophoresis gel shift assay was used to investigate polyplexes formation at different nitrogen/phosphate (N/P) ratios starting from 0.5 up to 5. A complete complexation of the siRNA was achieved at the N/P ratio of 3. The interaction thermodynamic between the cationic polymer and ONs was explored by Isothermal Titration Calorimetry (ITC). The polyplexes were characterized by Dynamic Light Scattering (DLS) showing a mean size in the range of 50-75 nm and a surface charge in the range from -5 mV to +11 mV depending on the N/P ratio. A narrow polydispersity index (PDI) was observed confirming that polyplexes formulations were monodispersed. Polyplexes formed at N/P ratio 3 and 5 showed the most performing physico-chemical features and were thus further characterized and tested *in vitro*.

Morphological analysis of these formulations were performed by Transmission Electron Microscopy (TEM) showing a rod-shape particles. Moreover, polyplexes showed also a satisfactory serum stability and remarkable siRNA protection from nucleases. The strength and the stability of the polymer/siRNA interaction was confirmed by the heparin

displacement test performed by electrophoresis. In fact, 2.5 IU/mL heparin concentration, about 16 fold higher compared to the heparin concentration in blood (0.15 IU/mL[4]) was required to achieve total siRNA displacement from polyplexes.

Preliminary *in vitro* studies were performed on human MCF-7 breast adenocarcinoma cells, human KB cervical carcinoma cells and murine MC3T3-E1 embryonic fibroblast showing a good biocompatibility and cell uptake of the polyplexes. In addition, the different composition and structure of the polyplexes was also found to affect the cell uptake: polyplexes with smaller aspect ratio were taken up more efficiently than polyplexes with larger aspect ratio. The hemolytic activity was also assessed by measuring red blood cells (RBCs) lysis and negligible hemolysis was observed for both the formulations tested.

To enhance the site-selectivity of the system, targeted polyplexes towards tumor cells were formulated. To this aim, the cationic polymer was functionalized at one end-chain with folic acid (Agm_6-M-PEG-FA). The silencing activity of polyplexes decorated with different amount of folic acid was evaluated and polyplexes formed with 25 %w/w of Agm_6-M-PEG-FA were found possesses the better activity. In this contest, a comparative study between folate and non-folate polyplexes was performed.

Aiming at identify the best *in vitro* and *in vivo* model, several cell lines were screened for the expression of the folate receptor finally selecting the human MDA-MB-231 breast adenocarcinoma cells. Silencing and toxicity studies of polyplexes were then performed on HeLa and MDA-MB-231 cells. For this purpose, siRac1 was used as a therapeutic siRNA for its ability to inhibit cell migration, metastatization and cell invasion[3]. The folate and non-folate polyplexes were found highly biocompatible (cell viability >80% for all the concentration tested assessed by MTT assay) and immuno-compatible (assessed by immune stimulation). Folate-targeted polyplexes showed a gene silencing about two folds higher compared to non-folate polyplexes (86% and 53%, respectively). The ability of the polyplexes to inhibit cell migration was assessed by wound healing assay. The gap closure was observed after 12 hours and the results showed a 40% inhibition of the cell migration when cells were treated with 500 nM siRNA equivalent dose for folate polyplexes. On the contrary, non-folate polyplexes inhibited cell migration of only 10%.

Despite the different silencing activity and inhibition of cell migration, no relevant differences in the cell uptake were observed between the targeted and non-targeted system by confocal analysis. Intracellular trafficking studies were then performed. Folate-targeted polyplexes were found in the cytoplasm and did not co-localize with early endosomes and lysosomes. Conversely, non-folate polyplexes fully co-localized with early endosomes.

The cell internalization mechanism was also evaluated by immunostaining the caveolin-1 and clathrin heavy chain, responsible for the caveolae and clathrin-mediated uptake, respectively. Caveolae- mediated internalization was observed for folate-targeted polyplexes while a clathrin-mediated mechanism was assessed for non-targeted polyplexes. These results highlighted the folic acid involvement on the caveolae mediated uptake which was found to enhance the gene silencing activity.

Finally, the systemic toxicity of folate and non-folate polyplexes using a siRNA concentration ranging from 1 to 6 mg/kg was evaluated on Nu/Nu female mice by stepwise escalation dose administered by intravenous injection until the maximum tolerated dose for short period. No toxicity was found for all the doses used for both formulations. Finally, folate polyplexes accumulation in the tumor was investigated observing a ~500-fold and ~65-fold increase of Rac1 siRNA tumor accumulation in comparison with saline or scramble siRNA (siEGFP) treatment, respectively. It was possible to detect a linear correlation between the size of the tumor and the polyplexes accumulation. Histologic studies confirmed the accumulation in the tumor tissue.

Introduction

In the recent years, pharmaceutical industries, research center and universities, discovered or synthesized several new molecular entities which demonstrated strong pharmaceutical effect on the treatment of several diseases such as cardiovascular, neurodegenerative or genetic disorders, infections and viral-mediated diseases and cancer[5]. However, due to their poor water solubility, short half-life or immune-stimulating properties, the development of promising drugs appears very challenging. On the other hand, recent advances in the nanotechnology field allowed the development of nano-sized carriers which can improve the pharmacological profile of new and old drugs thus revolutionizing the drug discovery world. To date, a good number of nanoscale therapeutics are on the market, and more are under clinical trials. As example, in 1995 Food and Drug Administration (FDA) approved the liposomal formulation of doxorubicin (Doxil®) for the Kaposi's sarcoma treatment. Compared to the free drug, Doxil® showed a higher anticancer efficacy and a reduced cardiotoxicity[6].

Compared to classical formulations, drug delivery systems (DDSs) provide several advantages such as enhance the therapeutic activity, prolong the *in vivo* drug half-life, reduce potential immunogenicity, and allow for the creation of formulations for a controlled drug release. All these features permit to reduce the administration frequency and, therefore, the side effects of the drug.

Aiming to a safe and efficient administration, nanoparticle vehicles must possess defined structural characteristics namely size, surface charge, shape, molecular architecture and hydrophobic/hydrophilic balance which affect the fomulation bio- and immune-compatibility and its bioelimination. Considering all these features, several drug delivery systems have been developed in the last decades such as micelles, liposomes, dendrimers, polymerosomes, polymer therapeutics and inorganic nanoparticles.

These nanocarriers can be used to improve the solubility and chemical stability of drugs. Indeed, drug delivery systems promote the delivery of the payload in the desired tissue.

As example, paclitaxel, capecitabine, tamoxifen are example of drugs which were encapsulated in drug delivery system to enhance their biopharmaceutical properties[7-9].

Among the several applications of these nanocarriers, delivery of genes and interfering RNA (iRNA) represent a great promise in medical field. Indeed, thanks to their unconventional mechanism which inhibit the production of selected proteins involved in

pathophysiological pathways, siRNA and miRNA may be used to treat several disease which actually do not have a specific and effective treatments such as cancers, hereditary and infectious disease. However, could be still too early talk about clinical application of siRNA and more in general gene therapy.
Due to their structural fragility and limited cell entry, the systemic administration of these therapeutics is precluded, thus different strategies are under development to exceed all these limits. Cationic nanocarriers and all non-viral gene delivery systems represent a good approach thanks to the ability to complex siRNA, pDNA, miRNA increasing the blood half-life, the intracellular uptake and gene knockdown. Indeed, these vehicle offer a number of important advantages over viral vectors such as the lower immunogenicity and easier to prepare and scale-up. Moreover, cationic nanocarriers can be designed for several purposes providing targeting agent or features tailored on the payload characteristic and clinical application.

1.1 Cancer and its hallmarks

The "war on cancer" is a declaration launched in 1971 by USA President Richard Nixon that presented the tumor disease as the most dangerous threat to societies[10]. After more than 40 years, despite many efforts, investments and initiatives which helped to improve the knowledge on the nature of this disease, cancer is still one of the major causes of death in the world and leading of one quarter of all deaths in USA[11]. National cancer Institute defined the cancer as "diseases in which abnormal cells divide without control and can invade nearby tissues" [12]. Tumorgenesis in humans, is a multistep process which involves complexes mechanisms causing the progressive transformation of human cells in malignant ones. Cancer cells can invade other organ or tissue by migration from the native tissue (the tissue where they are generated) bypassing the immunosystem recognition using blood and lymphatic vessels. The six biological capabilities developed during the multistep development of human tumors may be summarized as follow[13-15]:

- Sustaining proliferative signal: compared to healthy cells, tumor cells display a greater ability to produce and release growth-promoting signals ensuring the abnormal cell growth, the cell division and therefore the chronic proliferation of cancer cells. Playing on a fine equilibrium between upregulated and downregulated mechanism, cancer cells can acquire the capability to sustain proliferative signaling by different ways such as produce growth factor themselves, overexpress receptors,

increase the sequestration of growth factors in the extracellular matrix and inhibit factor degradation. In some cases, cancer cells could induce healthy cells to produce growth factor for themselves. Malignant cells can also disrupt negative feedback mechanism that in normal condition can reduce the proliferative signaling.

- Evading growth suppressors: The ability to circumvent the pathways of cell proliferation down-regulation is another feature of cancer cells. Many tumor suppressors have been discovered. Among these, RB (retinoblastoma-associated) and TP53 proteins play a central role in cellular regulatory mechanisms that drive the decisions of cells to proliferate or die.

- Resisting cell death: apoptosis is a physiological pathway triggered in response to various chemical or physical stresses. Tumor cells display natural barriers which corrupt the apoptotic machinery resulting in hyper-proliferation. These “barriers” derives from the overexpression of specific genes called “oncogenes”. Several researches have demonstrated how apoptotic processes are inefficiently related to the stage of tumor progression. Tumor cells develop many strategies to bypass the apoptosis such as the production of anti-apoptotic proteins by themselves or the elimination of damage sensors from the apoptotic-inducing circuitry.

- Enabling replicative immortality: Normal cells undergoes to senescence (an unproliferative but viable status) and crisis, having the cell death as end point. Oppositely to healthy cells, tumor cells possess an unlimited replicative potential and the capability to circumvent both senescence and crisis thus reaching a new status called “immortalization”. Researchers have demonstrated that this capacity is related to a mutation in the gene associated to the production of telomeres, molecules responsible to protect and stabilize the end portion of DNA chromosomes. The continuous re-generation of telomeres leads to the cancer cells immortalization as they lose the senescence properties.

- Inducing angiogenesis: Tumor tissue develops the ability to recruit angiogenic factors for the creation of new vessels and obtain oxygen and nutrients to increase the uncontrolled growth.

- Activating invasion and metastasis: Among the six hallmarks of cancer, metastatization is still the less known and understood mechanism. During the growth progression, tumor cells activate the metastasis cascade which promote the local invasion of tumor cells in healthy tissue far from the tumor site.

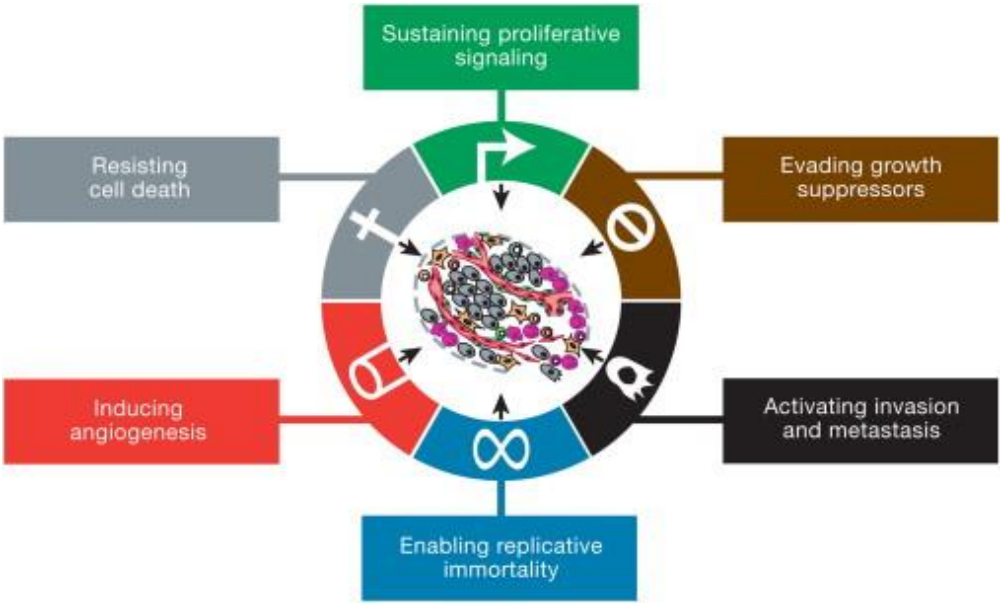

Figure 1. Representation of the hallmarks of cancer[14,16].

1.2 Molecular targeting: Rac1 gene

Angiogenesis and metastasis are two hallmarks of cancer development and propagation. These two processes involve a myriad of molecular pathways and therefore, many chemical processes providing an high spectrum of potential targets for therapeutic intervention. Indeed, in order to supply oxygen and nutrients, tumor cells release stimulating factors to induce capillary formations and therefore growth vessels. At the same time, new vessels could be form from the preexisting vasculature increasing the vessel network and permitting to the tumor to expanse its mass. On the other hand, metastasis consists in several complex steps including the local invasion of healthy tissue, the extravasation and cell migration into the blood stream until adhesion in different organs or tissue. Studies confirmed that for both the angiogenesis/vasculogenesis mechanism and the interactions of cancer cells with the endothelium, stroma, and extracellular matrix need of highly coordinated endothelial cell migration and cell-adhesions processes are required[16].

Rac1 is one of the Rho GTPase proteins which is responsible of the cellular growth and cell-cycle regulation[17], the formation of cell–cell adhesion[18], the contact inhibition process.

It alsodrives cellular mechanisms of healthy cells such as phagocytosis, mesenchymal-like migration, axonal growth, adhesion and differentiation of multiple cell types as well as reactive oxygen species (ROS)- mediated cell killing[3,17,19,20]. Due to its key role in all thesecell activities, researchers focused their attention on Rac1-mediated pathways involved in the tumor growth such as angiogenesis, invasion and metastasis. To date, different small molecules (from natural or synthetic) were studied to inhibit Rac1 and its molecular cascade in cancer cells. An example is NSC23766, a synthetic compound which bind Rac1 inhibiting its central role in cancer[21]. *In vitro* studies showed that cancer cells treated with NSC23766 displayed a reduced cell migration. NSC23766 was also tested *in vivo* on mouse bearing different tumor models showing a cytostatic activity and the ability to induce the apoptosis of tumor cells.

1.3 Traditional anticancer therapy

Traditional anticancer drugs are a class of small drugs that interfere with the regular cell cycle by inducing nucleus damage, inhibition of cellular replication, or promoting apoptotic pathways. Doxorubicin, paclitaxel, or cisplatin (Figure 2) are some examples of commonly used chemotherapeutics for cancer treatment[22].

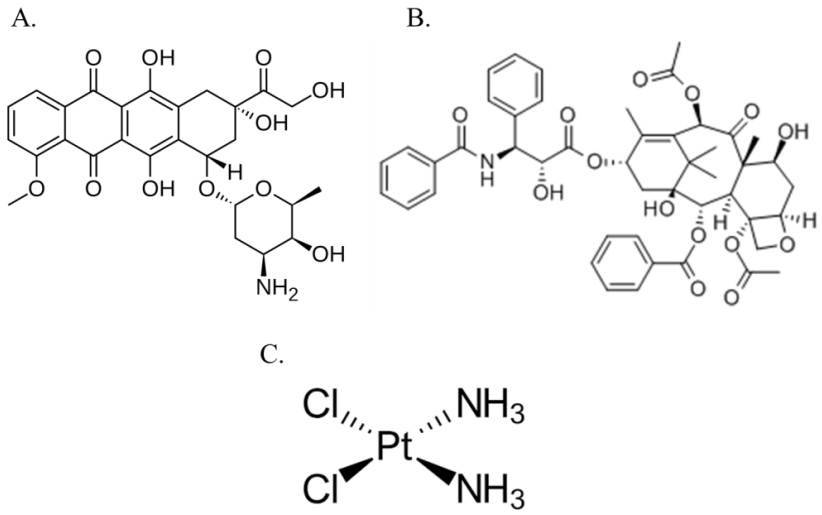

Figure 2. Chemical structures of common doxorubicin (A), paclitaxel (B) and cisplatin (C).

Doxorubicin is an anthracycline derivative used for the treatment of several cancers including breast, lung, gastric, ovarian, thyroid, non-Hodgkin's and Hodgkin's lymphoma, multiple myeloma, sarcoma, and pediatric cancers. Doxorubicin was isolated for the first time in 1970 by *Streptomyces peucetius var. caesius*[23]. To date, several doxorubicin

prodrugs and derivatives with a good anticancer activity have been synthesized. The major issue of these compounds is the cardiotoxicity which is related to its mechanism of action. As a matter of fact, doxorubicin interferes with topoisomerase II leading to DNA adduct formation and oxidative stress with the production of ROS species[24,25]. In this panorama drug delivery systems emerged as promising strategy to overcome these drawbacks. Doxil® was the first FDA-approved nano-drug in 1995 developed by Gabizon and Barenholtz and used for Kaposi's sarcoma, ovarian cancer and multiple myeloma treatment. This formulation is a pegylated liposome-encapsulated form of doxorubicin with an approximate mean size in range of 80–90 nm[26]. The advantage to use Doxil® is in the prolonged pharmacokinetics and highly reduced toxicity at heart level. Due to the steath properties of these liposomes, Doxil® can reach the tumor and accumulate in the desired site[6].

Paclitaxel is a chemotherapeutic isolated in 1960 from the bark of the Pacific yew tree (*Taxus brevifolia*) employed for the treatment of breast cancer, non-small cell lung cancer, bladder cancer, and cervical carcinoma[27-29] It was . The therapeutic efficacy of paclitaxel is due to the suppression of microtubule spindle dynamics resulting in the inhibition of mitosis process and induction of cellular apoptosis. The cellular target of paclitaxel is the tubulin a protein able to induce self-polymerization promoting the cellular replication. The pharmacokinetics parameters of paclitaxel were ameliorated by many different drug delivery systems, many of these are in clinical development. As example, Abraxane® is the physical conjugation of paclitaxel to human albumin. The choice of human albumin as drug delivery carrier allows to increase the intratumoral uptake of paclitaxel reducing its side effects such as the hypersensitivity to the drug. Abraxane® received the clinical approval for the treatment of advanced and meta-static prostate cancer and it is used as mono-therapy in metastatic breast cancer[30]. Paclitaxel conjugation to polymers is a common approach to improve the biopharmaceutical properties of this drug. Paclitaxel polyglumex is a poly-L-glutamic acid (PGA) derivative bearing paclitaxel. The molecular weight was finely tuned within the ideal range to selectively accumulate in tumor tissue by the enhanced permeability and retention (EPR) effect (further discussed in 1.6.1). Interestingly, paclitaxel polyglumex was obtained by coupling of PGA with paclitaxel through the 2′ hydroxyl moiety of paclitaxel, a site involved in the tubulin binding thus producing a prodrug which needs to be activated after been metabolized[31].

Cisplatin is a metal-organic compound able to intercalate the nuclear DNA, inhibit the cell proliferation and trigger the apoptosis process. To date, cisplatin is still a gold standard for

cancer treatment. At molecular level, cisplatin structure is formed by a central platinum atom surrounded by two chlorine atoms and two ammonia groups organized in cis configuration. National Cancer Institute indicates the administration of cisplatin towards bladder, ovarian and testicular tumors. The use of cisplatin is sometimes limited due to the nephrotoxicity of the drug. However, liposomal formulation of cisplatin (called "Lipoplatin®") displayed similar anticancer activity compared to the non-formulated drug with restricted side effects[32]. Actually, Lipoplatin® is used against pancreatic cancer in combination with gemcitabine as first line treatment[33]. In 2009, Lipoplatin® received the approval for the treatment of non-small cell lung cancer under the name of "Nanoplatin®".

1.4 Gene therapy

Many human genetic disorders are ascribed to DNA genome mutations which in many cases can affect the normal function of genes. The therapeutic strategy which involves the insertion of genetic material into diseased cells is generally defined as "gene therapy". In general, this approach induces the expression of a non-coded protein in the host cell. On the other hand, RNA or antisense oligonucleotide insertion is exploited to reduce the protein expression. The ability of RNA interference to silence gene expression was discovered and studied in 1998 when Fire and Mello published their works on Caenorhabditis elegans[34].

Nucleic-acid-based therapies involve a large class of drugs including plasmidic DNA (pDNA), small interfering RNA (siRNA), microRNA (miRNA), short hairpin RNA (shRNA) and oligonucleotides antisense. These compounds are used for the treatment of several diseases such as familiar hypercholesterolemia, hemophilia, cystic fibrosis, wound healing, neurodegenerative disorders and cancer[35-37]. Indeed, nowadays, many nucleic acid-based drugs are in the clinical trials. As example, ALN-RSV01 represent one of the recently published siRNA delivery system in clinical trials. ALN-VSP is a lipid formulation loaded with two different siRNAs in a 1:1 molar ratio. These two siRNA sequence possess different target. In fact, one is directed against vascular endothelial growth factor-A (VEGF-A) useful to inhibit the angiogenesis and the other against kinesin spindle protein (KSP), avoiding the mithosis and the cell proliferation[32]. This formulation and consist of a nasal spray of an siRNA against respiratory syncytial virus (RSV) displaying a good safety profile and a significant decrease (38%) of in the number of infected patients.

Another formulation in clinical trials, is Atu027 which is a lipoplex-based delivery system. This formulation was used to deliver siRNA that silence the expression of the protein kinase N3 (PKN3) with purpose of reduce the vascular permeability of tumor and of metastatic cells.

However, ALN-VSP and Atu0027 displayed a mils activation of immune system and complement in a dose-dependent way which could preclude the use of these promising carriers[32,33].

In general, a successful gene therapy involves 3 main sequential steps:

- Identificate the mutant gene or protein responsible for the disease;
- Clone the identical healthy gene or create a gene sequence which can inhibit the protein synthesis;
- Load the new gene on a nanocarrier towards the diseased cells.

siRNAs are short sequences of RNA (19-23 oligonucleotides per strand) which inhibit the production of targeted protein by mRNA interference.

At cellular level, siRNAs are produced by cleavage of longer RNAs mediated by DICER enzyme.[38]. Here, siRNAs are associated in a supramolecular complex called RISC (RNA-induced silencing complex, which is activated by a multifunctional protein called Argonaute-2 (AGO2) that in turn cleaves the sense strand (or passenger strand) of the siRNA[39]. The activated RISC-siRNA complex binds the complementary sequence of mRNA in cytosol and degrades it thus resulting in inhibition of protein traduction. Activated RISC-siRNA complex can then move on to cleave additional mRNA targets resulting in a potent gene silencing[40].

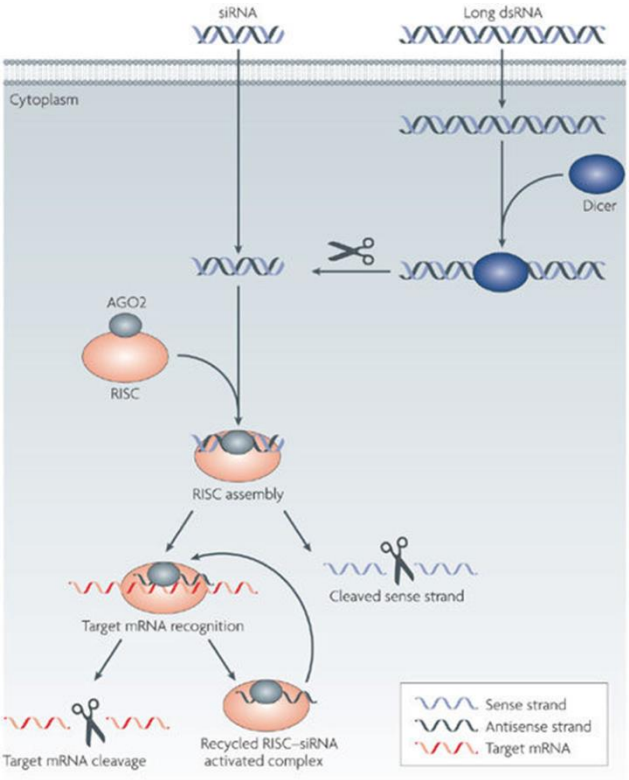

Figure 3. Mechanism of action of siRNA[40].

The therapeutic effect of siRNA could be modulated by a proper design of siRNA sequence which can silence similarly any gene in the body, ensuring the same therapeutic effect of classical small drugs. However, due to the high negative charge and molecular weight, these molecules are not stable in human plasma are unable to overcome the physiological barriers and can be immunotoxic[41]. Notably, the immune-response is siRNA sequence specific meanings that siRNA can elicit inflammation and complement activation as will discuss in section 1.11[42].

In the years, several strategies have been studied to reduce the limits of siRNAs. Chemical modifications on the backbone by introducing stabilizing groups or chemical conjugation with steroids or polymers were performed to increase their plasma stability and biopharmaceutical properties[43]. As example, the conjugation to cholesterol represent an interesting strategy for siRNA delivery. The cholesterol conjugation since it improves the biodistribution of siRNA used for the selective Apolipoprotein B inhibition by binding with serum proteins and good gene knockdown in mouse models was observed.[44]. The conjugation with cholesterol, In order to reduce the binding with Toll-like receptor, responsible of the inflammation pathways, and improve the endonuclease stability, 2'-O-methyl modification into the ribose was introduced.

Further modification of the sugar backbone on 2' hydroxyls generated a 2′-O-(2-methoxyethyl)-modified single stranded RNA molecule called Mipomersen[45]. This drug was used to silence ApoB48, a protein that has been implicated in cardiovascular disease.
Other chemical modifications were explored such as 2' hydroxyl substitution with fluorine on the ribose ring or the replacement of phosphodiester bond with phosphorothioate linkages[46].
However, most of these approaches led to an enhanced stability and biocompatibility of siRNA affecting the silencing activity. Despite many efforts, the need to develop new gene delivery systems is crucial for the clinical application of these potent class of drugs.

1.5 Gene delivery systems: an overview

1.5.1 Physical methods

Physical methods are attractive tools to transfect the cells with genetic material[47]. These techniques exploit physical forces to induce the passage through the plasmatic membrane of DNA/RNA resulting in high gene transfection. For this purpose, many different techniques could be used such as electroporation, sonoporation, ballistic DNA and microinjection[48].
Electroporation consists into the nanopore formation induced by an external electric field. These nanopores allow the genetic material to cross the cell membrane. The strength of electric field, amplitude, time of application and pulse duration can modulate and reverse the pore formation avoiding the cell death. In general, low field strength with long pulse is used for cancer cells transfection[49].
In analogy with electroporation, sonoporation has emerged as technique to deliver genetic materials using ultrasound. After the incapsulation of DNA or iRNA within microbubbles, the ultrasound waves are able to permeabilize the cell membrane and, at the same time, to cavitate the microbubble resulting in gene transfection[50].
Another interesting method is called "ballistic DNA" in which DNA coated heavy metallic particles (e.g. gold, silver or tungsten) with 1.0 μm size are shot into the cell cytosol[51].
Finally, microinjection is the simplest and safest method of gene transfer and is used to inject DNA into tissues or organs. Basically, DNA is administered in the desired site without the help of any carrier through a microneedle carrying syringe [52].

1.5.2 Viral vectors

Nowadays, viral vectors represent the 69% of gene delivery investigations[53]. Taking advantage of the natural mechanism of transfection of viruses, genetic materials can be introduced by the use of these vectors. After replacing the virus genome with the therapeutic oligonucleotides, viruses were transformed in gene-delivery carriers. Typical viruses employed for gene delivery purpose are retrovirus, lentivirus (for example, HIV), herpes simplex virus, pox virus and adenovirus or adeno-associated virus. However, the production of viruses-based gene delivery systems is very expensive and sometimes disadvantageous[43]. In fact, safety and cell-selectivity in the uses of viruses is the main problem in the use of viral vectors. Viral vectors suffer of bio- and immuno-compatibility and the possibility that the viruses will revert to a wild-type virion is always open. In addition, undesired effect could happen. As example, in 1999 adenovirus which was in clinical trials as gene therapy vector causes patient death the day after the virus-based formulation administration[54]. Moreover, studies in monkeys have showed that the adenovirus capsid proteins, might elicit an early inflammatory cytokine cascade[55].

1.5.3 Polymer therapeutics and polyplexes

Polymer-based systems represent the most promising strategy to deliver genetic materials to diseased cells thanks to their chemical variability and their potential functionalization. Complexes obtained by the charge interaction between cationic polymers and oligonucleotides are generally called polyplexes and represent the most used non-viral gene delivery system[1].

The ON complexation with positively charged polymers prevent the enzymatic degradation of the genetic material and the opsonization, allow to deliver the ONs on the tumor target, overcome the physiological barriers, promote the cell uptake and release the oligonucleotides.

For this purpose, polymers with different architecture and composition have been designed and studied during the years to increase the serum stability, biocompatibility, poly- or oligonucleotides complexation capacity and transfection activity[56]. Importantly, polycationic polymers can also be exploited to induce the endosomal escape of the genetic cargo. Endo-lysosomal compartments are acidified by proton pumps on their membranes. Once reached these endocytic vesicles, the cationic polymer undergo to protonation thus causing the rupture of the endosome membrane and the polyplexe release from the endosome. This process is called “proton sponge”[57]. In order to meet the need of proton

sponge effect in the endo-lysosomal compartment, several polymers where derivatized with histidine which contain the imidazole group. This chemical group shows the pKa in the optimal range able to induce the proton sponge effect and ensuring for a good biocompatibility of the nanocarrier.

Poly(ethylenimine) (PEI), poly cationic-aminoacid (e.g. polylysin, poly-arginine, etc.), polyamidoamine (PAMAM), and cationic cyclodextrin are some examples of widely used cationic polymers used to complex DNA or siRNA which had demonstrated both *in vitro* and *in vivo* efficacy.

Since 1995, PEI (linear or branched) has fascinated researchers working in gene delivery field because of its simply structure and high effective gene knockdown[58]. The high capacity to promote the gene silencing could be ascribed to the efficient endosomal escape through the proton-sponge mechanism. Indeed, despite the high content in amines, only the 15-20% of these are protonated at pH 7.4, ensuring for a high proton sponge ability. In order to increase the target specificity, PEI has been decorated with different ligands, namely antibodies[59], folic acid, transferrin[60].

In spite of its interesting properties, PEI with a molecular weight above 2000 Da shows a relevant cytotoxicity and is an off-the-shelf material. On the contrary, PEI with low molecular weight (<2000 Da) shows a good biocompatibility but is totally ineffective in terms of transfection and, therefore, gene knockdown. PEGylation, or coating with negatively charged polymers (e.g. hyaluronic acid) permits to reduce the PEI toxicity in *in vitro* and *in vivo* studies[61].

Polylysine (PLL) was the first polymer used applied in gene delivery[62]. However, PLL/DNA complexes showed a low gene knockdown which was strongly increased by the use of targeting agents both *in vitro* and *in vivo*[63,64]. As example, polylysine polymer was functionalized with a glycoprotein ligand which possesses high affinity asialoglycoprotein receptor overexpressed on hepatocyte in a murine model. The results showed a better silencing compared to the non-targeted polyplexes. However the low silencing ability of PLL could be ascribed to the low endosomal escape. To enhance the proton sponge effect, polylysine was further functionalized with imidazole groups showing a better silencing profile[65].

PAMAM are polymeric dendrimers that display a large number of secondary and tertiary amines on the surface responsible of proton sponge effect. Studies involving PAMAM complexes with genetic materials showed an high gene delivery and good biocompatibility[66].

Cationic cyclodextrins (CCD) is a class of cationic polymers developed in 1999 able to self-assemble in presence of nucleic acids forming polyplexes with a mean size of 100 nm. The study of the cationic polymers cyclodextrin-based involved several steps including the investigations on the size of cyclodextrin (α-, β- or γ-cyclodextrin), the chemical nature of cationic groups and the spatial distance between the cationic moiety and the cyclodextrins. Several studies reported in literature highlighted a higher biocompatibility of the CCDs compared to PEI and PLL both *in vitro* and *in vivo*. To increase the biocompatibility of the system and impart stealth properties to the nanocarriers, Davies and co-worker have decorated the PEG grafted with adamantane which form host-guest complexes with the cationic cyclodextrins cavity[67]. The external side of PEG chain was functionalized with transferrin as targeting agent. These polyplexes, called CALA-001, reached the phase II of clinical trials to treat solid tumors cancer.

Taking advantage to their unique pharmaceutical properties, cyclodextrins were also conjugated with PAMAM or PEI obtaining good transfection results[65,68].

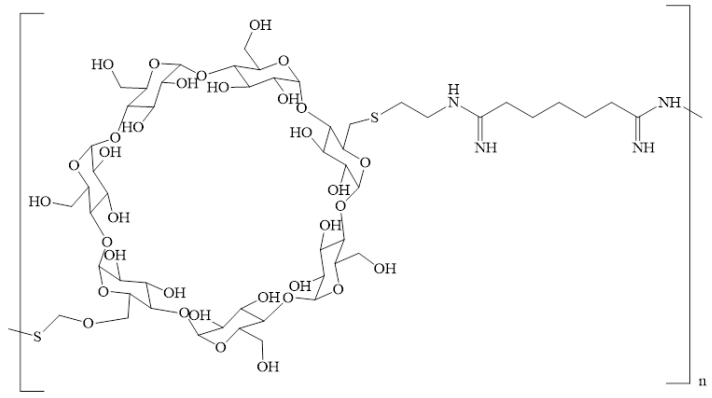

β-Cyclodextrin containing polycation

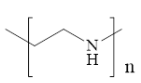

Linear PEI

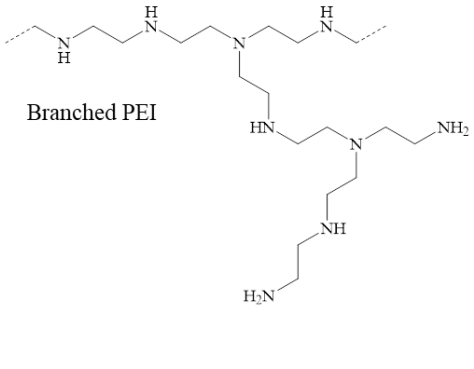

Branched PEI

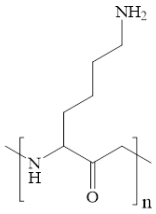

Poly(Lysine)

Figure 4. Chemical structures of cationic polymers used for delivery of oligonucleotides.

1.5.4 Liposomes and lipoplexes

Liposome decorated with cationic polymers (lipopolyplexes) or composed by cationic lipid (lipoplexes) and complexed with DNA or RNA are other non-viral carriers widely exploited for gene delivery application. Cationic lipids commonly used in gene transfection are characterized by a cationic head (usually an amino or guanidinic group) and two hydrophobic side chains characterized by saturated or insaturated bonds. These two portions are generally connected by an amidic or carbamate group, while the phosphonic group is avoided as it presents a strong negative charge that could interfere with the genetic material thus affecting the complexation efficiency. Mono-unsaturated tails showed high transfection efficacy, probably due to the effect on membrane fluidity[69]. 1,2-di-O-octadecenyl-3-trimethylammonium propane **(**DOTMA), 2,3-dioleyloxy-N-[2-(sperminecarboxamido)ethyl]-N,N-dimethyl-1-propanaminium (DOSPA), N-(2,3-Dioleoyloxy-1-propyl)trimethylammonium (DOTAP), (1,2- dimyristyloxy-propyl-3-dimethyl-hydroxy ethyl ammonium (DMRIE), 3β-[N-(N',N'-dimethylaminoethane)-carbamoyl] cholesterol (DC-cholesterol) or dioctadecylamido-glycylspermine (DOGS) are some examples of cationic lipids that have been used for liposomal gene delivery[40].

Several studies have showed that cationic lipids are involved in liposome stability and ON complexation but play a minimal role in the cell membrane interaction for the transfection pathway. In order to increase the transfection activity of lipoplexes, lipid “helper” which possesses neutral charge and fusogenic properties are used to promote the interaction with cell membranes, endosomal escape and gene knockdown. Limitations of lipoplexes applications include the poor serum stability, rapid clearance and inflammatory responses[40]. These drawbacks were overcome by the further decoration of lipoplex surface with PEG which increases the blood circulation time. Delivery of siRNA lipoplexes-mediated was successfully afforded using cationic liposomes formulated with DC-6-14, DOPE, and cholesterol[70]. Liposomes composed of DC-6-14, 1-palmitoyl-2-oleoyl-snglycero-3-phosphocholine, DOPE, and PEG_{2000}-DSPE were complexed with siRNA Argonaute-2 inhibitor and *in vivo* administered for the treatment of Lewis lung carcinoma. The results showed an efficient gene knockdown and significantly reduced tumor growth[71].

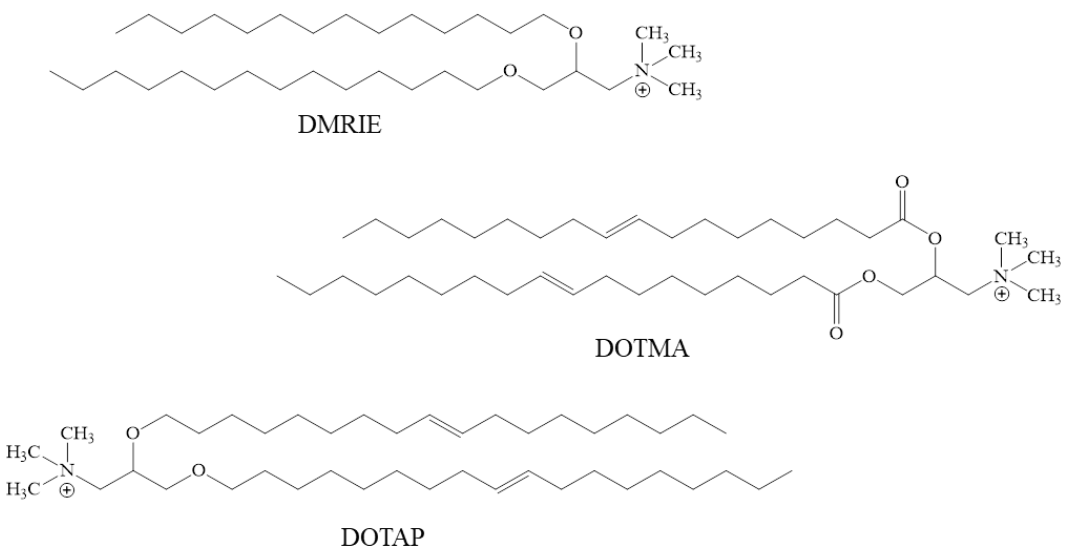

Figure 5. Chemical structure of 1,2- dimyristyloxy-propyl-3-dimethyl-hydroxy ethyl ammonium (DMRIE), 1,2-di-O-octadecenyl-3-trimethylammonium propane (DOTMA) and N-(2,3-Dioleoyloxy-1-propyl)trimethylammonium (DOTAP), cationic lipids commonly used for lipoplexes preparation.

1.6 Passive vs. Active targeting

Smart nanocarriers are developed taking advantage of the nature of the tumor. Exploiting the leaky vasculature, the overexpression of receptors or mutated proteins on the cell membrane and/or the tumor microenvironment, controlled and precise release of potent anticancer drugs (small active molecules or macromolecules such as oligonucleotides) can be performed with excellent results. In particular, three main approaches can be follow which are the passive targeting, the active targeting and stimuli-responsive targeting. These strategies could be used alone or associated.

1.6.1 Passive targeting

When a solid tumor reaches a size above 2 mm^3, the normal surrounding vasculature is no longer sufficient to provide oxygen and all the nutrient for its further proliferation[72]. In this contest, tumor cells release growth factors stimulating the grown of new blood vessels and this phenomena is called angiogenesis. However, the new blood capillary display a discontinuous epithelium and lack the basal membrane of normal vascular structures[73,74]. In this condition, fenestrations of the vessels can reach sizes ranging from 200 to 2000 nm[75] and can show little resistance to extravasation into the tumor interstitium. Another aspect of the rapid vessels formation is the defect of lymphatic system responsible for the drainage of the extracellular fluids. The absence of lymphatic vessels leads that extra-vasated solutes and colloids (i.e. nanoparticles) cannot go back to the circulation. This

synergistic effect was observed and described for the first time by Matsumura and Maeda in the 1980's years and is called enhanced permability and retention (EPR) effect[76,77]. The EPR effect has been comprehensively documented using various tumor types and animal models.

In order to develop nanocarriers which can efficiently accumulate in the tumor exploiting the EPR effect, several aspects have to be taken into account.. The hydrodynamic diameter of nanomaterial can influence the kinetics and therefore the tumor accumulation. Nanocarriers should be small enough to pass though the fenestrations in the neovasculature. Moreover, the nature of the cancerous mass should be considered. For example, Kataoka and co-workers[78] demonstrated the effect of nanoparticle size on low-vascular tumor. In particular, different polymeric micelles with sub-100 nm (30 nm, 50 nm, 70 nm and 100 nm) size were administered in mice bearing highly permeable tumors showing a good penetration and accumulation. At the same time, the administration of the same size micelles in poorly permeable human pancreatic adenocarcinoma, characterized by low vascularity and fibroses tissue, only small size nanoparticles (<50 nm in diameter) were able to accumulate in tumors. Similarly to the size, the surface charge plays an important role in tumor accumulation and penetration. Negative surface charges could show different effects on pharmacokinetics of nanoparticles due to the reduced absorption of serum proteins while positive surface charge generally provided for hemolytic properties and nonspecific uptake. However, positively charged particle promote endosomal release through mechanisms, such as the 'proton sponge effect', that is essential for oligonucleotides delivery.

Nanoparticle architecture can affect the intracellular and *in vivo* fate of nanoparticles. As described in literature discoidal, worm-like and spherical particles show geometrical parameters, such as curvature and aspect ratio (the ratio between the long axis and the small axis) , that modulate the cell uptake, macrophage internalization, renal filtration and tumor accumulation[79,80].

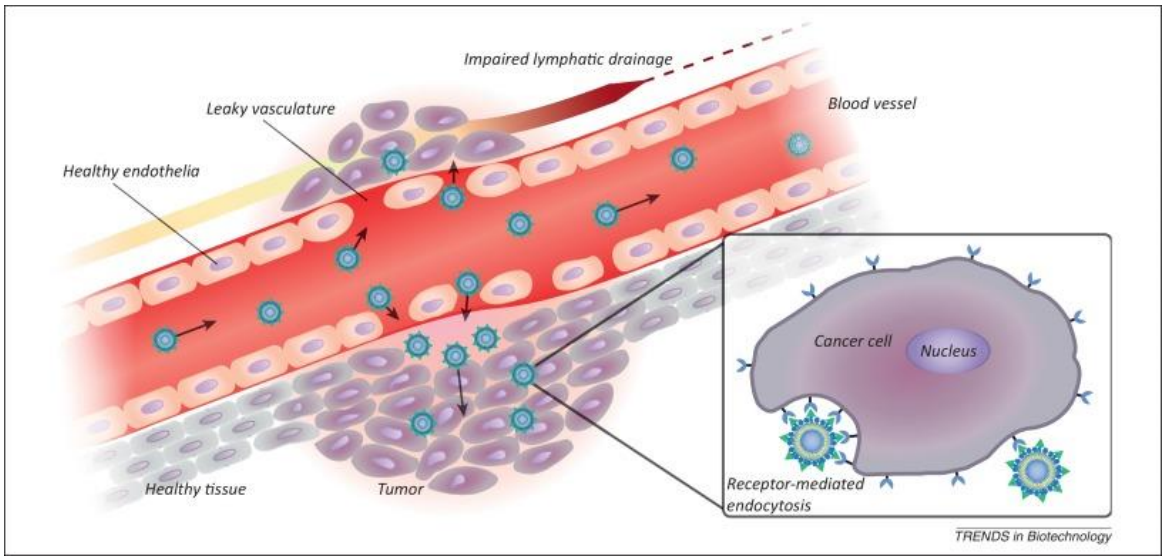

Figure 6. Enhanced Permeability and Retention effect (EPR) representation[81].

1.6.2 Active targeting

Active drug targeting involves the use of targeting ligands. The concept of "active targeting" concerns in the use of specific molecules which interact at the molecular level (ligand-receptor are close, <0.5 nm) with an overexpressed receptor on cell membrane, increasing the specificity of therapy[82-84].

Indeed, passive targeting strategies and long circulation time of drug delivery systems can facilitate accumulation of nanocarriers in the tumor interstitium but the cell uptake and drug accumulation could be still ineffective[85]. For this reason, researchers developed smart drug delivery systems bearing molecules on their surface that by a "trojan horse mechanism" are selectively internalized resulting in an increased therapy efficacy. The active targeting strategy is correlated to passive targetingas increasing the circulation time of nanocarriers (i.e. by modifying the surface of nanoparticles with PEG) the tumor accumulation by the EPR effect is improved and the targeting moiety is expected to enhance the tumor cell internalization.

In order to obtain a good ligand-receptor interaction, the ligand moiety for anticancer therapy should display different properties. Molecular weight, ligand-binding affinity and specificity, adaptability to different receptor topography, stability, immunogenicity and chemistry of conjugation are some parameters useful for the choice of the more suitable targeting agent. The ligand moiety could play a key role in nanocarrier therapy efficacy through the modulation of drug potency[86]. The targeting agent density on decorated nanoparticle could also affect the intracellular uptake[87]. On the other hand, the receptor

binding affinity and the receptor expression and distribution on tumor cells are non-negligible parameters[88].

The first example of active targeting nanocarrier was galactosamine-functionalized HPMA-Doxorubicin prodrug (also called PK2) employed for hepatocarcinoma treatment. So far, many targeting ligands have been investigated to actively target drug delivery systems such as peptides and proteins (e.g. transferrin whole antibodies or antibody fragments, aptamers and different receptor ligands (e.g. folic acid or galactosamine)[84].

1.6.3 Stimuli-responsive targeting

Stimuli-responsive nanocarriers represent a rather complex approach to deliver drugs. For this purpose, materials that are susceptible to specific stimulation based on different microenvironment of living tissues are needed. Protonation, hydrolytic cleavage, molecular or supramolecular conformational change in response to a specific stimulus are some example of the responsiveness that nanocarriers should display for an efficient and site-specific drug delivery[89].

Figure 7. Schematic representation of stimuli responsive nanocarriers, triggered by low pH, temperature, electric and magnetic fields, ultrasounds and enzymes[89].

Indeed, endogenous stimuli such as the lowered pH in the interstitium or in endo-lysosomes compartment, the higher glutathione concentration or an increased level of enzymes such as matrix metalloproteinases, represent good distinguishing conditions that can be exploited to obtain a site-selective uptake of nanocarriers or to realize a controlled drug release. As example, exploiting the different concentration of gluthatione in extracellular (from 2 to 10 μM) and intracellular (from 2 to 10 mM) compartements, drug delivery systems disulfide bond-based can be used for smart release of anticancer drugs into the tumor cells[90]. Several drug delivery were developed on the acidic tumor microenvironment. Indeed, the acidic extracellular pH of tumor tissue which is caused by anaerobic metabolites and hypoxia could be an perfect trigger for nanocarriers pH-sensitives. In similar manner, the acidic environment of endosomes and lysosomes was

widely used for therapeutic deliver in to cancer cells as described in section 1.10.05. Alternatively, heating, light, ultrasound or magnetic field are performing external physical stimuli that can be applied to induce a morphological rearrangement of the drug delivery system inducing the release of the drug in the site of action. These strategies are exploited for treatment several diseases namely, tumor, ischemia or infections.

1.7 Targeting moieties

The cancer targeting agents should be selected according to heterogeneity of tumor biology.the and the tumor growth and metastasis. As discussed before, the identity and characteristic of targeting ligand can affect the pharmacokinetics and cellular uptake of nanocarriers. In the recent years, targeting to markers involving neovasculature of angiogenesis, uncontrolled cell growth, and direct tumor targeting have been extensively studied. Here below a brief description of the main classes of targeting moieties exploited for the active targeting of drugs is reported.

1.7.1 Antibodies and antibodies fragment

Antibodies, or immunoglobulins (Ig), are large glycoproteins found in the serum. Among the different antibodies circulating in the blood (IgG, IgA, IgM, IgE), IgG is the main class of antibodies used for therapeutic and diagnostic applications. The classical antibody Y-shaped structure possesses two chains (heavy and light) linked by disulfide bonds.. The two arms of the Y structure are responsible of the antigen recognition and can be used for high selective tumor targeting, even as single fragment Antibodies targeted towards a specific receptor can interfer with specific pathways acting both asl targeting ligand and drug. Trastuzumab (anti-ERBB2, Herceptin®), bevacizumab (antiVEGF, Avastin®), etaracizumab (humanized anti-αvβ3 antibody, Abegrin) are some example of drug-ligand antibodies which regulate the proto-oncogenes responsible of cancer progression.

Furthermore, antibodies can be conjugated to chemotherapeutics to enhance their anticancer activity. The first immunoconjugate to have the clinical approval was gentuzumab ozogamicin (Mylotarg®). Gentuzumab is a monoclonal antibody which possess a stong affinity to CD33 receptor and was conjugated with ozogamicin, a cytotoxic drug. To date is used in US for the treatment of acute myeloid leukemia[91,92].

.

1.7.2 Transferrin

Transferrin is a serum glycoprotein involved in the transport of iron into proliferating cells which is overexpressed in malignant cells[93]. In healthy cells, upon binding to the transferrin receptors on the cell surface, transferrin is internalized through clathrin mediated endocytosis and the iron-protein dissociation is due to acidic pH value of endocytotic compartment. Cancer cells need of increased requirement of iron causing the transferrin receptor over expression[94]. Transferrin receptor targeting has been exploited for the delivery of different small anticancer drugs such as doxorubicin[95] and cisplatin[96] that are now in human clinical trials.

Mark Davis developed a transferrin targeted gene delivery nanocarrier based on cationic self-assembly polymers. These polyplexes have been used to target malignant tumor which is Ewing's sarcoma[68]. In another work, Davis et al. have studied the delivery of small interfering RNA (siRNA) in non-human primates using transferrin-conjugated liposomes. Moreover, transferrin-targeted liposomes co-encapsulating doxorubicin and verapamil have been shown to effectively overcome multi-drug resistance[97].

1.7.3 αvβ3 Integrin

Integrins are a class of transmembrane receptors with a large extracellular domain that connects the extracellular matrix (ECM) to the actin cytoskeleton during the cell motility. In particular, integrins are αβ heterodimers where the binding specificity is related to the extracellular domain which recognize and bind specific motifs within the matrix protein[98]. Among the integrins, αvβ3 integrin is highly expressed on neovascular endothelial cells and is important in the calcium-dependent signaling pathway leading to endothelial cell migration[99]. High efficient ligand for targeting the αvβ3 integrin is the small peptide Arginine-Glycine-Aspartic Acid (RGD). Chitosan and poly-L-lysine were conjugated with αvβ3 integrin targeting agent showing a strong enhancement of both antitumor and antiangiogenic activity with respect to the free drug[100].

1.7.4 Aptamers

In recent years, aptamers have emerged as good alternative to antibodies and antibody fragments for the sito-specific delivery of chemotherapeutic drugs. Aptamers are single-stranded DNA or RNA with high binding affinity towards various molecular receptors[101]. Oppositely to antibodies which display high molecular weight and structural fragility, aptamers have a small size and show high *in vivo* stability[102]. GMT8 aptamer, a short DNA

sequence used for human U87 glioblastoma cells targeting, was used to decorate docetaxel-loaded PEG-poly(ε-caprolactone) nanoparticles[103]. The *in vivo* imaging showed a 2-fold higher brain glioblastoma accumulation of targeted-nanoparticles than non-targeted controls. Langer et al. prepared a series of PEG-b-PLGA nanoparticles functionalized with increasing A10 aptamer densities which selectively recognized the extracellular domain of the prostate-specific membrane antigen (PSMA) overexpressed on prostate cancer cells[104]. The increasing percentage of aptamer on nanoparticles surface led to the increase of the uptake in PSMA overexpressing human prostate carcinoma LNCaP cells up to 5-fold for 5% mol/mol aptamer- decorated nanoparticles. However, over 5% functionalization, target delivery is *in vivo* compromised by high accumulation in liver and spleen[101].

1.7.5 Oligo- and polysaccharides

Saccharides (i.e. galactose, and galactosamine) and polysaccharides (i.e. hyaluronic acid) conjugated nanoparticles or liposomes have been developed for targeted cancer therapy. Due to their proper nature, nanoparticles functionalized with saccharides were mainly used for hepatocarcionoma drug delivery. The therapeutic efficacy of saccharides in targeted therapy was firstly assessed by galactosamine-decorated PEG-b-poly(acryloylcarbonate)-b-poly(ε-caprolactone) nanoparticles preparation for hepatocarcinoma paclitaxel delivery[105]. The biodistribution and antitumor efficacy studies of in hepatoma-tumor-bearing nude mice showed good results in terms of anticancer efficacy and site-specific tumor accumulation. Indeed, compared to non-targeted particles or commercially available formulation namely, Phyxol, galactosamine-decorated nanoparticles displayed highest tumor suppression efficacy. Hyaluronic acid (HA), a biocompatible polysaccharide composed of disaccharide units of N-acetylglucosamine and D-glucuronic acid linked through alternating β-1,3 and β-1,4 glycosidic bonds, showed interesting binding affinity with CD44 and RHAMM receptors[106]. Fattal and co-workers, developed a liposome and lipoplexebased-formulation with HA anchored on lipid bilayer as targeting agent showing high *in vitro* efficacy[107].

1.8 Targeting to breast cancer

Over the past 50 years, breast cancer showed the highest incidence among females worldwide. To date significant progresses have been done in diagnosis, therapy, and disease prevention. Nevertheless, the war against this cancer is still open. The efforts to

increase the efficacy of treatment include the use of active targeting nanoparticle systems towards specific markers overexpressed on breast cancer tumor[97].

Trastuzumab is a FDA-approved antibody which recognizes HER-2 receptor of HER-2-positive metastatic breast cancer cells. Many nanoparticles systems have been developed targeting HER-2 breast cancer tumors. Promising nanocarriers include crosslinked human serum albumin nanoparticles and quantum-dot loaded chitosan nanoparticles with absorbed siRNA[108] or micelles decorated with a model toxin against HER-2-positive tumors[109-111].

A novel widely used strategy involves the development of drug delivery systems displaying targeting agent against luteinizing hormone releasing hormone (LHRH) receptor localized on metastasized breast cancer. *In vitro* studies showed 9-fold accumulation of LHRH-conjugated superparamagnetic iron oxide nanoparticles (SPIONs) in MDA-MB-435 breast cancer cells compared to non-functionalized SPIONs. *In vivo* studies has demonstrated that LHRH-SPIONs accumulated in the tumor site suggesting the possible application for therapeutic purposes. Oppositely, non-targeted particles mainly accumulated in liver[108].

One of the most commonly used approach to targeted delivery of nanoparticles towards breast cancer is the nanocarrier surface decoration with folic acid. This promising approach was used also in the present work of thesis. For this reason, the role of folic acid and folate receptor will be further develop and discuss in the paragraph 1.9.

1.9 Folic acid and folate receptors

Folic acid (FA, Figure 8) is a low molecular weight (441 Da) essential vitamin involved in the biosynthesis of purines and pyrimidines in eukaryotic cells and needs to be acquired through the diet. Cell survival and proliferation are related on a cell ability to acquire this molecule. FA displays high binding affinity with its receptor (Kd< 1 nM), do not elicit toxicity and immunogenicity, possesses great stability in storage, is inexpensive and shows an easy chemistry of conjugation to carriers[112]. Indeed, cellular uptake of drug delivery systems decorated with FA similar affinity compared to the native FA (Kd ≈ 1 nM) and healthy cells transport folic acid only in reduced form such as 5-methyl-tetrahydrofolate across their membranes but do not transport folate conjugates of any type[112].

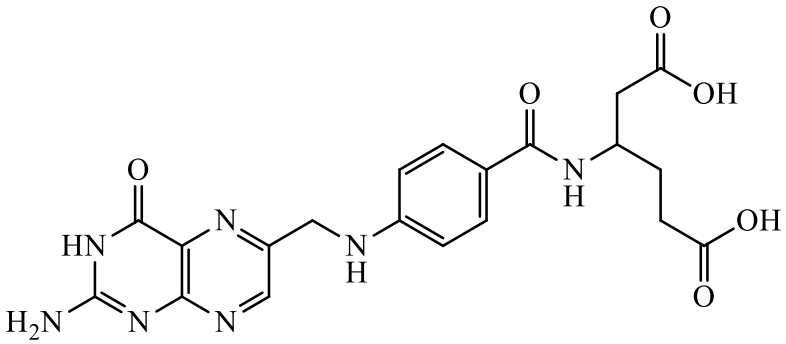

Figure 8. Chemical structure of folic acid.

FA uptake occurs by different route. The reduced folate carriers (RFCs) are anionic phosphates antiporters able to deliver FA in the tissues. The folate receptor (FR) is a 38 kDa glycosyl-phosphatidylinositol (GPI)-anchored glycoprotein whose expression levels in tumors are 100−300 times higher than in healthy tissues[110]. For this reason is one of the most highly exploited and investigated targets for cancer therapeutics[113]. Two main subclasses of folate receptors (FR_α and FR_β) are expressed on cell membrane and possess great binding affinity for folic acid in the oxidized form (Kd in the range of 1-10 nM). FR_α is commonly expressed on many surface tissues such as placenta, retinal pigment epithelium and choroid plexus but several studies have demonstrated a 40% increase of FR_α expression in human cancer cells compared to the healthy[114]. In the case of FR_β, this is expressed in the hematopoietic tissue and on activated macrophages[97,114]. As mentioned above, FRs are overexpressed on epithelial cancers of the ovary, mammary gland, colon, lung, prostate, nose, throat, and brain. Several studies revealed a correlation between the grade of histological stage in tumors and FR receptor expression. For all these reasons, folic acid is widely used targeting agent to specific deliver of anticancer drugs in order to reduce their toxicity and improve the therapeutic effect.

Molecular dynamic simulation studies have been carried out to evaluate the interaction of FA its receptor. FR_α showed a globular structure which contains a folate-binding pocket where, the pteroate moiety of FA is hidden inside; on the contrary, the FA glutamate moiety is exposed to the solvent and only the α-carboxy group is involved in interaction with the receptor meanings that γ-carboxy group is not responsible for the biological activity thus can be conjugated to drugs or nanocarriers[115].

To date, several drug delivery systems were targeted to tumors by FA. Liposomes bearing folic acid can be easily prepared by incorporating a phospholipid/flexible molecule (i.e PEG)-anchored folate into a liposome bilayer. Compared to the non-folate ones, liposomes decorated with FA show a reduction in nonspecific uptake by reticuloendothelial system

(RES)[116]. In order to avoid the shielding of FA by PEG (commonly used to give Stealth properties to liposomes), FA should be conjugated to a PEG molecule longer than that use to stabilize the liposomal formulation. This strategy enhance the folate accessibility to FR expressed on cell membrane[117]. Indeed, the use of folate receptor route for liposomal-based chemotherapeutic agents delivery, such as paclitaxel and doxorubicin is an interesting way to avoids the common multi-drug resistance experienced by cancer patient[97]. The FR overexpression was also exploited by Yoo and Park by functionalization of Doxorubicin loaded-PEG-PLGA micelles with FA. The in vitro results on human ovarian KB cells show a better uptake profile and therefore cytotoxicity compared to the non-folate micelles. Similarly, folate-micelles demonstrated be 2-folds efficient in tumor accumulation and the anticancer activity rather than non-targeted micelles[118]. The FA conjugation could improve the transfection of gene delivery tools. EG5-siRNA was efficiently complexed using cationic (oligoethanamino)amide-based polymers previously conjugated with FA for targeted delivery of in human cervix carcinoma cells. These polyplexes achieved folate receptor-specific cell targeting, and high in vitro and in vivo silencing of the EG5 gene in receptor-positive tumors. Biodistribution of these polyplexes show the absence of accumulation in non-target tissues demonstrating the selectivity of the drug delivery system. In similar manner, gold nanoparticles, cyclodextrin, dendrimers represents a suitable platforms targeted by folic acid[97].

1.10 Endocytosis mechanism

Endocytosis is defined as “the process of internalization of extracellular material within an invagination of the plasmalemma”[119]. Due to the fluidity and dynamism of cell membrane, cells form “gates” permitting nutrients, extracellular messangers and nanocarriers to overcome the lipidic bylayer and be internalized. Moreover, the need to understand the cell recruitement and internalization of nanocarriers and their intracellular fate is actually unsatisfied. For these reasons, several research groups focused the attention on cellular processing of nanoparticles. The mechanism of uptake behind the endocytosis of nanocarriers is rather complex and involve dynamic processes such as cellular uptake kinetics, structure of carriers (size, charge and shape), targeting ligand and many different characteristics proper of the cell type[120]. To date, endocytosis has been divided into three classes namely phagocytosis, macropinocytosis and pinocytosis. Pinocytosis pathway can be further divided in 3 classes: endocytosis clathrin-madiated, endocytosis caveolae-mediated and clathrin- and caveolae- independent mediated.

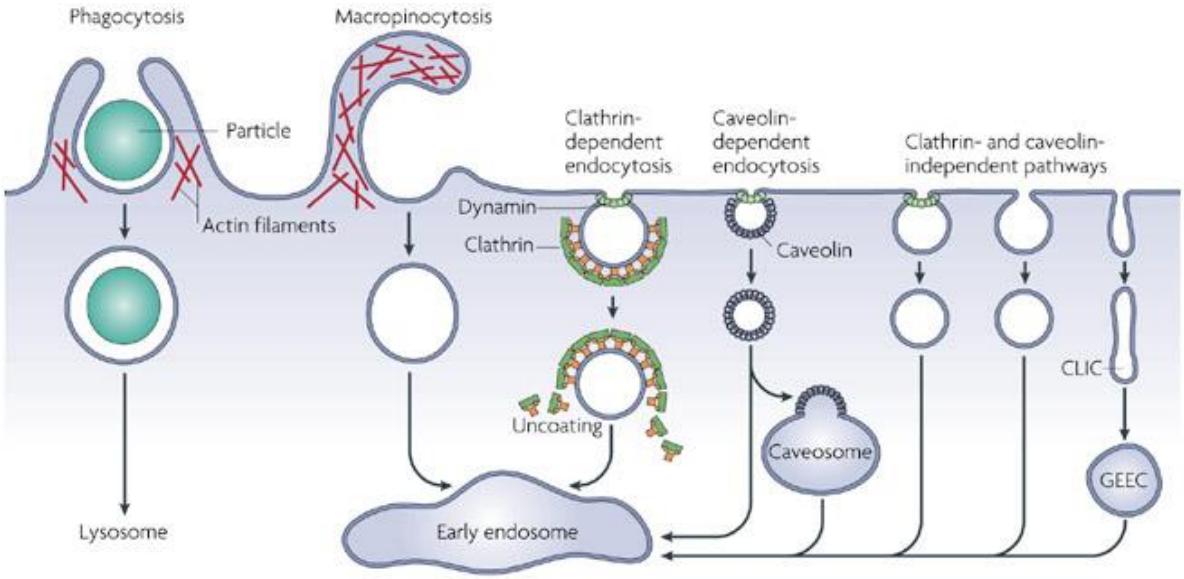

Figure 9. Multiple portals of nanocarriers entry in living cells.

1.10.1 Phagocytosis

Phagocytosis means the uptake of large solid particles with few micrometer of diameter. In general, phagocytosis uptake is a typical feature of macrophages, monocytes, neutrophils, and dendritic cells which are specialized to internalize foreign substances with broad size ranges (25 nm to several μm's in diameter)[121].

Phagocytic process by macrophages involves a cascade mechanism which the main important step is the opsonization of particle by IgG antibodies or complement proteins in the blood stream. Particles coat by opsonine are recognized by the Fc-receptor that interact with macrophages. Several studies have demonstrated that also by fibroblasts, endothelial and epithelial cells can used phagocytosis as endocytic pathway. It was observed how polyplexes could be internalized by epithelial cells via phagocytosis, after size increase induction by their association with heparan sulfate proteoglycans on the cells surface[122,123].

1.10.2 Macropinocytosis

Macropinocytosis is an essential process of cellular processes which is involved in cell motility and antigene sampling. In presence of determinate substances (i.e. growth factors or cell penetrating peptides), cellular membrane create engulfment of 0.2–10 μm in diameters, also called macropinosomes. The process that lead to macropinosomes formation is still poorly known and appears to show only a few distinct molecular

regulators, when compared to the other endocytotic ways. Luini and co-workers shows the role of brefeldin A-ADP ribosylated substrate (BARS), which was reported to play an essential role in macropinosome closure[124]. Compared with phagocytosis, micropinocytosis is characterized by the absence of solid particles meanings that the internalization involves only large volumes of fluid.

1.10.3 Clathrin-mediated endocytosis

Clathrin-mediated endocytosis is the most studied and well-characterized endocytic mechanism. The first observation of invagination, then defined as "clathrin" was more than 50 years ago by thin electron microscopy[125]. Clathrin-coated pits are small invagination of 120 nm in diameters which are originated by (i) clathrin heavy and light chains[126], from which this pathway origin its name and (ii) the subunits of the adaptor protein 2 (AP2) complex[127]. At molecular level the clathrin were bound by AP2 complex coating the membrane bilayer and become the mainly receptor-recognition molecule[128]. This process is assisted by clathrin-associated sorting proteins (CLASPs)[129,130], which interact with clathrin and AP2 molecules therefore increasing the range of receptors-molecule. Clathrin formation involves several steps such as clathrin-coated pits initiation, receptor binding, clathrin-coated pits growth and maturation, scission and clathrin-coated vesicles release, and, finally, uncoating. However, the final clathrin a three-leg shape formed by three clathrin heavy chain and three light chains. The formation of clathrin-coated pits is a process clathrin polymerization-mediated and dynamin-induced. After the pits formation, the clathrin chain undergoes to de-polymerization and the vesicles will fuse with early endosomes. Clathrin-mediated endocytosis is promoted by different ligands uptake in eukaryotic cells such as low-density lipoprotein[125], transferrin and Epithelial Growth Factor (EGF).

1.10.4 Caveolin-mediated endocytosis

In recent years, others intracellular pathways were discovered and studied such as caveolin-mediated endocytosis, flotillin mediated endocytosis, the clathrin-independent carriers/ GPI-enriched compartments endocytosis and Arf_6- dependent endocytosis[120]. These endocytic gates, in literature referred as clathrin-independent endocytosis causes the internalization of the 70% of the total fluid uptake. It was observed that these endocytic mechanisms are originate from regions cholesterol- or sphingolipids-rich in cell membranes, responsible of improve the fluidity of the membrane. Among the clathrin-

independent pathways reported above, caveolin-mediated endocytosis is the most well-characterized and studied transcytotic route. Caveolin-1 is a small integral membrane protein localized in the membrane bilayer and is able to bind the cholesterol molecules. The result of this interaction is the formation of flask or omega-shaped plasma membrane invaginations with a diameter of 60-80 nm, known as caveolae. However, these vesicles are involved not only in endocytosis; it was found that caveolae have a role in several processes such as lipid metabolism or cell surface tension sensing. The presence of caveolae is cell type dependent; they represents the 20% of the surface in found in endothelial cells, fibroblasts and adipocytes but any traces of caveolae was detected in leukocytes or neurons[131]. After caveolae formation, the invaginations are internalized in cytosol and trafficked in neutral pH- vesicles called caveosomes. Into the cytosol, caveosomes can fuse with endosomes or be internalized into Golgi apparatus or endoplasmatic reticulum. The different intracellular ways that caveosomes can take make caveolin-mediated endocytosis an interesting way suitable for drug delivery system. In matter of fact, when the payload possess high structural fragility or high sensitivity to enzymes (i.e. nucleic acids, peptides or proteins),exploiting caveolin-mediated internalization could be advantageous to by-pass the lysosomal degradation route. Hovewer, caveolin-mediated pathway possess a slower rate than that of clathrin-mediated endocytosis.

Folic acid and albumin are examples of molecule which are internalized by caveolin-mediated endocytosis.

1.10.5 Endosomes and lysosomes

Upon cell internalization, nanoparticles are in a well-known intracellular compartment called endosome. This organelle, is characterized by the maturation into the cell related to the decreasing of pH value. Indeed, the early (or “sorting”) endosomes display a pH in the ranging of 6.8-6.5. Progressively, more acidic pH were found in late endosomes (pH 6.0-5.5) until fuses with the lysosomal compartments that display the strongest pH value (pH 5.0-4.0). The pH decreasing is due to the presence of ATP-dependent proton pumps on endosome membrane surface. In these conditions, the ligand-receptor is compromise by the low pH resulting in the regeneration of the receptor on the cell membrane. On the other hand, the strong acidic milieu and the presence of acid hydrolases promote the degradation of nanocarriers[132].

1.10.6 Intracellular trafficking of delivery systems

In literature are reported many internalization route of gene delivery systems. On the basis of the intracellular pathway differences in transfection efficiency were found. On these basis, is current opinion that the intracellular trafficking (from the cell uptake to payloads release) of nanocarriers transporting nucleic acids is closely related to the gene knockdown.

The influence of surface charge, size and shape on the intracellular fate of lipo- polyplexes have also been investigated.

Surface charge of nanocarriers can impact on cell uptake due to the negatively charged features of cell membrane. For example,two formulation Poly(lactic acid)-PEG nanoparticle-based were prepared and tested on HeLa cells. The first one were used as well (ζ= - 35 mV), the second were further further coated with stearylamine in order to give a strong positive charge (ζ= + 35 mV) on nanoparticle surface. The uptake studies reveals that the positive nanoparticles show a better uptake profile mediated by chlatrin-mediated uptake instead of the negatively charged particles which are taken up by caveolin-mediated mechanism[133].

The impact of size of polyplexes was studied on mechanism of internalization and therefore on gene silencing. As example, fluorescent microspheres of 50, 100, 200, 500 and 1000 nm in diameter were incubated with non-phagocytic mouse melanoma B16-F10 cells. The study highlighted how increasing size, it was a shift from caveolae-mediated internalization to chlatrin mediated uptake.

The effect of the shape of particles on endocytosis uptake has been studied only recently. Studies seems suggested the preferential cell uptake of rod-shaped or cylindrical particles than spherical nanoparticles[134].

Also the cell-type can affect the internalization pathway of gene delivery system leading the transfection efficiency. As example, Douglas et al. treated three different cell lines (293T cells from human embryonic kidneys, COS-7 from african green monkey kidney fibroblast-like, and CHO from Chinese hamster ovary cells) with alginate-chitosan nanoparticles complexed with DNA. Results show that 293T and COS-7cells, which demonstrate a good transfection efficiency, internalize complexes primarily through clathrin-mediated processes. In contrast, CHO cells internalize polyplexes mainly by caveolin-mediated route and were not transfected[135].

1.11 Polyplexes and nanotoxicity

One of the major obstacle for the clinical approval of gene delivery systems is related to the toxicity of the synthetic cationic transfectants. Cell and molecular mechanisms behind the cytotoxicity of some lipo- polyplexes are rather complexes and involve apoptotic and necrotic pathways.

The heart of cytotoxicity is the membrane disruption properties of polycations and cationic nanoparticles which cause pore formation and membrane thinning. On the cell membrane interface, polyplexes may induce several membrane perturbation events due to the interaction between the positive charge of nanoparticles and the polyanion on cell surface. These membrane destabilization generate the gates used by polyplexes to entry in the cytosol and can explain the resulting cytotoxicity. Several studies suggest that cytotoxicity of polyplexes could be related to lysosomes membrane destabilization. After the endocytotic internalization, polyplexes are localized in endosomes and successively in lysosomes. The progressive lowering of pH value can induce the protonation of polyplexes which became able to distrupt the lysosome membrane thus release lytic enzymes and cell damage. Other investigations assume the relation between the polyplexes toxicity and mithocondria's membrane distruption or the Reactive Oxygens Species (ROS) at the cationic materials interface.

Hemolysis is one of the most significant parameter to evaluate the biocompatibility of cationic polymers. With some analogy with the living cells cytotoxicity, the red blood cell lysis-cationic polymers assisted could be due to the production of nanosized pores in the cell membranes responsible of rupture or global destabilization of red blood cell membranes resulting in release of all hemoglobin. Another supposed mechanism involve the buffering capacity of some cationic polymers which lead the lysis of red blood cells[136].

Many nucleic acid nanocarriers can promote the local inflammation by stimulation of immune system. Indeed, the interaction of polyplexes with Toll-like receptor can induce the secretion of cytokines and chemokines such as IL-6, IL-1β or TNF-α which are responsible of local inflammation. The excessive stimulation of immune system can produce an excessive release of immunogenic factors and inflict significant damages to tissues and organs (e.g., liver or kidneys toxicity)[137].

Another important aspect concerning the polyplexes toxicity is the complement activation. The complement system is a complex mechanism which involve more than thirty different proteins causing adverse reaction and immune cell stimulation. After intravenously

administration, the interaction of nanovehicles complexed with nucleic acid with plasma protein can induce the opsonization and consequent activation of complement cascade due to the cleavage of C3 complement protein. The complement activation could be also ascribed to nanocarriers/proteins aggragation or uptake in off-target cells[126].

Several studies demonstrated that toxicity of gene delivery nanocarriers depends on its molecular weight (MW), the functionalization, the polymer architecture (linear or branched). Many ways were evaluate to improve the biocompatibility of lipo- and polyplexes. The goal is create a safe non-viral vector for gene delivery whithout loss in efficacy. Poly-aminoacid such as poly(L-lysine), polyornithine, polyarginine, histones, and protamines that have excellent ability to condense DNA cell transfection and display an acceptable citotoxicity.

However, PEGylation remain the most common and successful approach to increase the compatibility with cell membrane. Kataoka and co-workers, synthesized a polymer with high complexation charactheristics. Furthermore, due to its low biocompatibility, the same polymer was further derivatized with PEG. Results showed a reduced cytotoxicity, a good cells internalization and silencing efficacy[138]. Poly-Lysine conjugates with PEG displayed to be improve the DNA passage cross the membrane and the biodistribution characteristic. Also chitosan was studied as efficient gene delivery vehicle for the high biocompatibility and significant transfection efficacy. Polymers such as dendrimers, synthetic amino derivatives of dextran and cationic acrylic polymers displayed good levels of gene transfer activity.

1.12 Atom Transfer Radical Polymerization (ATRP)

One of the most used reaction for yield polymers with precise molecular weight and functionality is the Atom Transfer Radical Polymerization (ATRP). In different condition of polymerization such as solvents, temperature and pressure, polymers can be synthesized for drug delivery, tissue engineering and imaging applications. The heart of ATRP reaction is the equilibrium between active species involved in propagations step and monomers (also called as “propagating radicals” and “dormant species”, respectively). The atom transfer process is promoted by catalyst a and the radicals were generated by a reversible redox process[139]. In this process, represented in Figure 10, radical formation is due to the removal of an halogen atom (generally a chlorine or bromine, X) from the macroinitiator (here referred as I_n-X) by the catalyst. This reaction occur when the transition metal (M) is in the lower state of oxidation (M^n). For this purpose, a ligand take part to the reaction and

complex the metal forming the transition metal complex (M^n/L). The reaction between I_n-X and M^n/L induce the formation of radicals (I_n°) with high reactivity with the monomers, which generate the polymers by "living polymerization". On the other hand, M^n/L undergoes the oxidation due to the abstraction of halogen atom (X) from the macroinitiator I_n-X forming (M^{n+1}/L)-X. This reaction is driven by constants of activation k_{act}, and deactivation k_{deact}. The polymer growth rate constant is called k_p.

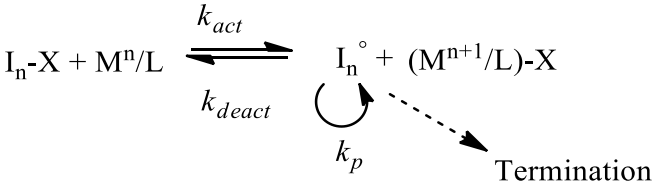

Figure 10. Schematization of ATRP process.

In order to promote the reaction a small aliquote of reducing agent (such as ascorbic acid) occoured to keep the transition metal complex in the lower state of oxidation.

The rate of ATRP reaction is related to different parameters such as , the catalyst, the ligand, the solvent and the concentrations of reagents and their chemical nature, are some of the aspects which take in consideration for a synthesis ATRP-mediated.

As known ATRP is a catalytic reaction and the nature of catalyst play a key role in the "living polymerization". Many redox-active transition metal complexes were studied including Cu, Ru, Fe, Mo and Os. However, copper is most commonly used metal catalyst in ATRP due to its safety compared to the other transition metals. In order to reduce the passage from Cu (I) to Cu (II), the reaction could be performed under nitrogen or argon flow (Figure 11).

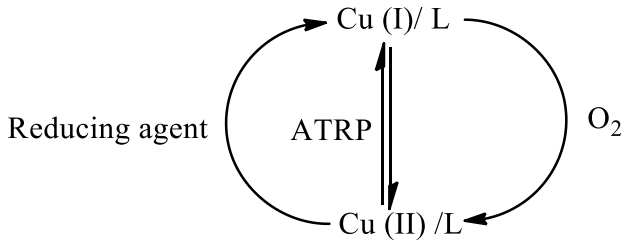

Figure 11. Schematization of oxidation/reduction cycle of copper in a general ATRP reaction.

Ligands are used to stabilize the catalyst in the lower state of oxidation. If the catalyst is Cu, in general ligands are tri- or tetra-dentate amines such as tris(2-dimethylaminoethyl)-amine (Me6TREN), tris(2-pyridylmethyl)amine (TPMA) or 2,2′-bipyridine. The choice of

ligands depends on the solvent and on macroinitiator nature. The impact of solvent on this type of polymerization is less than the ionic polymerization. However, the medium has an effect on ATRP equilibrium due to the polar character of Cu(I) complexes, less stable in high polar solvents.

The chemical structure of macroinitiator play a key role in the radical formation. Indeed, the chemical environment has an impact on the ability to remove the halogen from the structure and therefore to start the polymerization.

In these years, ATRP undergoes several development to increase the efficiency of the "living" polymerization. Activator Generated by Electron Transfer (AGET) ATRP which do not need of freeze-pump-thaw cycles or Activators Regenerated by Electron Transfer (ARGET) ATRP which used ppm level of copper are some example of the expamsion of this synthetic route.

For all its advantage, ATRP has been used to prepare many amphiphilic block polymers useful for drug delivery applications. As example, polyester-based amphiphilic block copolymers with hydrophilic poly(meth)acrylates or polysaccharides backbone were modified to form ATRP macroinitiators. Also polymers such as poly(N,N-dimethylaminoethyl methacrylate) (PDMAEMA) and PHEMA were synthesized by ATRP reaction[140].

Part A

Design and characterization of a novel efficient oligo-guanidyl nanocarrier for oligonucleotide delivery

2.1 Materials

Maltotriose, 6-aminocaproic acid, acetic anhydride, 2-bromoisobutyryl bromide, trimethylamine, ascorbic acid, agmatine sulfate, 1-ethyl-3-(3-dimethylaminopropyl) carbodiimide hydrochloride (EDC), N,N'-dicyclohexylcarbodiimide (DCC), N-hydroxysuccinimide (NHS), xylen cyanol, acryloyl chloride, copper bromide, tris(2-pyridylmethyl)amine (TPMA), deuterated solvents (D_2O, DMSO-d6, $CDCl_3$), glycerol, tris(hydroxymethyl)aminomethane chloride (Tris), boric acid, ethylenediaminetetraacetic acid and thiazole orange were purchased from Sigma Aldrich (St. Louis, MO, USA).

All products for cell biology including Dulbecco's modified Eagle medium (DMEM), L-glutamine, trypsin, antibiotic, and antimicotic solution, fetal bovine serum (FBS), phosphate saline buffer with and without Ca^{2+}/Mg^{2+}, 3-(4,5-dimethylthiazol-2-yl)-2,5-diphenyltetrazolium bromide (MTT) were obtained from Sigma-Aldrich (St. Louis, MO, U.S.A.).

Linear 5 kDa α-methoxy-ω-amino-polyethylene glycol ($mPEG_{5kDa}$-NH_2) was obtained from Iris Biotech GmbH (Marktredwitz, Germany).

Chamber slides BD Falcon for confocal microscopy were purchased from SACCO (Cadorago, Italy). Vectashield mounting medium with 4,6-diamidine-2-phenylindole (DAPI) was provided by Vector Laboratories Inc. (Burlingame, CA, U.S.A.). Cell lines from human cervical carcinoma (KB), human breast cancer (MCF-7), from murine embryonic fibroblast (MC3T3-E1) and from human cervical carcinoma (HeLa) were provided by the cell bank ATCC (Manassas, VA, USA).

Double-strand DNA (dsDNA) and cyanin-3 labeled ds-DNA (Cy3-dsDNA; 19 nucleotides per strand) were purchased from Biomers.net GmbH (Ulm, Germany). The GelRed (ds-DNA intercalating agent) was purchased from SICHIM (Rome, Italy).

SiRNA (Rac1 siRNA, Luciferase siRNA) sequences were from QBI Enterprise (Ness Ziona, Israel).

Lipofectamine 2000 was obtained from Life Technologies, (Grand Island, NY, USA)

The psiCHECK reporter assay was purchase from Promega Cat#E1960 (Madison, Wisconsin, USA).

Solvents were furnished by Carlo Erba (Milan, Italy), VWR International (Lutherworth, UK), Sigma Aldrich (St. Louis, MO, USA).

All the other reagents or salts were obtained from Fluka Analitical or Sigma-Aldrich.

2.2 Methods

2.2.1 Synthesis of maltotriosyl-N-acetyl-amino-hexanoic acid (M-COOH)

A 30 mL solution of 34.7 mg/mL (0.264 M) 6-aminohexanoic acid in methanol acidified with 1% v/v acetic acid was added of 1 g (1.98 mmol) of maltotriose and heated to 60°C until complete dissolution. The solution was maintained under stirring for 14 h at 50°C and, after reduction to half volume under vacuum, was added of 22.6 mL of acetic anhydride (237.6 mmol) over 60 min and then maintained under stirring at room temperature. After 24 h the volume was reduced to about 5 mL and dropped into 100 mL cold diethyl ether. The precipitate was recovered by centrifugation at 4000 rpm for 5 min and then desiccated under reduced pressure. The product yield was 1.1 grams (1.67 mmol, 84.2% mol/mol). The final product was analyzed by ^{1}H-NMR, ESI-TOF mass spectrometry, FT-IR and elemental analysis.

^{1}H NMR (400 MHz, D_2O) δ 5.39 (s, 1H, anomeric proton), 5.20 (s, 1H, anomeric proton), 4.12 – 3.33 (m, 18H, sugar region), 2.45 – 2.32 (m, 2H, ε-CH_2), 2.06 (s, 3H, CH_3-CO-), 1.75 – 1.44 (m, 4H δ- CH_2 and β-CH_2), 1.41 – 1.20 (m, 2H, α-CH_2).

ESI-MS [m/z]: 658.23 $(M\text{-}H^{+})^{1-}$ (calcd for 659.26)

FT-IR (KBr): ν (cm^{-1}) 3340 (-OH), 2931 (-CH), 1716 (-COOH), 1601 (acetyl CO-N);

Elemental analysis: C, 44.92%; H, 6.92%; N, 2.78%; (O, 45.38%) [calcd for maltotriosyl-N-acetyl-amino-hexanoic acid ($C_{26}H_{45}NO_{18}$), C, 47.34%; H, 6.88%; N, 2.12 %; O, 43.66%.].

2.2.2 Synthesis of star-like (2-bromoisobutyryl)$_6$-maltotriosyl-N-acetyl-amino-hexanoic acid (M-(Br_6)-COOH)

The synthesis of (2-bromoisobutyryl)-malytotryosyl-N-acetyl-amino-hexanoic acid was performed according to the modified protocol described by Stenzel-Rosembaum et al.[141]. A suspension of 1.0 g (1.52 mmols) of maltotriosyl-N-acetyl-amino-hexanoic acid in 40 mL of anhydrous chloroform was added of 4.21 mL (30.2 mmol) trimethylamine and maintained at 0°C under stirring for 15 min and then of 3.48 mL (30.2 mmol) of 2-bromo-isobutyryl-bromide over 30 min. The reaction mixture was maintained under stirring for 3 hours at 0°C and then for 72 hours at room temperature. The mixture was poured in a separating funnel containing 100 mL of water and washed three times with 300 mL of cold water, three times with 300 mL of 0.1 N NaOH and finally three times with 300 mL of cold water. The organic layer was recovered and dried with anhydrous Na_2SO_4. The

suspension was filtered and the solvent was removed under reduced pressure. The final product, 1.7 g (1.09 mmol, %mol/mol 71.7%) red-brown oil, was analyzed by ^{1}H-NMR, FT-IR and elemental analysis

^{1}H NMR (400 MHz, $CDCl_3$) δ 5.58 (s, 1H, anomeric proton), 5.25 (s, 1H, anomeric proton), 4.63 – 2.47 (m, 20H, glycosyl scaffold and ε-CH_2), 2.15 – 1.74 (m, 36H, CO-$(CH_3)_2$), 1.60 (s, 3H,-CO-CH_3 acetyl moiety), 1.45 – 1.06 (m, 4H, δ- CH_2 and β-CH_2), 1.01 – 0.67 (m, 2H, α-CH_2).

FT-IR: 3472 (-OH), 2978 (-CH), 1744 (isobutyryl -CO-O), 1650 (acetyl -CO-N).

Elemental analysis: found C, 40.02%; H, 4.89%; Br, 31.12%; N, 0.84%; (O, 23,13%). [calcd for (2-bromoisobutyryl)$_6$-maltotryosyl-N-acetyl-amino-hexanoic acid ($C_{50}H_{78}Br_6NO_{24}$), C, 38.66%; H, 4.87%; Br, 30.86%; N, 0.90%; O, 24.72%.].

2.2.3 Synthesis of acryloyl-agmatine (Acry-Agm)

Arcyloyl-agmatine was synthesized according to the modified protocol reported in the literature [142]. Briefly, 2.0 g (8.76 mmol) of agmatine sulfate were dissolved at 0°C in 15 mL of $NaHCO_3$ saturated water solution The solution was added of 0.75 mL (9.64 mmol) of acryloyl chloride in 30 min under vigorous stirring. After 1 h, the solution pH was adjusted to 1.0 with 1.0 N HCl and the mixture was saturated with sodium chloride. After filtration, the solution was washed in a separating funnel using 150 mL ethyl acetate and finally mixed three times with 50 mL of a 1:1 of isopropanol/ethyl acetate solution. The organic fractuins were collected, pooled and concentrated under reduced pressure. A pale yellow oil was recovered, dissolved in water and freeze-dried. The final product (1.0 g, 5.43 mmol, %mol/mol 62%) was analyzed by ^{1}H NMR and ESI-TOF mass spectrometry.

^{1}H NMR (400 MHz, D_2O): δ 6.27 (dd, *J* = 17.1, 9.7 Hz, 1H,CH_2=C-), 6.21 – 6.12 (m, 1H, C=CH-), 5.76 (dd, *J* = 9.7, 1.9 Hz, 1H, CH_2=C-), 3.29 (dd, *J* = 10.6, 4.2 Hz, 2H, α-CH_2), 3.03 (t, *J* = 6.9 Hz, 2H, δ-CH_2), 1.66 – 1.54 (m, 4H, β,γ-CH_2).

ESI-TOF [m/z]: 185.14 $(M+H^+)^{1+}$ [calcd for 184.13].

2.2.4 Synthesis of star-like (agmatntyl)$_6$-maltotriosyl-N-acetyl-amino-hexanoic acid (Agm$_6$-M-COOH)

CuBr (460.47 mg, 3.21 mmol), tris[(2-pyridyl)methyl]amine (TPMA, 932.05 mg, 3.21 mmol) and ascorbic acid (11.3 mg, 0.0642 mmol) were dissolved in 10 mL of anhydrous DMSO under nitrogen flow over 30 min and added to a degassed DMSO solution of acryloyl-agmatine (1181.28 mg, 6.42 mmol) and heated to 65°C. The solution was added of 500 mg of (2-bromoisobutyryl)$_6$-malytotryosyl-N-acetyl-amino-hexanoic acid (0.321

mmol) previously degassed under nitrogen flow. The mixture was stirred for 72 hours under nitrogen flow and then was exposed to the air. After 30 min the solution was poured in 200 mL of 1:1 v/v diethyl ether/acetone mixture supplied with 1% v/v of acetic acid. The precipitate was collected and desiccated under vacuum. The product yield was 542 mg (0.204 mmol), corresponding to 65%.

The guanidinium group content was determined by Sakaguchi assay[143]. The experimental data were referred to a calibration curve obtained with standard solutions of 0-100 μM guanidinium content (y= 9.1724x-0.0075, R^2=0.9965).

The final product was analyzed by ^{1}H-NMR (DMSO-d6), FT-IR and elemental analysis.

FT-IR : ν (cm^{-1}) 3373 and 3182,[$NHC(NH_2)_2^+$]; 2930 (CH_2) ; 1750 (C=O); 1300 (C-H bending).

Elemental Analysis: found, C 37.58 %, H, 5.51 %, N, 10.98 %; Br, 31.90 % (O, 14.03%). [Calcd for (agmatinyl)$_6$-maltotriosyl-N-acetyl-aminododecanoic acid HBr salt ($C_{93}H_{161}Br_6N_{25}O_{30}$·6HBr): C, 36.33%, H, 5.48%, N, 11.39%, Br, 31.19%, O, 15.61%].

2.2.5 Synthesis of star-like (agmatinyl)$_6$-maltotriosyl-N-acetyl-amino-hexanoate-α-methoxy poly(ethylene glycol)$_{5kDa}$ (Agm$_6$-M-PEG)

(Agmatinyl)$_6$-maltotriosyl-N-acetyl-amino-hexanoic acid (Agm$_6$-M-COOH, 500 mg, 0.188 mmol) was dissolved in 10 mL of 1:2 v/v DMSO/100 mM morpholino-ethan-sulphonic acid buffer (MES), pH 4.7. The solution was added of 291.9 mg (1.88 mmol) of 1-ethyl-3-(3-dimethylaminopropyl)carbodiimide (EDC) and 216.3 mg (1.88 mmol) of N-hydroxysuccinimide (NHS). The solution was stirred for 30 min and then added of 785 mg of (0.157 mmol) of mPEG$_{5kDa}$-NH_2 previously dissolved in 1:2 v/v DMSO/100 mM MES buffer, pH 4.7. The solution was stirred for 72 hours and then dialyzed against water for 48 hours using a 3.5-5.0 kDa MWCO dialysis membrane. The product was lyophilized and characterized by UV-Vis. The final product yield was 820 mg (0.102 mmol, %mol/mol 65.3%). The yield of conjugation determined by Sakaguchi assay for the guanidine content and by the iodine assay (y=0.0663x-0.0183, R^2=0.9933) for the PEG detection[144] was 96%.

2.2.6 Gel permeation chromatography

Molar mass of Agm$_6$-M-PEG polymer was analyzed by Malvern Viscotek TDA 302 system, equipped of Refractometer, Light Scattering (low-angle light scattering-LALS and right-angle light scattering-RALS) and Differential Viscosimeter, triple detector. The system was operated with TSKgel G3000 (7 μm, 7.8×300 mm) and TSKgel G4000 (10 μm, 7.8 ×300 mm) paired Tosoh columns thermostatted at 40°C and eluted with 0.1 M

$NaNO_3$ (supplemented of NaN_3 0.02% w/w), pH 7.4, at a flow rate of 0.6 mL/min. The columns were calibrated with standard pullulans.

2.2.7 Electrophoretic mobility shift assay

Agm_6-M-PEG/dsDNA samples were prepared by mixing 2.58 μL of 10 μM scrambled 11619 Da dsDNA solution (300 ng, 2.58×10^{-11} mol) in 10 mM phosphate buffer, 0.15 M NaCl (PBS), pH7.4, with 10 μL of 0.705-7.05 μg/mL Agm_6-M-PEG solutions in PBS, pH 7.4, in order to yield 0.5, 1.0, 2.0, 3.0, 4.0, 5.0 N/P ratio. The mixtures were maintained for 30 min under mild mixing at room temperature and then added of 3 μL of loading buffer (50:50 v/v glycerol/water supplied with and 0.25% xylene cyanol). The Agm_6-M-PEG/dsDNA samples were analyzed by gel-electrophoresis using 12% polyacrylamide gel in Tris-Borate-EDTA (TBE) 1X buffer at 100 V. The dsDNA was stained by immersion of the gel in a marker solution obtained by dilution of 15 μL of GelRed™ Nucleic acid Gel Stain 10000 X in 30 mL of milliQ water. The gel image was taken using a Perkin Elmer UV-Transilluminator Geliance 600 Imaging System.

2.2.8 Thiazole orange association assay

The degree of Agm_6-M-PEG/dsDNA complexation was evaluated by thiazole orange (TO) exclusion assay. Agm_6-M-PEG/dsDNA mixtures in PBS buffer, pH 7.4 were prepared by adding increasing amounts of Agm_6-M-PEG to dsDNA solution to yield a final dsDNA concentration of 100 μM and 1.0, 2.0, 3.0, 5.0, 7.0, 10.0 N/P molar ratio. To 17.5 μL of Agm_6-M-PEG /dsDNA mixtures were added of 8.25 μL of 100 μM TO solution in DMSO to yield a TO:dsDNA molar ratio of 0.5:1.0. After 15 min, the TO association with dsDNA of the dsDNA/Agm_6-M-PEG complex was determined by fluorescence analysis (λ_{ex} 508 nm, λ_{em} 530 nm).

2.2.9 Isothermal Titration Calorimetry

Isothermal titration calorimetry (ITC) analyses were carried out using a Malvern MicroCal, LLC VP-ITC microcalorimeter system (Worcestershire, UK). The ITC analyses were performed under two different titration conditions: a. 141.2 μM Agm_6-M-PEG was titrated with 40 μM dsDNA; b. 20 μM Agm_6-M-PEG was titrated with with 100 μM dsDNA. Both Agm_6-M-PEG and dsDNA solutions were prepared by using 10 mM tris(hydroxymethyl)aminomethane (TRIS) buffer, 0.15 M NaCl, pH 7.4 and the solutions were degassed and thermostatted at 25°C before the analysis. The ITC analysis was

performed at 25°C. Every 5 min, 10 µL (a.) or 6 µL (b.) of dsDNA solution were injected into the cell containing 1.5 mL Agm_6-M-PEG solutions.

ITC blank titrations were carried out by dsDNA injection into plain buffer and by buffer injection into Agm_6-M-PEG solutions.

All measurements were replicated three times and the experimental data obtained by Agm_6-M-PEG titration with dsDNA were subtracted of the blank data and processed with the VP-ITC Microcal Origin 7 software.

2.2.10 Dynamic Light Scattering (DLS) and Zeta potential analysis

Dynamic light scattering (DLS) and zeta potential (ζ-potential) analyses were performed at 25°C using a Malvern Zetasizer NanoZS (Malvern Instruments Ltd., U.K.) supported by a Zetasizer Software (version 6.12). Agm_6-M-PEG/dsDNA samples (1 mL) in PBS, pH 7.4, were prepared by mixing 0.5 mL of 0.5 mg/mL Agm_6-M-PEG with 0.5 mL of 1.0-10.0 µM dsDNA solutions to yield Agm_6-M-PEG/dsDNA mixtures corresponding to 1.0, 2.0, 3.0, 5.0, 7.0, 10.0 N/P molar ratio.

2.2.11 Transmission Electron Microscopy (TEM)

Agm_6-M-PEG/dsDNA complexes were prepared by mixing 10 µL of 5.0 mg/mL Agm_6-M-PEG with 33 µL and 18.6 µL of 10 µM dsDNA in order to obtain 3 and 5 N/P ratios and the solutions were diluted to 500 µL with PBS buffer, pH 7.4. The samples were deposited on a small copper grid (400 mesh), covered by "holey film" carbon layer and analyzed in negative staining mode analyzed by Transmission Electron Microscopy (TEM, Tecnai G2 microscope (FEI)) using 1% w/v uranyl acetate as contrast agent. The Aspect Ratio (ratio between the major axis and minor axis) of polyplexes was calculated by use ImageJ software.

2.2.12 Size stability test of Agm_6-M-PEG/dsDNA complexes

Agm_6-M-PEG/dsDNA samples were prepared by mixing 50 µL of 5.0 mg/mL Agm_6-M-PEG with 16.4 µL and 9.85 µL, respectively, of 100 µM dsDNA to obtain 3 and 5 N/P ratios in PBS, pH 7.4, or DMEM supplemented with 10% FBS (Fetal Bovine Serum), 2 mM L-glutamine, 100 IU/mL penicillin, 100 µg/mL streptomycin and 0.25 µg/mL of amphotericin B (complete DMEM) filtered using MWCO 0.22 µm filter. The samples were maintained at 37°C analyzed by DLS for 12 hours.

2.2.13 Cell lines and cultures

The human MCF-7 breast adenocarcinoma, human KB cervical carcinoma, murine MC3T3-E1 embryonic fibroblast and human HeLa cervical carcinoma cell lines were grown at 37°C, in 5% CO_2 atmosphere, using DMEM medium supplemented with 10% FBS (Fetal Bovine Serum), 2 mM L-glutamine, 100 IU/mL penicillin, 100 μg/mL streptomycin and 0.25 μg/mL of amphotericin B.

2.2.14 Cytotoxicity of Agm_6-M-PEG/dsDNA complexes

MCF-7, KB, MC3T3-E1 cells were seeded in 96 well plate (5 x 10^3 cell/well). After 24 hours the medium was removed and the cells were incubated at 37°C with increasing concentrations of Agm_6-M-PEG and increasing dsDNA concentrations (125 nM-500 nM) of Agm_6-M-PEG/dsDNA samples with 3 and 5 N/P ratio. Following 24 and 48 hours, the cell survival was assessed through 3-(4,5-dimethylthiazol-2-yl)-2,5-diphenyltetrazolinium bromide (MTT) assay. 20 μL of 5 mg/mL MTT solution in PBS buffer were added in each well and the plates were incubated at 37°C. After 3 hours the medium was removed and replaced with 200 μL of dimethyl sulfoxide (DMSO) and incubated at room temperature in gentle rocking for 15 min.

2.2.15 Flow cytometry analysis

Cell uptake study was performed using MCF-7, KB and MC3T3-E1 cells using flow cytometry analysis. In order to evaluate dsDNA uptake into the cells, the complexes were prepared with labeled Cyanine 3-dsDNA (Cy3-dsDNA). Cells were seeded in six well plate at a density of 1.5 x 10^6 cells/well. After 24 hours the DMEM medium was removed and the cells were washed twice with PBS, pH 7.4, and then treated with 500 μL of Agm_6-M-PEG/Cy3-dsDNA complex solutions at fixed concentrations of 125 nM labelled ONs. After 6 hours of incubation time at 37°C, the wells were washed three times with PBS, pH 7.4, and transferred into cytometer tubes. After centrifugation at 1500 rpm for 5 min, the supernatants were discharged and the pellets were re-dispersed in 300 μL of PBS, pH 7.4, and analyzed by using the mean fluorescence intensity. Data collection was carried out with 10000 counts per sample.

2.2.16 Confocal microscopy observation

MCF-7, KB and MC3T3-E1 cells were seeded at density of 5 x 10^4 cells/cm^2 and grown for 24 h at 37°C and 5% CO_2. The medium was removed and the cells were washed with

PBS, pH 7.4. 500 µL of Agm_6-M-PEG/Cy3-dsDNA complexes in cell culture medium at concentration of 125 nM of Cy3-dsDNA were prepared by simple mixing of Agm_6-M-PEG with Cy3-dsDNA as described in previous section and added in each wells. Cells were treated at 37°C in the dark for 6 hours and then gently washed three times with 500 µL PBS, pH 7.4. Cells were fixed with 500 µL of 1% w/v paraformaldehyde solution in PBS, pH 7.4 for 15 min at room temperature. The wells were washed three times and incubated with 500 µL of 5.0 µg/mL of DAPI solution for nuclei staining for 15 min at room temperature. In order to stain the membranes, the fixed cells were treated with 4.5 µg/mL solution of wheat germ agglutinin 488 AlexaFluor. The wells were washed three times with PBS solution and the three times with milliQ water.

The samples images were acquired using a Zeiss LSM 800 confocal microscopy equipped of an immersion lens with 63 X magnification. The lasers were fixed at 405 nm, 488 nm and 561 nm to detect DAPI, 488 AlexaFluor and Agm_6-M-PEG/Cy3-dsDNA complexes.

2.2.17 *In vitro* silencing studies

In vitro siRac1 gene knockdown by complexes of Agm_6-M-PEG/siRac1 was evaluated using psiCHECK reporter assay following the psiCHECK™-2-based construct preparation for the Rac1 activity as reported in Polyak et al.[145]. One copy of a consensus target sequence of Rac1 was cloned into the multiple cloning site located downstream of the *Renilla* luciferase translational stop codon in the 3′-UTR region. HeLa cells (1×10^6) were incubated at 37 °C and 5% CO_2. Following 24 hours, the cells were transfected overnight with 4 µg Rac1-psiCHECK™ 2-based plasmids using 4 µL Lipofectamine® 2000. The transfected cells were reseeded in 96-wells plate in 150 µL and final concentration of 2.5×10^3 cells/well. After 6 hours, the cells were transfected with the Agm_6-M-PEG/siRac1 complexes prepared with increasing concentration of siRac1 (125 nM-500 nM). In order to evaluate the specificity of the silencing, cells were treated with complexes with Agm_6-M-PEG and scramble siRNA (siLuc). 50 nM siRac1 or siLuc siRNA were complexed with Lipofectamine® 2000 as positive control or left untreated. Following the treatment, cells were washed three times with PBS buffer, pH 7.4 and lysed using 50 µL of 1X passive lysis buffer. The Rac1 gene silencing was evaluated using Dual-Luciferase® Assay kit according to manufacturer procedure and misured by luminescence micro plate reader (Mithras LB 940 Multimode Microplate Reader, Berthold Technologies, Germany). The silencing activity results were normalized by the value obtained with the untreated cells transfected with the psiCHECK™-2 plasmid only.

2.2.18 Statistical analysis

All the results are expressed as mean ± SD. The statistical analysis was performed by using two-way ANOVA. P value < 0.05 were considered to be significant.

2.3 Results

2.3.1 Synthesis and characterization of Agm_6-M-PEG polymer as a novel oligonucleotides carrier

Agm_6-M-PEG was synthesized according to a multi-step process described in Scheme 1.

In the first step, the maltotriose unit (M) was derivatized with an amino terminating aliphatic acid (NH_2-R-COOH) to produce the intermediate M-COOH that could be further functionalized with polymers, targeting agents or other physicochemical or biological modifiers.

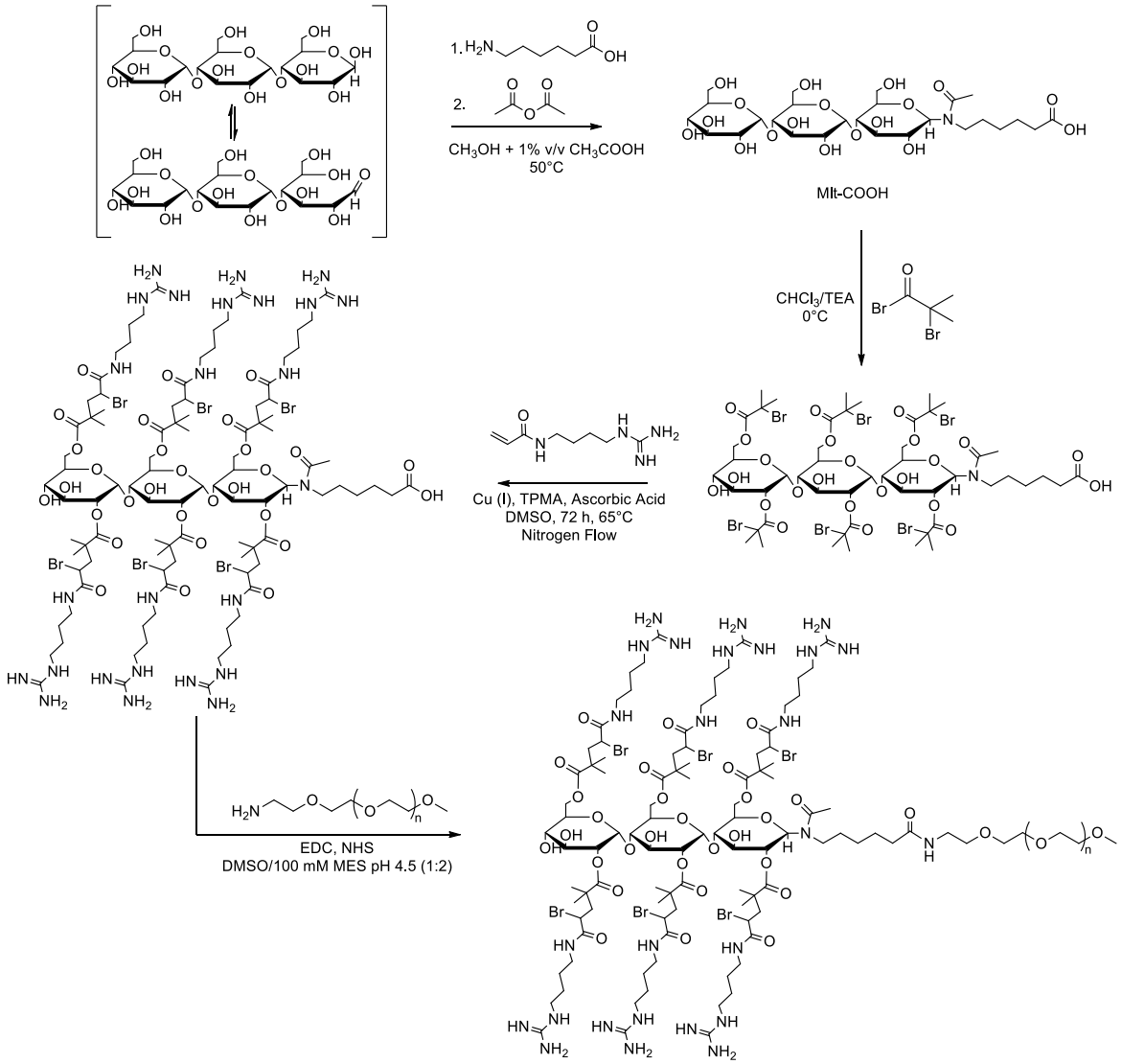

Scheme 1. Synthesis of star-like $(agmatinyl)_6$-maltotriosyl-N-acetyl-amino-hexanoate-PEG_{5kDa}-OMe [Agm_6-M-PEG].

Accordingly, the anomeric oxygen of maltotriose was derivatized with a short aliphatic spacer, namely ε-aminocaproic, and the resulting Shiff base was stabilized by nitrogen acetylation. The ^{1}H-NMR, FT-IR and ESI analyses (Figure 12) analysis confirmed the

chemical identity of the final product (M-COOH), which was obtained with a 84.3% molar yield.

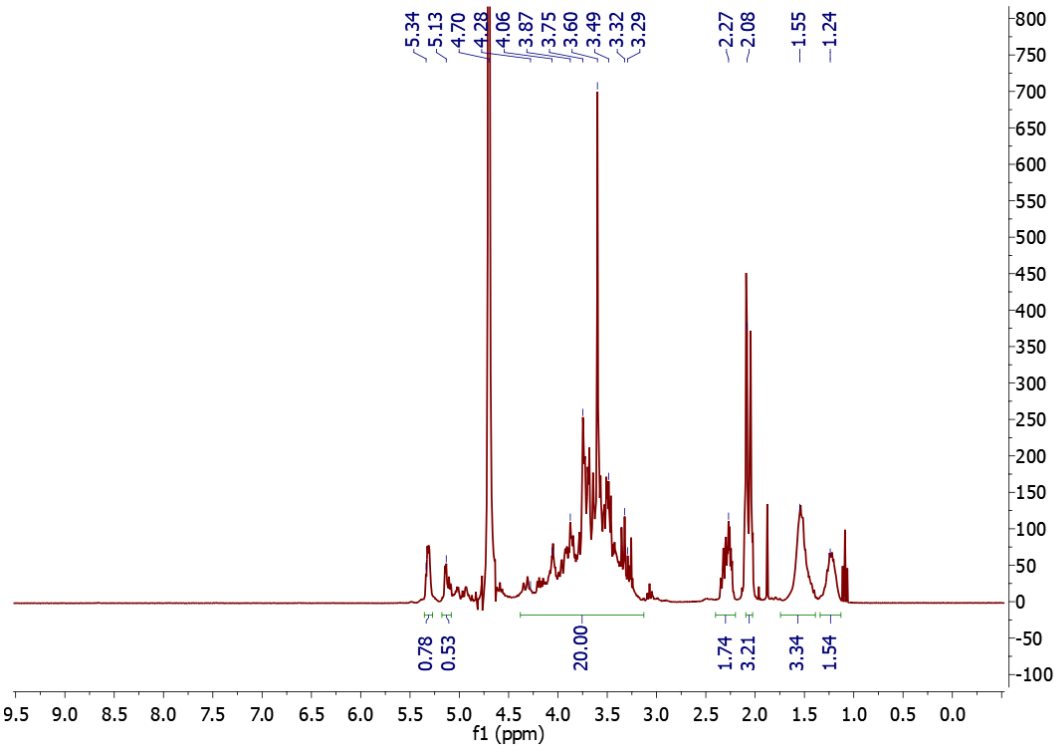

Figure 12. ^{1}H-NMR of M-COOH, performed in D_2O.

In the second step, the hydroxyl groups of maltotriose were derivatized with agmatines by Atom Transfer Radical Polymerization (ATRP) to obtain the oligoguanidyl "polycationic head". The oligosaccharide derivatization included the hydroxyl group functionalization with α-bromoisobutyryl bromide to produce a star-like macroinitiator. The elemental analysis of the resulting product showed that the reaction yielded a mean of 6 α-bromoisobutyryl unit out of 10 -OH groups with 71.7 % yield [M-(Br_6)-COOH /M-COOH], which produced the intermediate M-(Br_6)-COOH (1553 Da mean mol wt).

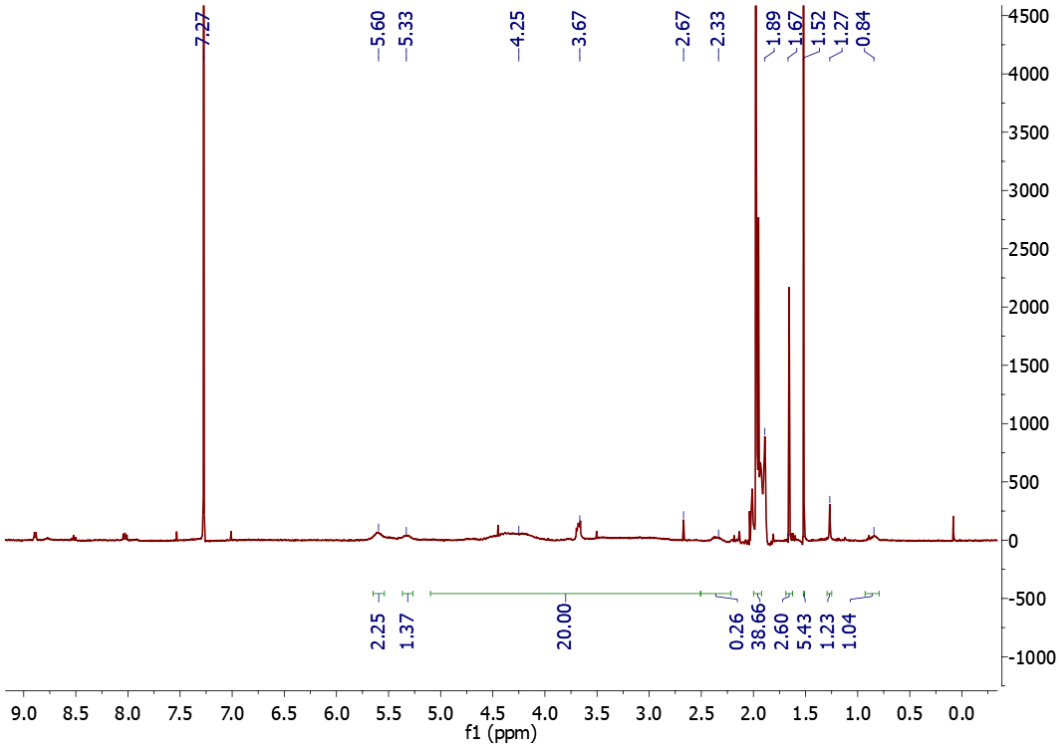

Figure 13. ^{1}H-NMR spectrum of M-(Br_6)-COOH. The analysis was performed in $CDCl_3$ solvent.

The M-COOH reaction with α-bromoisobutyryl bromide resulted in the reduction of the intensity of the characteristic ^{1}H-NMR (Figure 13) signals of the sugar (δ 4.12-3.33 ppm) and the ester formation was confirmed by FT-IR (Figure 14), which showed the disappearance of the typical signal of –OH at 3500 cm^{-1}.

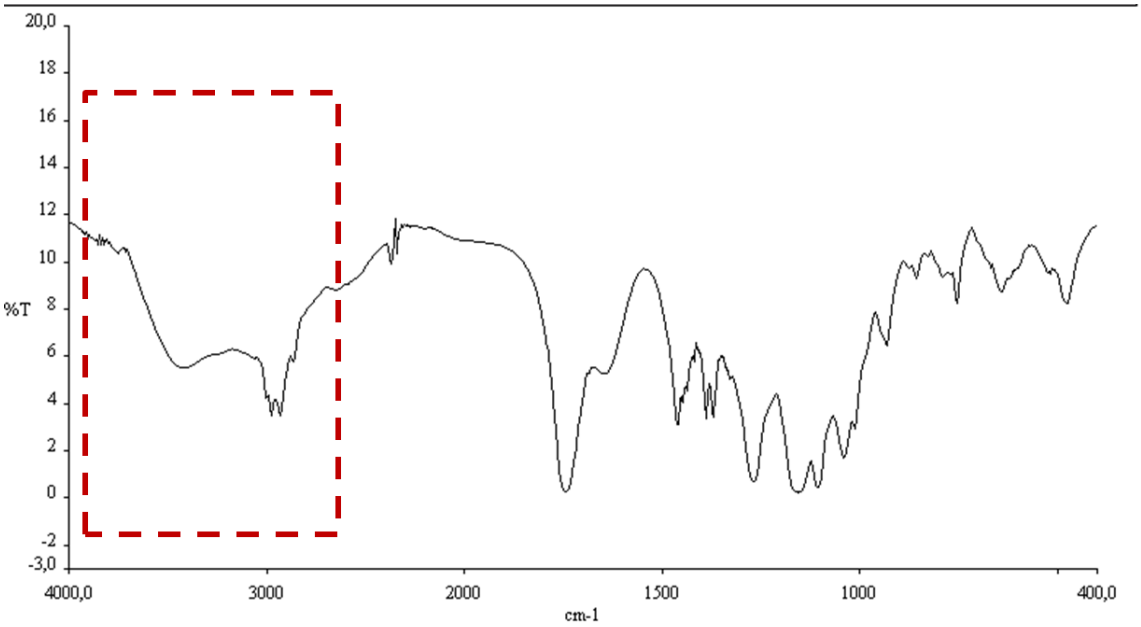

Figure 14. FT-IR spectrum of M-(Br_6)-COOH. In the red square is reported the –OH signal reduction.

The agmatine conjugation to M-(Br_6)-COOH was obtained by using acryloyl agmatine, which was previously synthesized by agmatine reaction with acryloyl chloride (Figure 15).

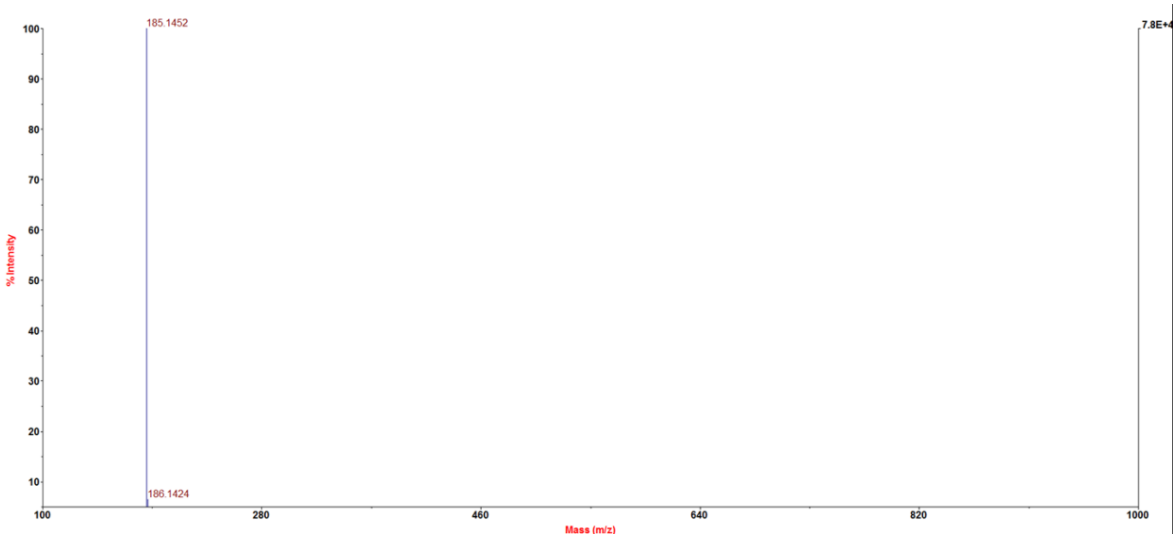

Figure 15. ESI-TOF spectrum of acryloyl agmatine.

The ATRP reaction was carried out in the presence of Cu(I) as catalyst and tris[2-pyridyl)methyl]amine (TPMA) as complexing agent in the presence of ascorbic acid under nitrogen to avoid the Cu(I) oxidation. The FT-IR spectrum (Figure 16) of the final product (Agm_6-M-COOH) showed the presence of a strong signal at 3373 cm^{-1} corresponding to the guanidinium group. The colorimetric Sakaguchi assay for guanidinium determination and the elemental analysis demonstrated the presence of a mean of six guanidyl moieties/maltotriosydic unit (Agm_6-M-COOH).

Agm_6-M-COOH was finally conjugated to linear 5 kDa α-methoxy-ω-amino-polyethylene glycol ($mPEG_{5kDa}$-NH_2) by EDC/NHS coupling. The colorimetric analyisis of the final product showed the complete conjugation of the PEG to the polycationic head and the GPC analysis show that the product had the expected molecular weight (about Mn = 8000 Da, PDI= 1.182).

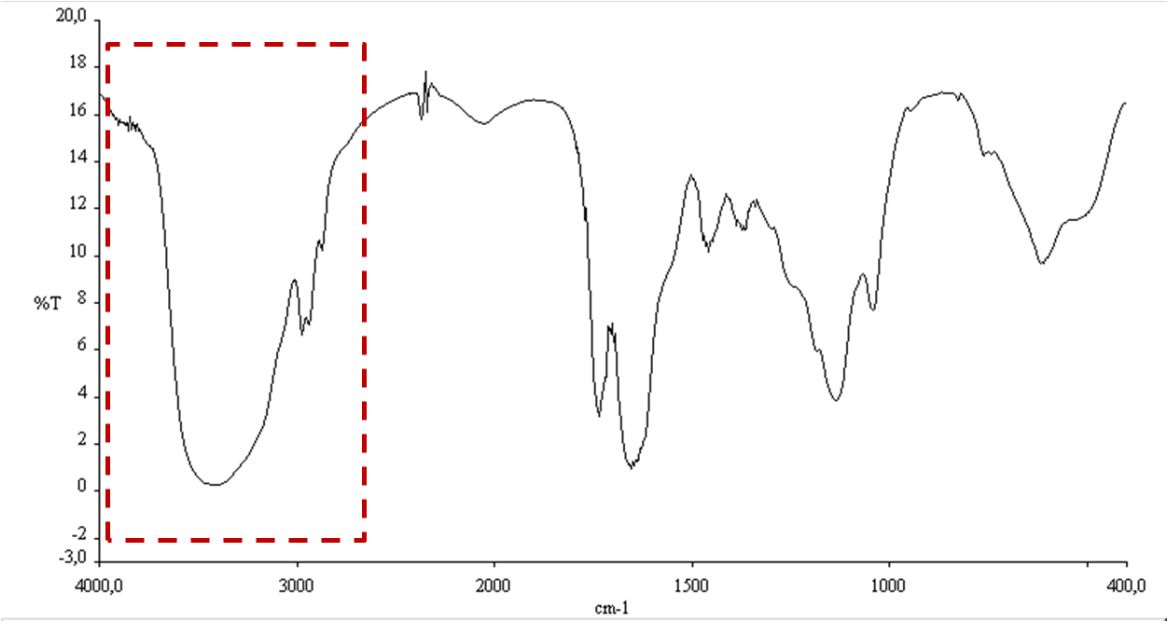

Figure 16. FT-IR spectrum of Agm_6-M-COOH. In the red square is reported the guanidinium signal.

2.3.2 Agm_6-M-PEG and oligonucleotides complexation

The ability of Agm_6-M-PEG to complex oligonucleotides (ONs) was assessed by gel electrophoresis, thiazole orange association and Isothermal Titration Calorimetry (ITC) analysis using 19 pb dsDNA (11 kDa) as model ON.

The gel electrophoresis analysis was carried out under physiological conditions, pH 7.4, by using samples with increasing Agm_6-M-PEG/ON ratio determined as N/P ratio, guanidyl groups (N) of Agm_6-M-PEG and phosphate groups of ON, (0.5-5.0 N/P), which were prepared by mixing a fixed amount of dsDNA with increasing amounts of Agm_6-M-PEG.

The free dsDNA in the gel was stained using Gel Red Nucleic Acid Gel Stain and visualized using UV-transilluminator as described in our previous work [146]. Figure 17 shows that no free dsDNA was detected at ≥ 3 N/P ratio indicating the complete ON complexation.

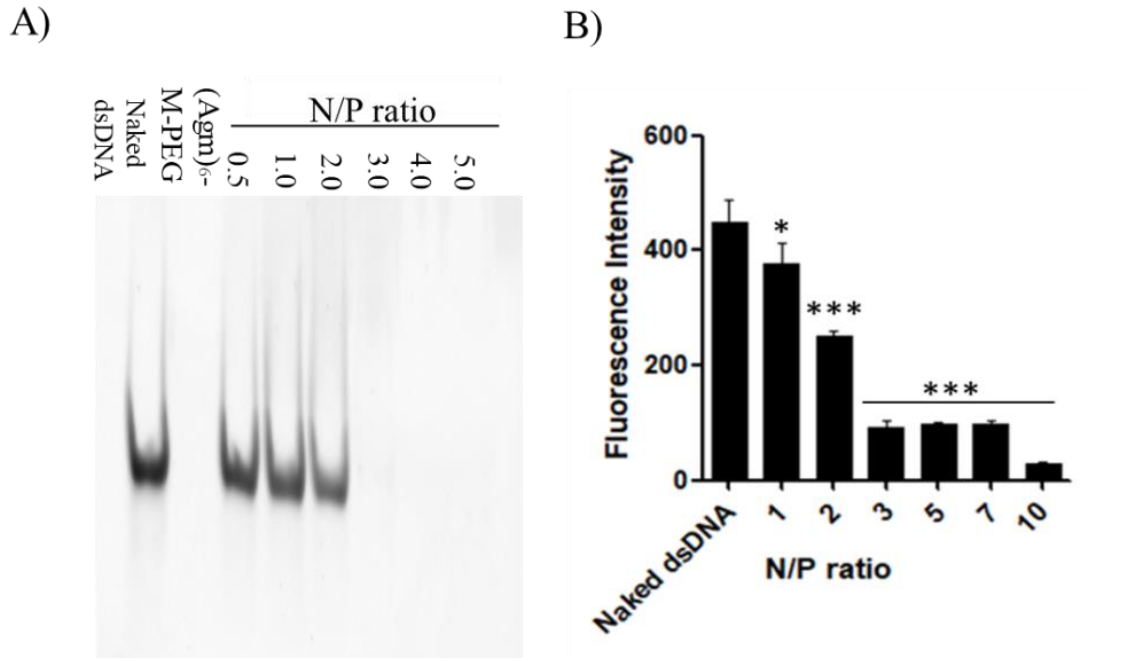

Figure 17. A) Gel mobility assay profiles of Agm_6-M-PEG/dsDNA complexes with N/P ratio in the range of 0.5-5 at pH 7.4. The samples were run in polyacrylamide gel using TBE as running buffer. B) Fluorescence intensities of thiazole orange association with naked dsDNA and polyplexes at increasing N/P ratio value in PBS, pH 7.4. Data are mean of fluorescence intensity ± SD, *p< 0.05; **p< 0.01; ***p<0.001 vs naked dsDNA (n=3).

The degree of complexation of dsDNA by Agm_6-M-PEG polymer was evaluated by thiazole orange (TO) association assay. The free dsDNA in solution was intercalated by TO and a characteristic fluorescence intensity was recovered at 530 nm. The fluorescence intensities were decrease following increasing amount of Agm_6-M-PEG due to the sequestration of free dsDNA into the polyplexes and TO displacement. The fluorescence analysis show an significantly fluorescence intensity reduction starting from 3 N/P ratio (Figure 17B) meaning that Agm_6-M-PEG is complexed with ONs and dsDNA is shield from TO association.

The ITC profiles obtained by Agm_6-M-PEG titration with dsDNA at high N/P ratio range (400-3 N/P ratio) (Figure 18A). Under these experimental conditions a typical exothermic ($\Delta H<0$) behavior was obtained. The experimental data were found to fit one binding site model. The calculated association constant (Ka) was $9.7\pm5.45\cdot10^7$ and the complete complexation was achieved at 6.5 N/P ratio. The association between the polymer and the ON underwent under enthalpic control (ΔH -2.49 ± 0.0677 10^4 cal/mol) while a decreased entropy was registered (ΔS -46.9 cal/mol/deg) [147,148].

The ITC profile obtained in the low N/P ratio range (3-0.05 N/P ratio) reported in Figure 18B shows that the Agm_6-M-PEG complexation with dsDNA is controlled by an entropic process (ΔS47.4 cal/mol/deg) while the enthalpic content increased (ΔH 4811± 80.63 cal/mol) [149,150]. The experimental data were found to fit one binding site model, which yielded an association constant of $6.98\pm1.20\cdot10^6\ M^{-1}$.

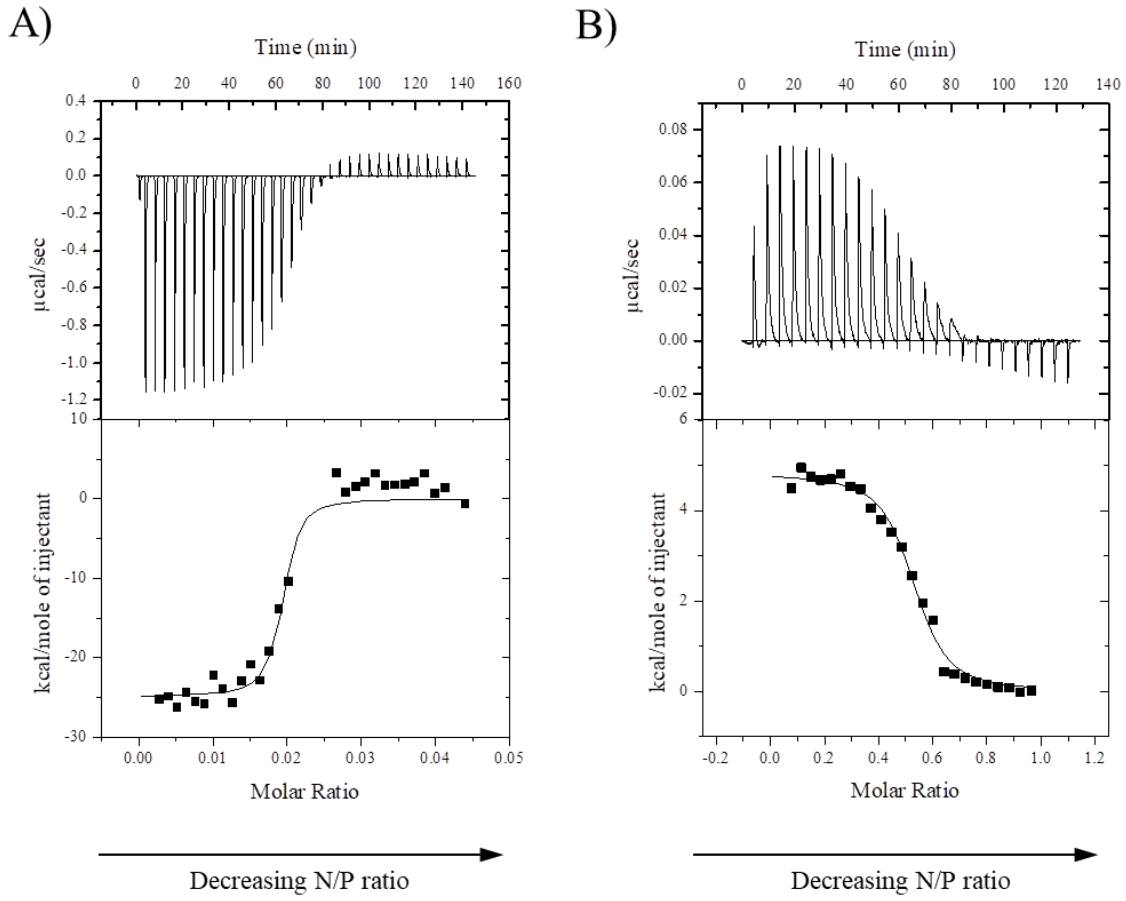

Figure 18. Isothermal Titration Calorimetry profile of dsDNA in Agm_6-M-PEG solution. A. Agm_6-M-PEG titration with dsDNA at high N/P ratio. B. Agm_6-M-PEG titration with dsDNA at low N/P ratio. The upper panel reports the raw ITC data and the lower panel reports the plot of the heat flow per mole of Agm_6-M-PEG with dsDNA.

2.3.3 Agm_6-M-PEG/dsDNA complexes: charge, size and shape

The surface charge (ζ-potential) and size of Agm_6-M-PEG/dsDNA complexes was evaluated by Dynamic Light Scattering (DLS) at 25°C in 10 mM phosphate, 0.15 M NaCl, pH 7.4, at increasing N/P ratio (from 1 to 10).

The ζ-potential profile reported in Figure 19A shows that at 1 and 2 N/P ratio the surface is negative, which switches to positive when the N/P ratio increases from 2 to 3. The surface positive charges continues to increase as the N/P ratio increases. Figure 19B shows that the

size of the Agm_6-M-PEG/dsDNA complexes increases from 50 70 75 nm as the N/P ratio increases from 1 to 3. At N/P values ≥ 2 no significant differences have been observed. The polydispersity index (PDI, Figure 19C) was found to decrease from of 0.275 ± 0.009 ti 0.246 ± 0.014 as the N/P ratio increased from 1 to 2 and remained stable at higher N/P rario values.

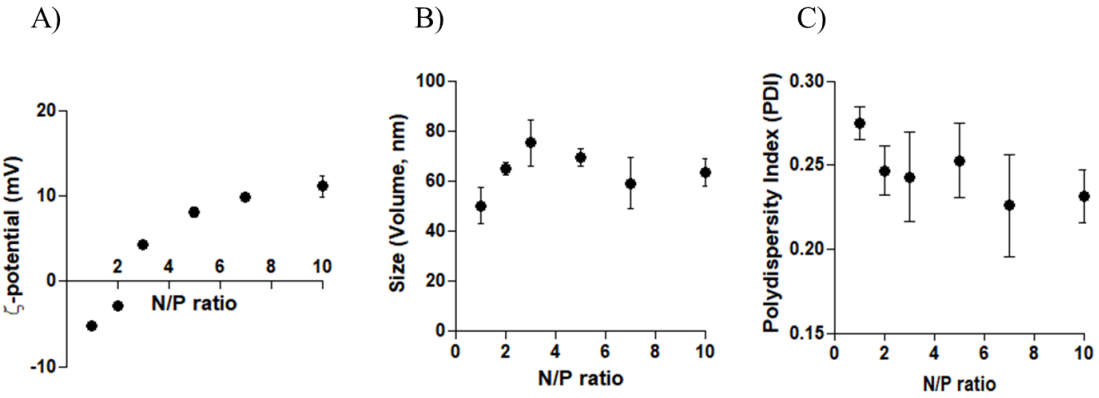

Figure 19. Zeta potential, size and PDI of Agm_6-M-PEG/dsDNA complexes are reported in panel A, B and C, respectively. Data are reported as mean values ± SD, with n= 3 experiments.

Figure 20A and 20B report the Transmission Electron Microscopy (TEM) images of Agm_6-M-PEG/dsDNA complexes at 3 and 5 N/P ratio, which show that the complexes have a rod-shape structure. The aspect ratio calculated for 3 and 5 N/P ratio was 3.26 ± 0.61 and 5.98± 1.57, respectively.

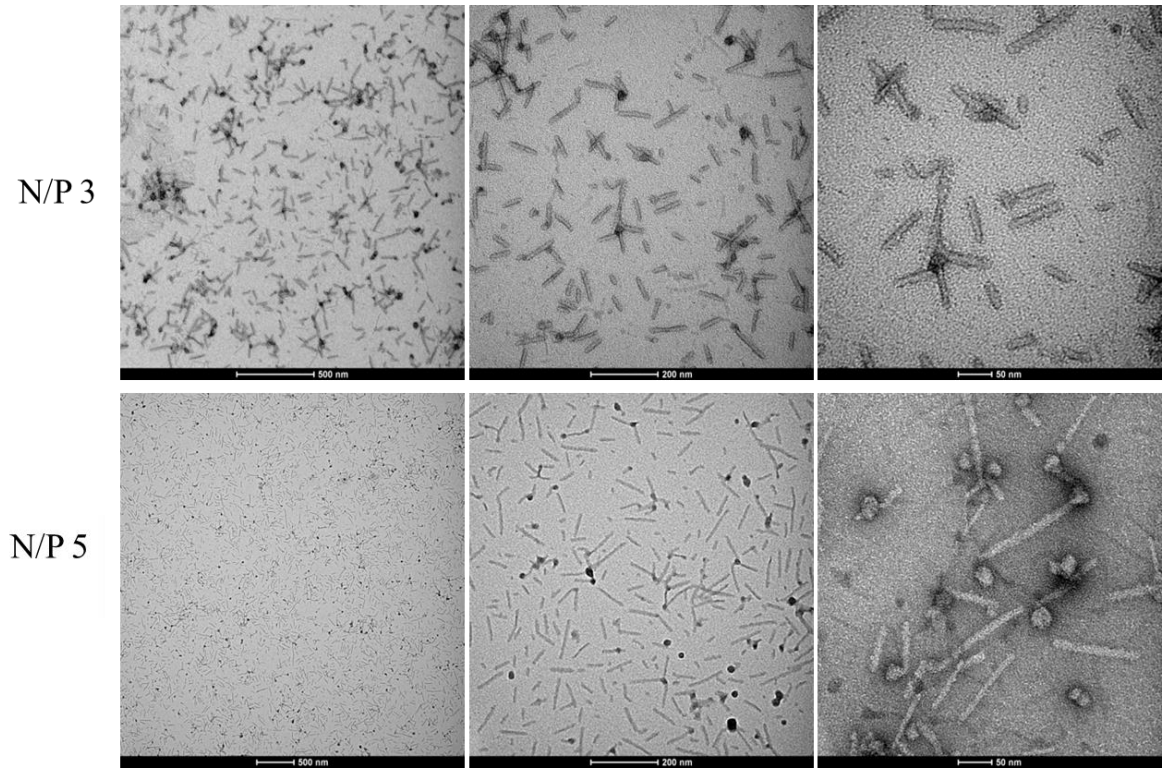

Figure 20. TEM images of Agm_6-M-PEG/dsDNA complexes with 3 N/P ratio (A) and 5 N/P ratio (B).

2.3.4 Size stability studies

Stability studies were performed by 12 hours incubation of 3 and 5 N/P ratio Agm_6-M-PEG/dsDNA complexes at 37°C in PBS, pH 7.4, and in complete DMEM supplemented with 10% FBS (Figure 21). In plain buffer the 3 and 5 N/P ratio complexes did not show significant size changes over 12 h incubation. In complete DMEM/FBS both formulations, (3 and 5 N/P ratio) underwent size increase during the first 1.5-2 hour incubation and then remained stable over the 12 hour incubation.

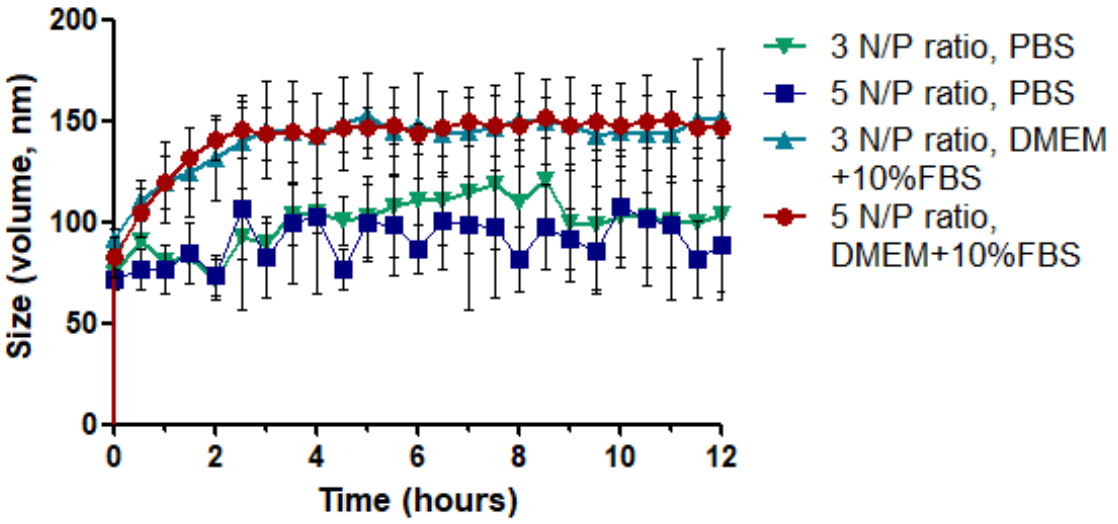

Figure 21. Size of Agm_6-M-PEG/dsDNA polyplexes with 3 and 5 N/P ratio in PBS and DMEM medium supplemented with 10% FBS (Fetal Bovine Serum) at 37°C. Data are reported as mean values ± SD, with n= 3 experiments.

2.3.5 Agm_6-M-PEG/dsDNA cytotoxicity and cell uptake

Cytotoxicity studies were carried out by MCF-7, KB and MC3T3-E1 cell line incubation with increasing concentrations of 3 and 5 N/P ratio Agm_6-M-PEG/dsDNA complexes.

The two formulations displayed negligible toxicity against the three cell lines with no significant differences after 24 and 48 hour incubation at all the tested complex concentrations (Figure 22).

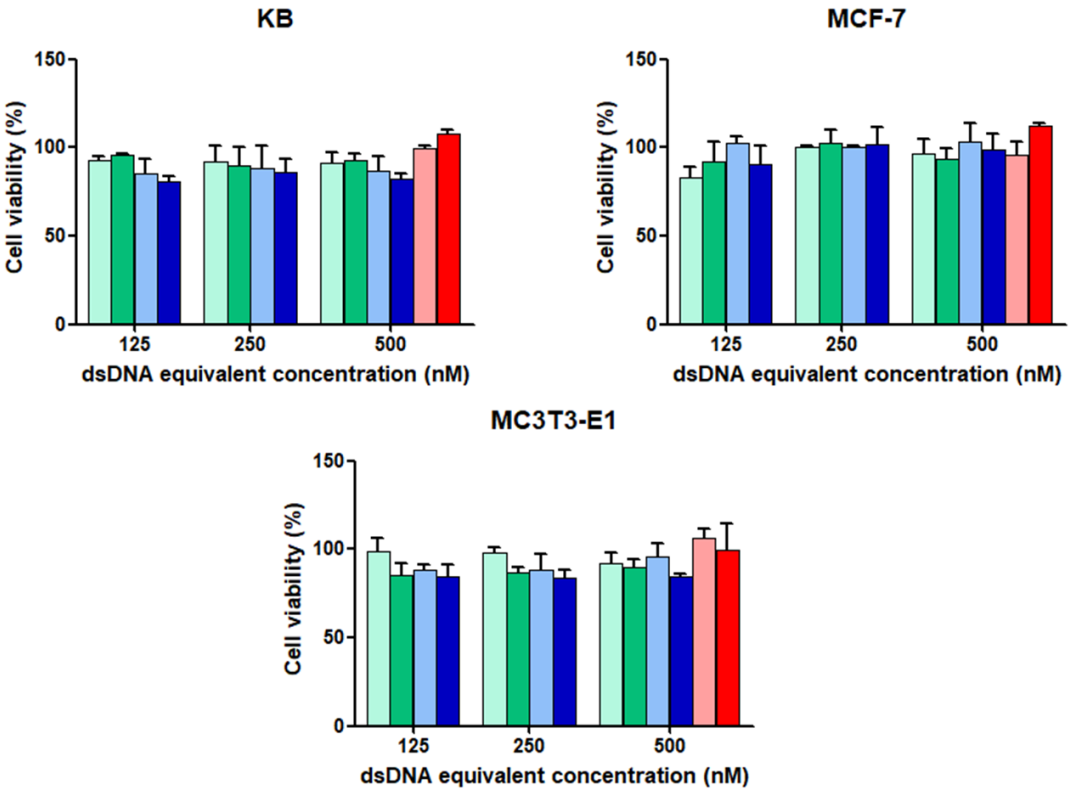

Figure 22. Viability of KB (A), MCF-7 (B) and MC3T3-E1 (C) cells incubated with Agm_6-M-PEG/dsDNA complexes with 3 N/P ratio at 24 hours ( ) and 48 hours ( ), Agm_6-M-PEG/dsDNA complexes with 5 N/P ratio at 24 hours ( ) and 48 hours ( ). dsDNA at 500nM was used as control in 24 hour ( ) and 48 hours ( ) experiments . Data are reported as mean values ± SD, with n= 6 experiments

The Agm_6-M-PEG/dsDNA cell up-take was investigated by flow cytometric and confocal microscopic analyses of KB, MCF-7 and MC3T3-E1 cells incubates for 6 hours at 37°C with Agm_6-M-PEG/Cy3-dsDNA 3 and 5 N/P ratio complexes prepared using Cy3 labelled dsDNA (Cy3-dsDNA).

The flow cytometric profiles reported in Figure 23 show that both 3 and 5 N/P ratio complexes are efficiently taken up by all the cell lines even though cell up-take differences were observed either with the three cell lines or between the 3 and 5 N/P ratio complexes. KB and MCF7 cells internalized the Agm_6-M-PEG/dsDNA complexes much more efficiently than the MC3T3-E1 cells.

Indeed, the case of KB and MCF-7 cells, the 3 and 5 N/P ratio complexes underwent massive cell internalization even though the 3 N/P ratio complex was taken-up by the cells more efficiently than the 5 N/P ratio formulation. Only slight cell up-take was instead observed with MC3T3-E1 cells either for 3 or 5 N/P ratio complexes.

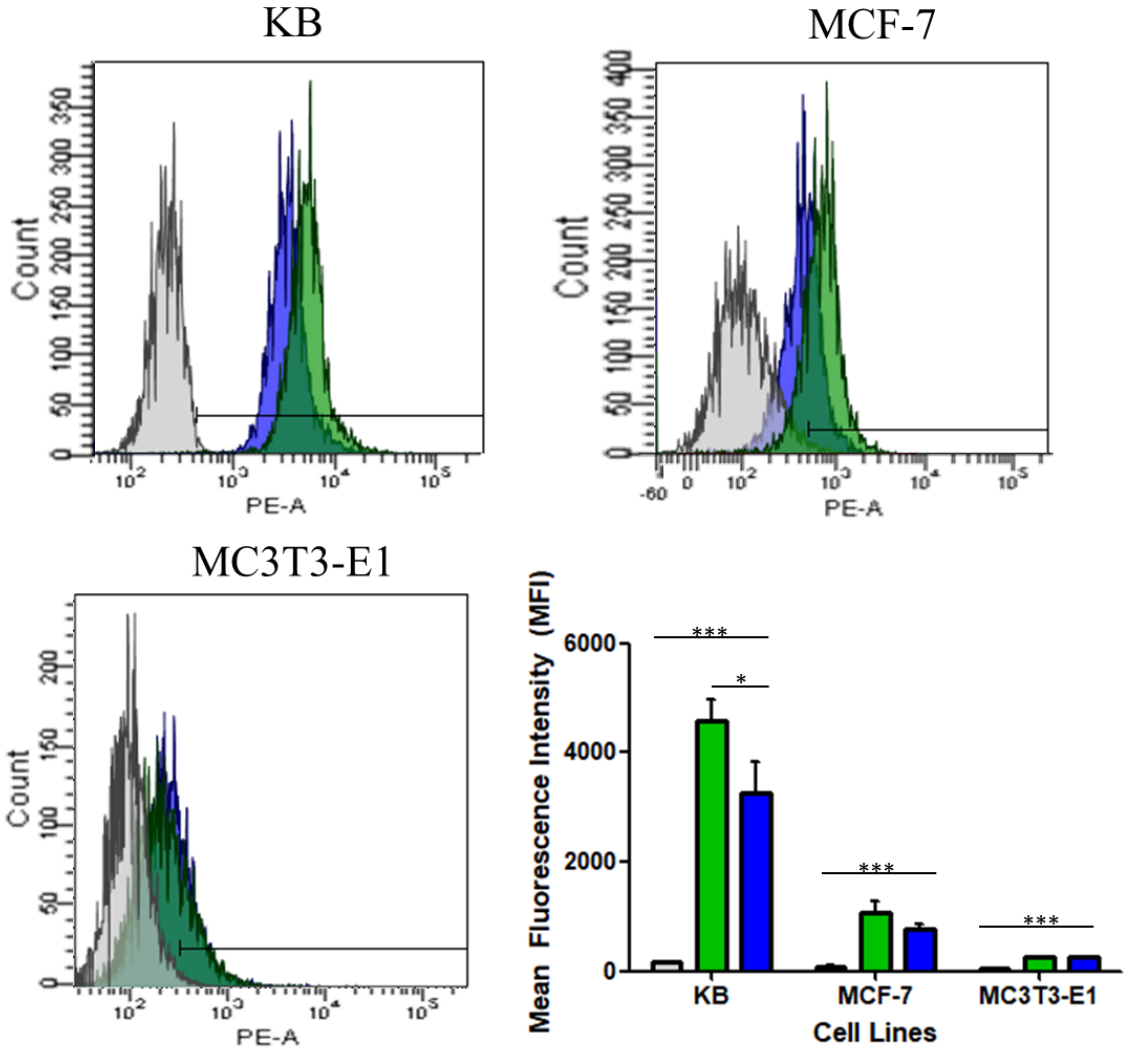

Figure 23. Cell cytometric profiles of KB, MCF-7 and MC3T3-E1 cells after 6 hour cell treatment with Agm_6-M-PEG/Cy3-dsDNA complexes with 3 and 5 N/P ratio. Untreated cells are used as control. Data are mean of fluorescence intensity ± SD, *p< 0.05; **p< 0.01; ***p<0.001 vs untreated cells, (n=3).

The confocal microscopy images reported in Figure 24 show the complexes (red), the cell membrane (green) and the nucleus (blue). The control cell images reported in Figure 24 A1, B1 and C1 show the membrane and nucleus only. The images of the cells treated with the complexes at 3 N/P ratio (Figure 24 A2, B2 and C2) and at 5 N/P ratio (Figure 24 A3, B3, C3) show a high localization of Cy3-dsDNA (red spots) in the cytosol of KB, MCF-7 and MC3T3-E1 treated with 3 and 5 N/P ratio Cy3-dsDNA/Agm_6-M-PEG complexes.

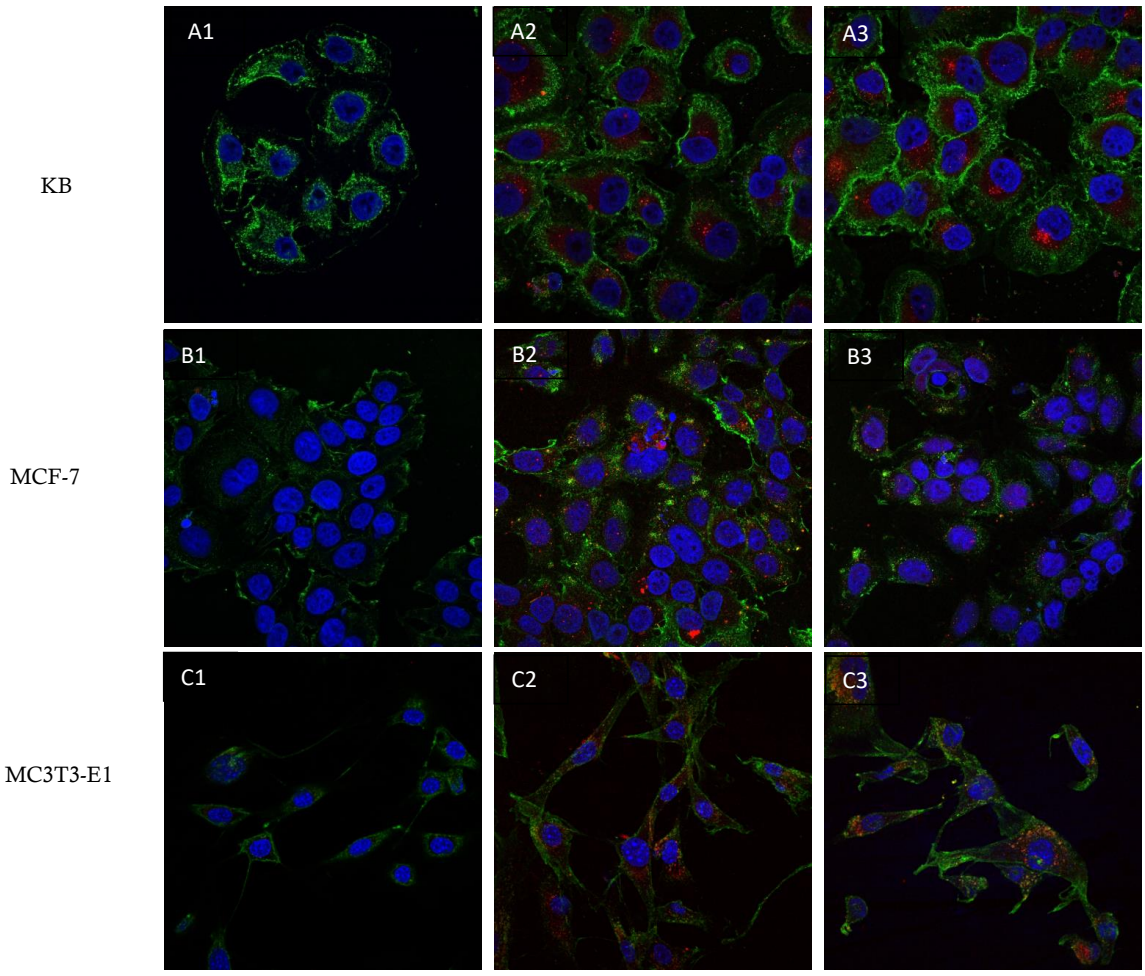

Figure 24. Confocal microscopy images of KB, MCF-7 and MC3T3-E1 cells treated with Agm_6-M-PEG/Cy3-dsDNA complexes with 3 and 5 N/P ratio. Untreated cells are used as control.

2.3.6 siRac1 *in vitro* gene silencing on HeLa cells

The ability of siRac1/Agm_6-M-PEG complexes to silence Rac1 was assessed by dual luciferase psiCHECK^{TM} reporter assay. 24 hours before the test, HeLa cells were transfected with Rac1-psiCHECK 2-based plasmids using Lipofectamine® 2000. In this plasmids there are two sequences 1) *Renilla* report gene which is fused with a targeted siRac1 gene sequence and 2) *FireFly* luciferase internal control. The transfection was espressed by decrease of *Renilla* luciferase activity but not in the activity of the *FireFly* internal control. After 24 hours, HeLa were reseeded and treated with Agm_6-M-PEG/siRac1 complexes (125-500 nM siRNA equivalent dose) for 72 hours with 3 and 5 N/P ratio and the *in vitro* silencing was evaluated by Dual-Luciferase® Assay kit. Complexes with 3 N/P ratio show 51 % of Rac1 silencing 500 nM without significative off-target gene knockdown. On the other hand, complexes with 5 N/P ratio show a similar

Rac1 silencing values but the off-target incidence is higher than 3 N/P ratio complexes at all the concentrations tested. These results suggest that for 5 N/P ratio complexes the silencing is mostly not related to the siRNA. Lipofectamine® 2000 was used as positive control and show 92% of Rac1 gene knockdown and high off-target silencing. This study was conduct in parallel with MTT assay on HeLa to exclude silencing-survival relation.

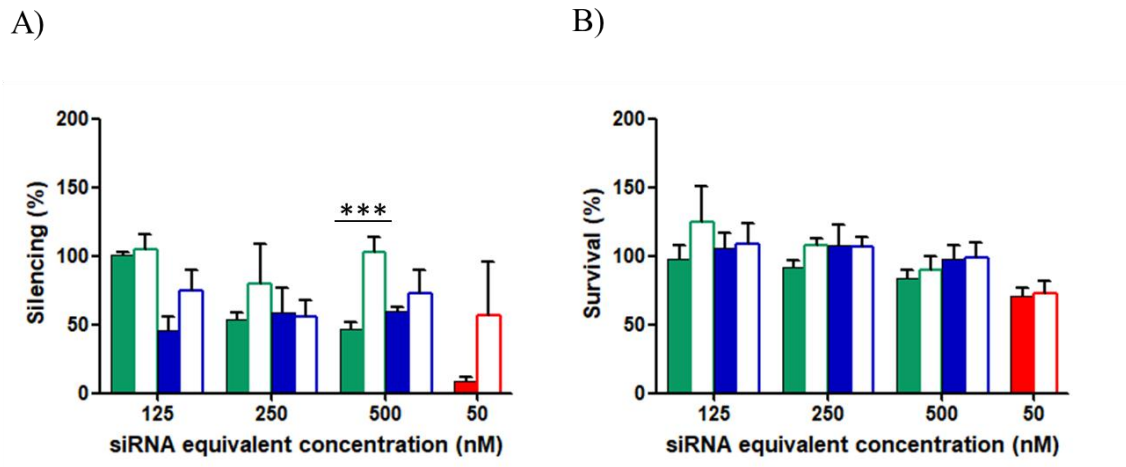

Figure 25. A) Rac1 gene knockdown and B) survival of HeLa cells after 72 hours of incubation with Agm_6-M-PEG/siRNA polyplexes. HeLa cells were treated with Agm_6-M-PEG/siRac1 polyplexes with 3 N/P ratio ( ) and 5 N/P ratio ( ) at three different concentration (125 nM – 500 nM). Agm_6-M-PEG/siLuc polyplexes at 3 N/P ratio ( ) and 5 N/P ratio ( ) were used to evaluate the non-specific silencing. siRac1 ( ) and siLuc ( ) at 50 nM either complexed with Lipofectamine 2000, were used as control. Data are reported as mean values ± SD, with n= 3 experiments. Statistical analysis *p< 0.05; **p< 0.01; ***p<0.001 vs siLuc complexed polyplexes.

2.3.7 Discussion

The new supramolecular bioconjugate (Agm_6-M-PEG) was designed in order to obtain a star-like cationic macromolecule that on one side forms polyplexes with oligonucleotides and on the other bears a chemical moiety available for functionalization with targeting agents.

Maltotriose was selected as platform for the construction of the novel supramolecular carrier by virtue of its multivalent structure and the peculiar reactivity of the anomeric carbon. The hydroxyls of maltotriose can in fact be functionalized with guanidyl moieties to generate a star-like oligocationic head while the anomeric carbon can be functionalized with a linker for conjugation of targeting agents or physicochemical or biological modifiers.

In a preliminary study, several attempts have been done to conjugate amino terminating PEG to the anomeric carbon of maltotriose, but the reaction yield was extremely poor even under stressed reaction conditions. Therefore, the anomeric carbon of maltotriose was functionalized with ε-aminocaproic acid, which could be further functionalized with polymers, lipids or other colloidal structures The resulting Shiff's base was stabilized by acetylation of the amino group. ESI, ^{1}H-NMR and elemental analysis showed that the chemical protocol yielded the expected derivative with high yield and purity degree.

The introduction of guanidyl groups into the maltotriose structure was achieved by a multistep process that involved the conjugation of 2-bromo-isobutyryl bromides to the hydroxyl groups of the sugar, which convert the oligosaccharide to a star-macroinitiator, followed by acryloyl-agmatine conjugation by ATRP. The incomplete hydroxyl functionalization with 2-bromo-isobutyryl bromide (6 out of 10 available hydroxyl groups per maltotriose unit) can be ascribed to steric hindrance phenomena that prevent the conjugation of 2-bromo-isobutyryl bromide to the vicinal hydroxyl groups of the maltotriose.

Acryloyl-agmatine was selected to introduce cationic moieties into the maltotriose structure because agmatine is an endogenous compound biosynthesized by decarboxylation of arginine that contains a guanidinium group positively charged under physiological conditions (pKa≈13)[151]. Furthermore, with respect to arginine, agmatine does not contain carboxylic groups, which could form charge associations with the guanidyl groups. ATRP reaction of the acryloyl moiety yielded 6 guanidyl groups/maltrotriose unit indicating the complete conjugation of acryloyl-agmatine to the activated maltotriose hydroxyls, which is in agreement with the results reported in a previous paper[152].

Finally, the new star-like cationic structure was conjugated to linear $mPEG_{5kDa}$-NH_2 to enhance the biopharmaceutical features of the carrier/oligonucleotide complex. mPEG can in fact convey to the system high solubility and hydrodynamic volume that prevents the rapid clearance of the polyplex by kidney ultrafiltration. Furthermore, X-PEG-NH_2 terminating with a reactive group (X) can be used in place of mPEG-NH_2 thus allowing for the conjugation of a targeting moiety for active delivery of oligonucleotides. The GPC analyses showed that the final supramolecular carrier (Agm_6-M-PEG) possessed the expected molecular weight (8000 Da) and good polydispersity index (PDI: 1.182).

Gel electrophoresis studies carried out using 19 pair basis dsDNA as model oligonucleotide (ON) showed that complete ON association was obtained with 3 N/P ratio, corresponding to 19 Agm_6-M-PEG/dsDNA. This result was confirmed by fluorescence analysis performed using thiazole orange, which assesses the ON non-complexed with Agm_6-M-PEG.

Isothermal Titration Calorimetry (ITC) analyses showed the thermodynamic complexity of the formation of Agm_6-M-PEG/ON polyplex. In order to get close information about the nature of the Agm_6-M-PEG/dsDNA association the ITC study was carried out by titrating the carrier with the ON under two different conditions: high and low Agm_6-M-PEG/dsDNA ratio (400-3 N/P ratio and 3-0.05 N/P ratio, respectively).

In the first case (high N/P ratio) the study was carried out above the N/P ratio threshold (N/P=3) of complete ON association with the carrier, which could provide information about the single ON chain association with multiple Agm_6-M-PEG molecules. Under this condition, the ITC profile showed that the Agm_6-M-PEG/dsDNA association is controlled by a characteristic exothermic process with an overall remarkable enthalpy decrease ($\Delta H<0$), which is ascribable to electrostatic interactions between the Agm_6-M-PEG and dsDNA[153]. The single dsDNA injection into the Agm_6-M-PEG solution yields a remarkable heat release ($si\Delta H<0$), which decreases as the titration proceed. The $si\Delta H$ is nearly 0 at 6 N/P ratio equivalent that means that the association driven by the enthalpic process is completed even though there is not a complete charge balance. However, below 6 N/P ratio the association proceeds according a different mechanism. Indeed, below 6 N/P ratio the single injection of dsDNA into the cell containing the Agm_6-M-PEG solution elicits small positive thermal changes ($si\Delta H>0$) suggesting that at this point the association process is driven by an entropic mechanism due to the displacement of solvent molecules bound to the few cationic groups still available to complex ONs[154]. Nevertheless, under

these conditions the decreased enthalpy ($\Delta H<0$) and entropy ($\Delta S<0$) dominate the overall association process.

When the ITC study was carried out with low N/P ratio, the carrier was titrated with the ON below the N/P threshold of ON association with Agm_6-M-PEG and the carrier associates with a large excess of ON. Under this condition the Agm_6-M-PEG/ON association was found to occur according an endothermic process ($\Delta H>0$) driven by a remarkable increase of entropy ($\Delta S>0$). This result is in agreement with the data obtained in the terminal step of titration at high N/P ratio. The reason of this behavior could be explained by the combination of conformational changes of ON and Agm_6-M-PEG and the repulsion among the negative charges of ONs at low polymer concentrations[153]. Therefore, when the ON concentration is low with respect to the carrier, the association is driven by an exothermic mechanism. On the contrary, when the ON concentration is high with respect to the carrier and the carrier is partially associated to the ON to form an hindered structure with low charge available for further ON association, the association process is dominated by an entropic mechanism.

The high association constants (K_a) calculated by ITC analyses indicate that structured and stable Agm_6-M-PEG/dsDNA complex are obtained. However, the K_a calculated at low N/P ratio is about 1 order of magnitude lower than that calculated at high N/P ratio, which seems to indicate that when a high amount of ON is combined with the carrier, the binding is a combination of strong and weak association which result in an overall lower Ka. On the contrary, when a little amount of ON combine with the carrier, only strong interactions are involved in the complex formation.

The dynamic light scattering analysis (DLS) showed that the combination of ON with Agm_6-M-PEG forms colloidal structures with size of about 75 nm. Neither the particle size nor the polydispersity (PDI) significantly change with the N/P ratio. Nevertheless, according with the results obtained by gel-electrophoresis and ITC, the ζ-potential profile shows that the composition of the colloidal polyplexes changes with the Agm_6-M-PEG /ON ratio. Indeed, the polyplex charge changes with the N/P ration, being negative at N/P <2 while switches to positive at N/P>2.

According to the ITC, gel electrophoresis, DLS and ζ-potential data, Agm_6-M-PEG/dsDNA polyplexes at 3 and 5 N/P ratio were chosen as candidates. These compositions display in fact complete carrier/ON association with high association stability, slight positive charge and nanometric size.

The transmission electron microscopy (TEM) analysis showed that the Agm_6-M-PEG/dsDNA polyplexes possess a rod shape. Interestingly, the polyplexes with different composition have a different aspect ratio, which confirms that the conformation of the structure of the complex changes with the N/P ratio (Agm_6-M-PEG/dsDNA ratio) hypothesized in the ITC data discussion. In particular, the polyplexes obtained with 3 N/P ratio are thicker and shorter than the polyplexes obtained with high 5 N/P ratio. This suggests that when a high number of ON combine with Agm_6-M-PEG, they conformationally arrange to form a thickset structure.

The DLS analysis of the polyplexes incubated in PBS and in cell culture medium showed that the size of both formulations does not substantially changes over the time indicating that these polyplexes are stable in buffer. In cell culture medium containing serum proteins, the polyplexes undergo a slight size increase during the first three hours of incubation to reach a stable size that is maintained throughout the time. The size enlargement observed under these conditions may be attributable to protein absorption on the polyplexes surface that could be due to coulombic interactions of charged proteins with the slightly positive polyplex. As reported in different work, serum proteins could wrap the polyplexes reducing the toxicity and the recruiting in RES organs[155].

The cell culture studies were performed to investigate the cell up-take and biocompatibility on different cell lines, namely MCF-7 are breast tumor cells, KB ovarian tumor cells and MC3T3-E1 murine fibroblasts. Importantly, both formulations, 3 and 5 N/P ratios, were found highly biocompatible even at high concentrations towards all the tested cell lines. The lack of cytotoxicity of these polyplexes can be ascribed to the peculiar physicochemical features of the carrier and low overall charge of the polyplexes.

The flow cytometric (FACS) and confocal analyses showed that both formulations are efficiently taken-up by the cells, even though the extent of internalization was found to depend on both polyplexes composition and cell line[156,157].

Regarding the polyplex composition, the 3 N/P ratio formulation was found to be internalized more efficiently compared to the 5 N/P ratio formulation, despite the latter is more positively charged than the former. Therefore, the different cell up-take of the two polyplexes is ascribable to the different structural conformation, suggesting that thin and long structures are taken up by the cells more efficiently than thick and short structures. It is in fact reported in the literature that rod-shaped particles preferentially enter the cells though the axial axis perpendicularly oriented to the cell membrane while the cell penetration with the axial axis parallel to the cell membrane is slower as longer is the

particle[156,158-160]. Accordingly, the cell up-take of the 5 N/P ratio particles that have a higher aspect ratio are taken up by the cells less efficiently than the 3 N/P polyplexes with smaller aspect ratio.

Interestingly, the three cell lines used for the cell internalization studies showed a significantly different up-take of the complexes. The KB cells displayed the highest cell up-take of the polyplexes while a little polyplexes internalization was obtained with MC3T3-E1 cells. This result may be due to different mechanisms of endocytosis or different membrane composition, including carriers or receptors that could unexpectedly be involved in the cell up-take process[157]. A preliminary evaluation about the Agm_6-M-PEG ability to transfect cells was performed using Rac1 siRNA as a oligonucleotide model for gene silencing. The results showed that the 3 N/P ratio polyplex have a higher silencing activity compared to the 5 N/P ratio polyplex. Both the formulation showed a slightly dose response with 51% gene knockdown with 500 nM siRNA equivalent dose 3 N/P ratio polyplexes.

Part B

Comparative study of folate and non-folate polyplexes towards cancer cells

3.1 Materials

All the reagents used for the synthesis of cationic polymers were purchased from Sigma Aldrich (St. Louis, MO, USA) or Merck (White House Station, NJ, US). Linear 5 kDa α-methoxy-ω-amino-polyethylene glycol ($mPEG_{5kDa}$-NH_2) and linear 6 kDa bis amino-polyethylene glycol (PEG_{6kDa}-$(NH_2)_2$) were obtained from Iris Biotech GmbH (Marktredwitz, Germany). Cy3-NHS and Cy5.5-NHS fluorescent probes were obtained from Lumiprobe GmbH. [^{3}H]-folic acid (FA) sodium salt was bought from American Radiolabeled Chemicals, Inc. (St. Louis, MO, USA).

All the cell lines used were provided by the cell bank ATCC (Manassas, VA, USA), unless otherwise indicated. All tissue culture reagents were purchased from Biological Industries Ltd. (Beit Haemek, Israel). Double-strand DNA (dsDNA), 19 nucleotides per strand) were purchased from Biomers.net GmbH (Ulm, Germany). SiRNA (EGFP siRNA, Rac1 siRNA, Luciferase (siLuc) siRNA, Cy5-labeled Rac1 siRNA) sequences were supplied by QBI Enterprise (Ness Ziona, Israel). Lipofectamine 2000 was obtained from Life Technologies, (Grand Island, NY, USA). psiCHECK reporter assay was purchase from Promega (Madison, Wisconsin, USA). ProLong Gold antifade with DAPI mounting medium was purchased from Invitrogen (Eugene, OR, USA). Organic solvents were furnished by Carlo Erba (Milan, Italy), VWR International (Lutherworth, UK) and Sigma Aldrich (St. Louis, MO, USA). All the other reagents or salts were obtained from Fluka Analitical or Sigma-Aldrich.

3.2 Methods

3.2.1 Synthesis of Agm_6-M-COOH and Agm_6-M-PEG cationic polymers

The synthesis of cationic moiety (Agm_6-M-COOH) and non-folate cationic polymers (Agm_6-M-PEG) used in the present work are described in the previous section.

3.2.2 Synthesis of Folate-α-amino-poly(ethylene glycol)$_{6kDa}$ (NH_2-PEG-FA)

FA-PEG-NH_2 was synthesized according to a literature procedure using a slightly modified protocol[161]. Folic acid (FA, 30 mg, 0.068 mmol) was dissolved in 500 μL of anhydrous DMSO at 40°C under stirring until complete dissolution. N-Hydroxysuccinimide (NHS, 9.44 mg, 0.082 mmol) and Dycyclohexilcarbodiimide (DCC, 16.8 mg, 0.082 mg) were added to the FA solution and the reaction was carried out overnight at room temperature. The Dicyclohexilurea (DCU) precipitate was then filtered off and the activated folic acid was precipitated in diethyl ether (30 mL × 3). The precipitate was re-dissolved in anhydrous DMSO, the obtained solution was sequentially added of triethylamine (TEA, 4.7 μL, 0.034 mmol), $(NH_2)_2$-PEG_{6kDa} (408 mg, 0.068 mmol) and stirred overnight. The reaction mixture was precipitated in Et_2O (3×30 mL) and then dried under vacuum. The crude product was purified from free folic acid by gel filtration chromatography using Sephadex G-25 resin and water with 0.05% v/v of NH_3, pH 9.0 as eluent. Fractions containing the conjugate were collected and lyophilized obtaining NH_2-PEG-FA as a yellow powder (372 mg, 0.0577 mmol, 84.9% mol/mol). MALDI-TOF mass spectroscopy of Folate-α-amino-poly(ethylene glycol)$_{6kDa}$ was performed using sinapinic acid matrix in 400 Plus MALDI TOF/TOF Analyzer, (AB Sciex-Framingham, MA, USA). MALDI TOF/TOF-MS [m/z]: 6532, [calcd [M + H] = 6442].

The conjugation degree as determined by comparing the iodine assay (y=0.0663x-0.0183, R^2=0.9933) results for PEG quantification[144] and UV-Vis detection of folic acid (ε_M = 6197 mol^{-1} cm^{-1})[162] was found to be 97%.

3.2.3 Synthesis of (agmatinyl)$_6$-maltotriosyl-N-acetyl-amino-hexanoate-poly(ethylene glycol)$_{6kDa}$-Folate (Agm_6-M-PEG-FA)

(Agmatinyl)$_6$-maltotriosyl-N-acetyl-amino-hexanoic acid (Agm_6-M-COOH, 500 mg, 0.188 mmol) was dissolved in 5 mL of 1:2 v/v DMSO/100 mM morpholino-ethan-sulphonic acid buffer (MES), pH 4.7. The solution was sequentially added of 1-ethyl-3-(3-dimethylaminopropyl)carbodiimide (EDC) (291.9 mg, 1.88 mmol), N-hydroxysuccinimide (NHS) (216.3 mg, 1.88 mmol) and left under stirring. After 30 minutes a NH_2-PEG-FA

(942 mg, 0.157 mmol) solution in 1:2 v/v DMSO/100 mM MES buffer, pH 4.7 (3 mL) was added. The mixture was stirred for 72 hours at room temperature and then dialyzed against deionized water for 48 hours using a 3.5-5.0 kDa MWCO dialysis membrane. After lyophilization the product was isolated as yellow powder (780 mg, 0.092 mmol, 55.2% mol/mol) and characterized by UV-Vis. The conjugation degree was calculated by normalizing the guanidine content[163] as determined with Sakaguchi assay by the PEG content resulted from iodine assay, as reported above, and was found to be 96%.

3.2.4 Synthesis of (agmatinyl)$_6$-maltotriosyl-N-acetyl-amino-hexanoate-poly(ethylene glycol)$_{6kDa}$-NH_2 (Agm$_6$-M-PEG-NH_2)

The synthesis of Agm$_6$-M-PEG-NH_2 was performed following a similar procedure to that described for Agm$_6$-M-PEG-FA. Briefly, Agm$_6$-M-COOH (100 mg, 0.038 mmol) was dissolved in 2 mL of 1:2 v/v DMSO/100 mM morpholino-ethan-sulphonic acid buffer (MES), pH 4.7. The solution was added of EDC (72.8 mg, 0.38 mmol) and NHS (43.7 mg, 0.38 mmol) followed by the addition of $(NH_2)_2$-PEG$_{6kDa}$ (248 mg ,0.0414 mmol) after 30 min. The solution was stirred for 72 hours at room temperature and then dialyzed against deionized water for 48 hours using a 3.5-5.0 kDa MWCO dialysis membrane. The lyophilization yielded the final product as white powder (210 mg, 0.025 mmol, 65.8% mol/mol) that was characterized by ^{1}H-NMR and UV-Vis spectroscopic analysis. The conjugation yield was 91%, as determined by Sakaguchi and iodine assays[144] for guanidine and PEG quantification, respectively.

3.2.5 Synthesis of (agmatinyl)$_6$-maltotriosyl-N-acetyl-amino-hexanoate-poly(ethylene glycol)$_{6kDa}$-Cyanine3 (Agm$_6$-M-PEG-Cy3)

Cyanine3-NHS (Cy3-NHS, 7.0 mg, 0.011 mmol) was dissolved in 500 μL of anhydrous DMSO. This solution was added dropwise to a Agm$_6$-M-PEG-NH_2 solution (112 mg, 0.013 mmol) in a 2:1 (v/v) mixture of DMSO/100 mM $NaHCO_3$ buffer, pH 8.5. The mixture was stirred overnight, then dialyzed against water for 72 hours in the dark using a 3.5-5.0 kDa MWCO dialysis membrane and finally lyophilized.

The final product yield was 90 mg (0.01 mmol, 91% mol/mol). The bioconjugate was analyzed by iodine assay and by UV-Vis spectroscopy to detect PEG and Cyanine3 content, respectively, in 10 mM phosphate, 0.15 M NaCl, pH 7.4 PBS buffer (ε_M =150,000 M^{-1} cm^{-1})[162]. The conjugation yield was found to be 93%.

3.2.6 Synthesis of Folate-poly(ethylene glycol)$_{6kDa}$-Cyanine5.5 (FA-PEG-Cy5.5)

Cyanine5.5-NHS (Cy5.5-NHS) was conjugated to FA-PEG-NH_2 as described above for Agm_6-M-PEG-Cy3. Briefly, Cy5.5-NHS (6.33 mg, 0.01 mmol) was dissolved in 100 μL of anhydrous DMSO. This solution was added to FA-PEG-NH_2 (60 mg, 0.0093 mmol) previously dissolved in a 2:1 (v/v) mixture of DMSO:0.1 M $NaHCO_3$ buffer, pH 8.5. The mixture was stirred overnight and then dialyzed against water for 72 hours in the dark using a 3.5-5.0 kDa MWCO dialysis membrane. The purified product was finally lyophilized and subjected to iodine test and spectrophotometric analysis (λ_{max} 675 nm, ε_{mol} 250,000 M^{-1} cm^{-1}) in phosphate buffer, pH 7.4 to determine PEG and Cyanine5.5 content, respectively[162]. A 97% conjugation degree was obtained. The final product (50 mg, 0.006 mmol, 68% mol/mol) was characterized by MALDI-TOF analysis. The measurement was performed as described above. MALDI TOF/TOF-MS [m/z]:6968, [calcd [M + H] = 7194].

3.2.7 Preparation of polyplexes

Polyplexes were prepared using different oligonucleotides (ONs). Scrambled dsDNA (19 pb, 11 kDa) was used as a model for preliminary studies. For all the *in vitro* and *in vivo* studies, siRac1 (19 pb, 13 kDa), siLuc (19 pb,13 kDa) and siEGFP (19 pb, 13 kDa) were used. Polyplexes were self-assembled by simple mixing Agm_6-M-PEG or 75:25 w/w % of Agm_6-M-PEG:Agm_6-M-PEG-FA with ONs in 10 mM phosphate buffer, 0.15 M NaCl (PBS), pH 7.4 at room temperature in order to obtain different Nitrogen (N)/Phosphate (P) ratios (N/P ratio). For flow cytometric analysis, 99:1 %w/w Agm_6-M-PEG:Agm_6-M-PEG-Cy3/siRNA and 74:25:1 %w/w Agm_6-M-PEG:Agm_6-M-PEG-FA:Agm_6-M-PEG-Cy3/siRNA polyplexes were prepared. For confocal microscopy observation, 99:1 %w/w Agm_6-M-PEG:Agm_6-M-PEG-Cy3/siRac1-Cy5 and 74:25:1 %w/w Agm_6-M-PEG:Agm_6-M-PEG-FA:Agm_6-M-PEG-Cy3/siRac1-Cy5 polyplexes were used. For the intracellular trafficking Agm_6-M-PEG/siRac1-Cy5 or 75:25 w/w % of Agm_6-M-PEG:Agm_6-M-PEG-FA/siRac1-Cy5 were used. The biodistribution experiments were performed using polyplexes prepared in PBS, pH 7.4 at a 60:25:15 Agm_6-M-PEG:Agm_6-M-PEG-FA:Agm_6-M-PEG-Cy3/siRac1 mass ratio. The ONs and polymer concentrations were selected in order to yield determined N/P ratio required for the specific analysis. These protocols were used for the preparation of all the polyplexes referred to here.

3.2.8 Dynamic Light Scattering (DLS) and Zeta potential analysis

DLS analyses were performed on 1 mL of Agm_6-M-PEG/dsDNA or 75:25 w/w % of Agm_6-M-PEG:Agm_6-M-PEG-FA/dsDNA samples in PBS, pH 7.4. Polyplexes suspensions were prepared at fixed polymer concentration of 500 μg/mL added of 33.0 μL of 100 μM dsDNA solution in PBS, pH 7.4 to yield a final mixture corresponding to 3.0 N/P molar ratio for both formulations.

Dynamic Light Scattering and Zeta Potential analysis were performed at 25°C using a Malvern Zetasizer NanoZS (Malvern Instruments Ltd., U.K.) supported by Zetasizer Software (version 6.12).

3.2.9 Transmission Electron Microscopy

100 μL of Agm_6-M-PEG/dsDNA and 75:25 w/w% Agm_6-M-PEG:Agm_6-M-PEG-FA/dsDNA samples were prepared at a polymer concentration of 100 μg/mL (Agm_6-M-PEG alone or 75:25 Agm_6-M-PEG:Agm_6-M-PEG –FA mixture) containing 18.6 μL of a 10 μM dsDNA solution to obtain a N/P ratio of 3. Samples were analyzed by Transmission Electron Microscopy (TEM). The samples were deposited on a small copper grid (400 mesh), covered by "holey film" carbon layer and analyzed in negative staining mode. 1% w/v uranyl acetate solution in milliQ water was used as contrast agent.

3.2.10 Electrophoretic mobility shift assay (EMSA)

Electrophoretic analyses were performed to evaluate the ability of Agm_6-M-PEG or Agm_6-M-PEG-FA to complex oligonucleotides. To obtain N/P ratios ranging between 0.5 and 5.0, polyplexes with increasing concentration of Agm_6-M-PEG or Agm_6-M-PEG-FA were complexed with 50 pmol of siRNA by simple mixing of polymeric mixtures and siRNA in PBS. 10 μL of polyplexes suspensions were added of 3 μL of loading buffer containing 50% v/v glycerol in PBS. The Agm_6-M-PEG/siRNA samples were loaded into 2% agarose gel supplemented with ethidium bromide (5 μL of a 10 mg/mL solution) and electophoretically run in Tris-Acetate-EDTA (TAE) 1X buffer at 100 V for 15 min. The migrated siRNA was visualized under UV light.

3.2.11 Plasma stability studies

The stability of polyplexes in plasma was investigated through incubation of siRNA polyplexes in 100% mouse plasma. 5 μL of Agm_6-M-PEG/siRac1 polyplexes (100 pmol siRNA equivalent dose) were prepared as describe above at N/P ratios of 3 and 5 and

incubated with 15 μL whole mouse plasma from 30 min to 24 hours. Afterwards, 10 μL of these samples were added of 5 uL of ultrapure water or heparin (90 IU/mL) and incubated for further 15 min. Samples were loaded on 2% agarose gel supplemented with ethidium bromide using Tris Acetate EDTA (TAE) as running buffer at 100 V for 15 min. The migrated siRNA was visualized under UV light.

3.2.12 Heparin-siRNA competition assay

The stability of polyplexes was evaluated by the siRNA release from Agm_6-M-PEG/siRNA polyplexes in presence of heparin as a poly-anion competitive molecule model. Agm_6-M-PEG/siRac1 polyplexes at 3 and 5 N/P ratio (50 pmol equivalent siRNA) were prepared in PBS, pH 7.4 and incubated with increasing concentration of heparin (0.25-15 IU/mL per 50 pmol siRNA). Following 15 min, 5 μL of 50% v/v glycerol solution in PBS buffer pH 7.4 were added to the polyplexes/heparin solution and the samples were run in 2% agarose gel as described above.

3.2.13 Hemolysis assay

2 mL of mouse blood were centrifuged at 1100 rpm for 5 min at 4°C. The supernatant was removed and the red blood cells (RBCs) were washed three times with saline solution (0.15 M NaCl in ultra-pure water). The pellets containing RBCs were dispersed in PBS, pH 7.4 at a final concentration of 2% w/w. RBCs suspension was incubated with an increasing concentration of Agm_6-M-PEG/siRac1 polyplexes (0.0001-1.0 mg/mL), corresponding to relevant in vivo concentration, at 37°C for 1 hour. 10% Sodium dodecyl sulfate (SDS) solution and Dextran (70.0 kDa) were used as positive and negative control, respectively. Then the samples were centrifuged at 1100 rpm for 5 min and 100 μL of the supernatant was transferred into a 96-well plate. The absorbance was measured at 550 nm using SpectraMax® M5e plate reader (Molecular Devices LLC., Sunnyvale, California, USA). Percent of hemolysis lysis was normalized to that of RBCs treated with 100% of Triton X-100 solution (100% hemolysis).

3.2.14 Cell lines

Murine 4T1 breast cancer, murine DA3 mammary adenocarcinoma, human MCF-7 breast adenocarcinoma, murine B16-F10 melanoma cells, human WM115 melanoma and human HeLa cervical carcinoma were cultured in Dulbecco's Modified Eagle's Medium (DMEM, Gibco-InVitrogen, Carlsbad, CA, US) supplemented of 10% fetal bovine serum (FBS), 100 IU/mL Penicillin, 100 μg/mL Streptomycin, 12.5 IU/mL nystatin, and 2 mM L-glutamine.

Murine Ret melanoma cells, human A375 melanoma cells and Human Mel 526 cells were cultured in RPMI-1640 (Roswell Park Memorial Institute, RPMI, Gibco-InVitrogen, Carlsbad, CA, US) supplemented of 10% fetal bovine serum (FBS), 100 IU/mL Penicillin, 100 μg/mL Streptomycin, 12.5 IU/mL nystatin, 2 mM L-glutamine and 2.5% v/v of HEPES. Human 131/4-5B1 melanoma cells were growth in RPMI 1640 supplemented of 10% fetal bovine serum (FBS), 100 IU/mL Penicillin, 100 μg/mL Streptomycin, 12.5 IU/mL nystatin, 2 mM L-glutamine. Murine D4M melanoma cells were cultured in DMEM/F-12 added of 10% fetal bovine serum (FBS), 100 UI/mL Penicillin, 100 μg/mL Streptomycin, 12.5 UI/mL nystatin, and 2 mM L-glutamine.

Human MDA-MB-231 breast adenocarcinoma were a gift from Phil Low Laboratories, Purdue University, and were cultured in DMEM medium supplemented with 10% fetal bovine serum (FBS), 100 UI/mL Penicillin, 100 μg/mL Streptomycin, 12.5 UI/mL nystatin, and 2 mM L-glutamine.

HUVEC (Human umbilical vein endothelial cells) were purchased from Lonza (Visp, Switzerland) and cultured in Endothelial Cell Growth Medium (EGM-2, Lonza, Visp, Switzerland). All the cells were growth at 37 °C and 5 % CO_2. Cells were splitted at 70% of confluence and cell culture media was changed every 3 to 4 days. If not otherwise specified, cells were purchased from American Tissue Culture Collection (ATCC).

To evaluate the folate receptor expression, all the cell lines were grown for one week in folic acid depleted RPMI-1640 (Roswell Park Memorial Institute, Folic Acid depleted, FF-RPMI) supplemented with 10% fetal bovine serum (FBS), 100 UI/mL Penicillin, 100 μg/mL Streptomycin, 12.5 IU/mL nystatin, and 2 mM L-glutamine. All the cell lines were grown at 37°C in humified 5% CO_2 atmosphere.

3.2.15 Folate receptor (FR) expression investigation

The folate receptor (FR) investigation was performed according to previously published protocols[117,164]. Briefly, all the cells in analysis were grown for two weeks in FF-RPMI. HUVEC were cultured in EGM-2 for one week before use. 1.0×10^6 cells/well were seeded in 24 well plates in 500 μL of FF-RPMI and were added of 10 μL of 2 μM folic acid (FA) previously dissolved in PBS, pH 7.4. After 3 hours of incubation at 37°C, 10 μL of 10 μM tritiated folic acid ([^{3}H]FA, 5μCi/mL, 0.2 μM in each well) were added and the cells were incubated for additional 3 hours. The cells were harvested with 500 μL of trypsin solution and the suspension was centrifuged for 5 min at 4000 rpm. The supernatant was removed and the pellet washed 3 times with PBS, pH 7.4. The supernatant

was discharged and the cells were lysed by addition of 500 μL of 0.5 N NaOH. After resuspension, the pellet was left overnight at room temperature with gentle rocking. After 12 hours, the suspension was neutralized with 500 μL of 0.5 N HCl. After 30 min, 600 μL of the neutralized solution was added to 3 mL of scintillation fluid. The amount of bound FA was determined by radioactivity emission (Tri-Carb® 2100TR liquid scintillation counter, Waltham, MA, USA).

3.2.16 Dual Luciferase reporter assay

The in vitro efficacy polyplexes was assessed by psiCHECK reporter assay (Promega Madison, Wisconsin, US) as described by Polyak et al[165]. To evaluate the better formulation to yield the higher silencing preliminary screening was performed on HeLa cells using polyplexes with increasing amount (% w/w) of Agm_6-M-PEG-FA. HeLa cells (1×10^6 cells/well) were incubated overnight at 37 °C and 5% CO_2 in DMEM supplemented of 10% FBS. The cells were then transfected with 4 μg Rac1-psiCHECK™-2-based plasmids using 4 μL of Lipofectamine® 2000 (Life Technologies, Grand Island, NY). Afterwards, 2.5×10^3 cells/well of transfected HeLa cells were reseeded in 96-wells plate in 150 μL of DMEM. Polyplexes decorated with different percentage of FA (25, 50 and 100%) were prepared at 3 and 5 N/P ratio with 125, 250, 500 nM equivalent siRac1 or siLuc concentration. These formulations were incubated with HeLa cells for 72 hours. siRac1 and siLuc, both complexed with Lipofectamine® 2000 (50 nM siRNA dose), were used as positive controls. After 72 hours, the medium was removed completely, the cells were washed 3 times with 500 μL of PBS and lysed by addition to each well of 50 μL of 1x passive lysis buffer. Renilla and firefly luciferase levels were evaluated using Dual-Luciferase® Assay kit (Promega Corporation, Wisconsin, USA) according to manufacturer procedure. Results were normalized to control untreated cells.

In similar manner, HeLa cells and MDA-MB-231 (1×10^6 cells/well) were incubated overnight at 37 °C and 5% CO_2 in DMEM supplemented of 10% FBS or FF-RPMI added of 10% FBS. The cells were then transfected with 4 μg Rac1-psiCHECK™-2-based plasmids using 4 μL of Lipofectamine® 2000 (Life Technologies, Grand Island, NY). Finally, 2.5×10^3 cells/well of transfected HeLa cells or MDA-MB-231 were reseeded in 96-wells plate in 150 μL of DMEM or FF-RPMI respectively. The cells were treated with Agm_6-M-PEG/siRac1 and 75:25 %w/w Agm_6-M-PEG:Agm_6-M-PEG-FA/siRac1 polyplexes with increasing concentration of siRac1 equivalent dose (125, 250 and 500 nM). Agm_6-M-PEG/siLuc and 75:25 %w/w Agm_6-M-PEG:Agm_6-M-PEG-FA/siLuc were

used as negative controls. After 72 hours, the cells were lysates as described before and levels of renilla and firefly luciferases were detected as described above.

3.2.17 Cell viability studies

HeLa and MDA-MB-231 cells were seeded in 96 well plate (2.5×10^3 cells/well) in DMEM supplemented with 10% FBS or FF-RPMI supplemented with 10% fetal bovine serum (FBS), respectively. The cells were incubated 24 hours before the treatment at 37°C and 5% CO_2. The medium was removed and the cells were treated with Agm_6-M-PEG/siRNA or 75:25 w/w % Agm_6-M-PEG:Agm_6-M-PEG-FA/siRNA polyplexes. The samples were prepared to yield a 3 N/P ratio with increasing concentrations (125, 250 and 500 nM) of siRNA equivalent dose using siRac1 and siLuc as controls. After 72 hours, the cell survival was assessed through 3-(4,5-dimethylthiazol-2-yl)-2,5-diphenyltetrazolinium bromide (MTT) assay[166]. 20 μL of a 5 mg/mL MTT solution in PBS buffer were added to each well. After 3 hours the medium was removed, replaced with 200 μL of dimethyl sulfoxide (DMSO) and incubated at room temperature with gentle rocking for 15 min. The absorbance of the solution in each well was evaluated at 570 nm by SpectraMax® M5e plate reader (Molecular Devices LLC., Sunnyvale, California, USA). The cell viability was normalized to untreated cells.

3.2.18 Wound healing assay

MDA-MB-231 cells were seeded in a 96-well plate 24 hours before the analysis at a density of 7.0×10^4 cells/well in 100 μL folate depleted RPMI medium supplemented of 10% of FBS and growth at 37°C in 5% CO_2.

A wound was made in each well using WoundMaker and the harvested cells were removed by washing three times with 100 μL of PBS 10 mM phosphate, 150 mM NaCl, pH 7.4. The wells were filled with 200 μL FF-RPMI containing Agm_6-M-PEG:siRac1 and 75:25% w/w Agm_6-M-PEG:Agm_6-M-PEG-FA/siRac1 polyplexes at 3 N/P ratio with 500 nM equivalent siRNA dose. Cell treated with Agm_6-M-PEG/siLuc and 75:25% w/w Agm_6-M-PEG:Agm_6-M-PEG-FA/siLuc polyplexes at N/P charge ratio of 3, both siRNA alone (siRac1 or siLuc) or PBS were used as controls. The plate was placed in IncuCyte ZOOM incubator and images were taken at scheduled times. After 12 hours, the Relative Wound Density was calculated using IncuCyte Software. The images were analyzed using ImageJ software.

3.2.19 Cell uptake of polyplexes on MDA-MB-231

In a 6 well plate, MDA-MB-231 cells (1.5×10^6 cells/well) were seeded in FF- RPMI supplemented of 10% of FBS. After 24 hours, at scheduled times (5, 30 min, 1, 3, 6 or 24 hours) the cells were treated with 99:1 %w/w Agm_6-M-PEG:Agm_6-M-PEG-Cy3/siRac1 and 74:25:1 %w/w Agm_6-M-PEG:Agm_6-M-PEG-FA:Agm_6-M-PEG-Cy3/siRac1 (125 nM siRac1-Cy5 equivalent concentration) at N/P ratio of 3. Afterwards, cells were washed 3 times with 500 μL of PBS with 0.5% w/v of BSA and treated with 250 uL of trypsin and re-suspended in RPMI without phenol red. The cells were centrifuged at 1100 rpm for 5 minutes at 4°C and the supernatants were removed. The pellets were re-suspended in PBS, pH 7.4 supplemented of 2% FBS and the samples were analyzed by ImageStream multispectral imaging flow cytometer (Amnis Corp., Seattle, WA).

3.2.20 Folate competition study

MDA-MB-231 or HUVEC cells (1×10^6 cells/well) were seeded in 24 well plate in 500 μL of FF-RPMI and treated with Folic acid (FA), Agm_6-M-PEG/siRNA, 95:5 w/w % Agm_6-M-PEG:Agm_6-M-PEG-FA/siLuc, 90:10 w/w % Agm_6-M-PEG:Agm_6-M-PEG-FA/siLuc, 50:50 w/w % Agm_6-M-PEG:Agm_6-M-PEG-FA/siLuc or Agm_6-M-PEG-FA/siLuc in PBS, pH 7.4, using 2 μM of FA-equivalent dose. After 3 hours of incubation at 37°C, 10 μL of [^{3}H]FA were added to each well and the cells were incubated for a further 3 hours. Afterwards, the medium was removed and the cells were harvested by addition of 100 μL of trypsin solution and centrifuged. To ensure complete removal of the excess of [^{3}H]FA, the pellets were washed 3 times with 300 μL PBS, pH 7.4 and lysed by overnight incubation with 500 μL of 0.5 N NaOH, followed by neutralization with 0.5 N HCl. 600 μL of the suspension was added to 3 mL of scintillation fluid and the amount of radioactivity was determined as described above.

3.2.21 Confocal microscopy

MDA-MB-231 (8×10^4 cell/well) cells were seeded on 35 mm slides in 24 well plates 24 hour prior the treatment in FF- RPMI medium. At the scheduled time points of 6 and 24 hours cells were treated with 99:1 %w/w Agm_6-M-PEG:Agm_6-M-PEG-Cy3/siRac1-Cy5 and 74:25:1 %w/w Agm_6-M-PEG:Agm_6-M-PEG-FA:Agm_6-M-PEG-Cy3/siRac1-Cy5 prepared as described in the previous section at the defined 3 N/P ratio and 125 nM siRNA equivalent concentration. Afterwards, the cells were washed 3 times with 250 μL of PBS and fixed with 500 μL of 4% v/v paraformaldehyde in PBS on ice for 20 min. Cover

glasses were mounted with Vectashild® DAPI containing medium (Vector Laboratories, USA) and analyzed using Leica SP8 confocal imaging systems (60x Magnification). Lasers with emission wavelengths at 405, 568 and 666 nm were used to detect DAPI, Agm_6-M-PEG-Cy3 and siRac1-Cy5, respectively. The slides were kept at 4°C in the dark until the analysis was performed. The images were processed with ImageJ version 1.51f software.

3.2.22 Immunofluorescence analysis

The intracellular fate of polyplexes was monitored by immunostaining analysis.

In a 24 well plate, MDA-MB-231 cells (8.0×10^4 cell/well) were seeded 24 hours prior the treatment in FF-RPMI medium. The cells were treated with Agm_6-M-PEG/siRac1-Cy5 and 75:25% w/w Agm_6-M-PEG:Agm_6-M-PEG-FA/siRac1-Cy5 polyplexes at 3 N/P ratio with 200 nM equivalent siRac1-Cy5 concentration. After 3 hours, cells were washed with 250 µL of PBS and fixed with 500 µL 4% of paraformaldehyde solution in PBS on ice for 20 min. The membrane permeabilization was performed by incubating cells with Triton X-100 (0.25% v/v) solution in PBS, pH 7.4. After 10 min, cells were washed 5 times with 250 µL PBS supplemented of 50% of Fetal Bovine Serum (FBS). The intracellular trafficking of FA-PEG alone was studied by treating MDA-MB-231 cells with 0.001 mg/mL of FA-PEG-Cy5.5 for 30 min.

Staining of early endosomes and lysosomes was performed with mouse anti-EEA1 (Early endosomes Antigen 1) (BD, New Jersey, US) and rabbit anti-LAMP-1 (Lysosomal-associated membrane protein 1) (Cell Signaling Technology, Massachusetts, US) antibodies (each antibody was diluted with 1:100 dilution in PBS, pH 7.4) respectively. After 1 hour, cells were washed three times with 250 µL of PBS, pH 7.4 supplemented with 50% FBS and three times with 250 µL of PBS only, pH 7.4. Cells were then treated with goat anti-mouse-rhodamine and goat anti-rabbit-AlexaFluor 488 secondary antibodies (each antibody was diluted with 1:100 dilution in PBS, pH 7.4) (Santa Cruz, Heidelberg, Germany) for 30 min at room temperature in the dark.

Caveolae and Clathrin were stained with mouse anti-Caveolin-1 and rabbit anti-Clathrin heavy chain antibody (each antibody was diluted 1:100 in PBS, pH 7.4) (Abcam), respectively. After 1 hour, cells were washed three times with PBS, pH 7.4 supplemented with 50% Fetal Bovin Serum (FBS) and three times with PBS pH 7.4. The cells were treated with goat anti mouse-rhodamine and goat anti rabbit-AlexaFluor 488 (1:100 in PBS) (Santa Cruz, Heidelberg, Germany) for 30 min. The slides were washed with PBS,

pH 7.4 and cover glasses were mounted with Vectashild® DAPI containing medium and analyzed using Leica SP8 confocal imaging systems (60x Magnification). Lasers with emission wavelengths at 405, 525, 583 and 666 nm were used to detect DAPI, AlexaFluor 488, Rhodamine and siRac1-Cy5, respectively. Representative images of each dye were captured and the images were processed with ImageJ version 1.51f software. Cells treated with secondary antibodies only were used as control.

3.2.23 TNF-α cytokine secretion from human peripheral blood mononuclear cells

50 mL of whole blood leukocyte enriched from human healthy donors by Sheba Medical Center Blood Bank were diluted to 215 mL with PBS, pH 7.4 supplemented with 2 mM EDTA. The solution was gently overlaid onto 15 mL lymphoprep™ (Ficoll) (Axis-Shield). Suspensions were centrifuged at 20 ℃, 400 g for 40 min without brake. The upper layer was removed and the opaque-light PBMCs rings were collected and suspended in 50 mL of PBS, pH 7.4 supplemented with 2 mM EDTA. The suspension was centrifuged at 200 g for 15 min at 20°C. The supernatant was completely removed and PBMCs were dispersed in RPMI 1640 growth medium supplemented with 10% Fetal Bovine Serum (FBS), L-Glutamine, Penicillin-Streptomycin-Nystatin to yield a concentration of 3.0×10^6 cells/mL. PBMCs (1.5×10^6 cells/well) were seeded in 12 well plates at 37 °C in humidified 5% CO_2/air. Cells were treated with Agm_6-M-PEG/siRac1 or 75:25% w/w Agm_6-M-PEG:Agm_6-M-PEG-FA/siRac1 polyplexes at 3 N/P ratio (125 – 250 nM siRac1 equivalent dose), Agm_6-M-PEG and 75:25% w/w Agm_6-M-PEG:Agm_6-M-PEG-FA polymers and siRac1 alone. Lipopolysaccharides (LPS) at a concentration of 4 μg/mL and PBS were used as positive controls and negative controls, respectively. After 12 hours, cells were centrifuged at 800 g for 7 min and TNF-α cytokine secreted from PBMCs were evaluated by DuoSet ELISA kits (DY210, R&D Systems, Minnesota, USA).

3.2.24 Animals and Ethics Statement

All animal procedures were performed in compliance with Tel Aviv University guidelines approved by the Institutional Animal Care and Use Committee (IACUC)**.** Nu/nu nude mice were purchased from Harlan Biotech (Rehovot, Israel). Animals were used at 7 weeks of age and housed in ventilated cages and clinically controlled rooms. Athymic Nu/nu nude mice were anesthetized (ketamine/xylazine) and human MDA-MB-231 breast adenocarcinoma tumor cells (2.0×10^6 cells/100 μL) were inoculated intramammary. Seven days post inoculation mice body weight and tumor progression were monitored

twice a week for tumor formation using a caliper and randomized according to tumor size. After 21 days, which lead to the development of MDA-MB-231 orthotropic tumor with an approximate volume of 100 mm^3, mice were used for experiments.

3.2.25 Maximum tolerated dose (MTD)

Maximum tolerated dose was tested up to 4 mg/kg of siRNA in female Nu/Nu nude mice. Administration was performed by i.v. injection of 100 μL Agm_6-M-PEG:siRac1 or 75:25% w/w Agm_6-M-PEG:Agm_6-M-PEG-FA/siRac1 polyplexes at 3 N/P ratio per day for 3 days and the interval between treatments was 24 hours. Mice were monitored up to 1 month.

3.2.26 Tumor accumulation of siRac1-polyplexes

100 μL of 75:25% w/w Agm_6-M-PEG:Agm_6-M-PEG-FA/siRac1, 75:25% w/w Agm_6-M-PEG:Agm_6-M-PEG-FA/siEGFP polyplexes at 3 N/P ratio (4 mg/kg siRNA equivalent dose) or PBS, pH 7.4 were administered by i.v. injection for three day with 24 hours between each injection. Mice were euthanized 24 h following the 3rd injection and tumors were collected and weighted. Then, the tumors were homogenized and lyophilized. The final lysates were obtained by addition of 0.25% v/v Triton X-100 in ultrapure water and siRac1 was quantified by stem-loop qPCR method using SYBR Green on Applied Biosystem 7300 PCR System.

3.2.27 Biodistribution of polyplexes in tumor-bearing mice

100 μL of 60:25:15 %w/w Agm_6-M-PEG:Agm_6-M-PEG-FA:Agm_6-M-PEG-Cy3/siEGFP polyplexes (4 mg/kg equivalent siRNA dose) were administered by i.v. injection in female Nu/Nu nude mice. At scheduled times of 30 min, 3 hours and 6 hours, mice were sacrificed and tumor, spleen, liver, lungs, heart and kidneys were collected and analyzed by CRI Maestro^{TM} non-invasive Intravital fluorescence imaging system. Multispectral image-cubes were used through 500–720 nm spectral range in 10 nm steps using excitation (554 nm) and emission (568 nm longpass) filter set. Organs auto-fluorescence and background signals were eliminated by spectral analysis and linear un-mixing algorithm. A quantitative analysis of the fluorescence intensity was carried out using the Maestro software and each intensity measurement was normalized according to the tumors/organs size.

3.2.28 Histology studies from tumor tissue

After biodistribution evaluation, female Nu/Nu nude mice were euthanized and tumors were fixed in 4% paraformaldehyde solution in PBS for 3 hours followed by D-Sucrose

(BioLab) 0.5 M for 1 hour and D-Sucrose 1 M overnight. Then, tumors were embedded in OCT (Scigen) on dry ice and stored at -80°C. Immunohistochemistry of intramammary tumor was performed using 5 μm thick OCT frozen tissue sections. Staining was performed using the BOND RX autostainer (Leica). Frozen tumor sections were stained for blood vessels using rat anti mouse CD31 antibody (BD biosciences 1:25 dilution in PBS, pH 7.4) and goat anti rat-Alexa-488 secondary antibody for immunofluorescence (Jackson ImmunoResearch, 1:300 dilution in PBS, pH 7.4). Prior to antibodies incubation, slides were incubated with Peroxidase Block (Leica) for 5 min to quench endogenous peroxidase activity, followed by incubation with 10% of goat serum in PBS, pH 7.4 + 0.02% Tween 20 in PBS + 0.02% Gelatin in PBS, for 1 hour. The tissues were fixed and mounted on a glass microscope slide with a glass coverslip, and the nuclei were counterstained with ProLong™ Gold antifade reagent with DAPI (Invitrogen). Fluorescence images were captured using a fluorescence microscope (Evos FL Auto, life technologies) at 10x and 40x magnification. Lasers with emission wavelengths at 405, 525 and 555 nm were used to detect DAPI, Alexa-488 and -Cy3 labelled polyplexes. Untreated tumor was used as control.

3.2.29 Statistical Analysis

All the experiments were performed in triplicate, unless otherwise stated. Values are given as means ± s.e.m. Two-way ANOVA tests were used where appropriate. * $p < 0.05$, ** $p < 0.01$ or *** $p < 0.001$ were considered to be statistically significant.

3.3 Results

3.3.1 Synthesis of cationic polymers

The cationic polymers used in the present work are shown in Scheme 2.

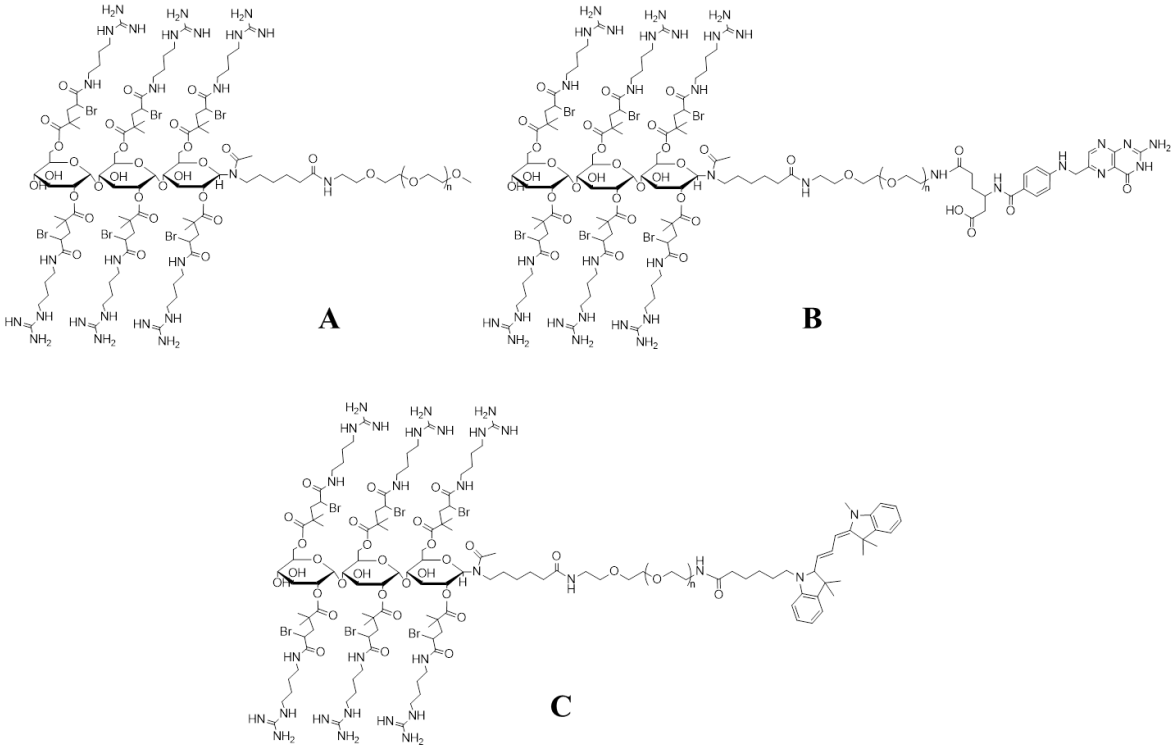

Scheme 2. Chemical structure of star-like polymers: $(agmatinyl)_6$-maltotriosyl-N-acetyl-amino-hexanoate-α-methoxy poly(ethylene glycol)$_{5kDa}$ (Agm_6-M-PEG, **A**), $(agmatinyl)_6$-maltotriosyl-N-acetyl-amino-hexanoate-poly(ethylene glycol)$_{6kDa}$-Folate (Agm_6-M-PEG-FA, **B**) and $(agmatinyl)_6$-maltotriosyl-N-acetyl-amino-hexanoate-poly(ethylene glycol)$_{6kDa}$-Cyanine3 (Agm_6-M-PEG-Cy3, **C**).

Agm_6-M-COOH and Agm_6-M-PEG were synthesized as described in the previous section. With the aim of generating a cationic polymer displaying a targeting agent, folic acid (FA) was activated with DCC/NHS and conjugated to linear 6 kDa bis-amino-polyethylene glycol PEG_{6kDa}-(NH_2).

The final conjugate was analyzed by MALDI-TOF analysis and UV-Vis spectroscopy with a yield of conjugation of 97%. The obtained Folate-PEG-NH_2 polymer was further conjugate with the cationic star-like head Agm_6-M-COOH. The reaction was carried out using EDC/NHS coupling agents and the UV-Vis analysis (ε_M = 6197 mol^{-1} cm^{-1})[162] of the final product showed a conjugation degree of 96% (Scheme 3).

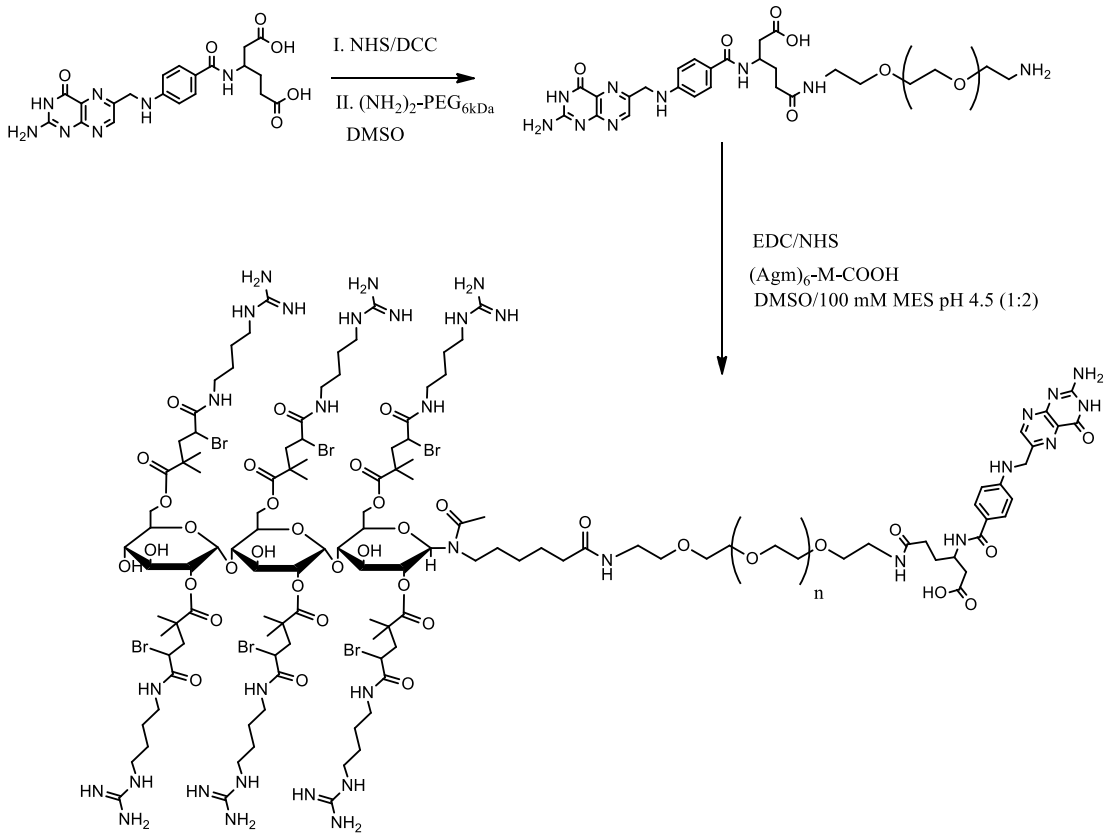

Scheme 3. Synthesis of (agmatinyl)$_6$-maltotriosyl-N-acetyl-amino-hexanoate-poly(ethylene glycol)$_{6kDa}$-Folate (Agm$_6$-M-PEG-FA).

The synthesis of Agm$_6$-M-PEG-Cy3 was carried out to track the polymer during the *in vitro* and *in vivo* experiments. Cyanine3 was conjugate to Agm-M-PEG-NH_2 via a standard coupling procedure and the polymer labelling degree, corresponding to the yield of conjugation, was measured by UV-Vis spectrophotometric analysis.

3.3.2 Physico-chemical characterization of folate and non-folate polyplexes

To efficiently deliver a shielded oligonucleotides, folate and non-folate polyplexes were prepared. The non-folate polyplexes were prepared using 100% of Agm$_6$-M-PEG polymer complexed with ONs. On the other hand, a mixture of 75:25 %w/w of Agm$_6$-M-PEG:Agm$_6$-M-PEG-FA polymers was used for ONs delivery.

The size of polyplexes was evaluated by dynamic light scattering (DLS) analysis and Agm$_6$-M-PEG/dsDNA polyplexes showed an hydrodynamic diameter of 75±5 nm (as described in the previous section). Similarly, 75:25 %w/w of Agm$_6$-M-PEG:Agm$_6$-M-PEG-FA/dsDNA polyplexes displayed a size diameter of 82±10 nm. The size of polyplexes was also investigated by TEM analysis (Figure 26) and in both preparations a rod-shape structure was observed indicating that the presence of 25% w/w of Agm$_6$-M-

PEG-FA polymer did not affect the shape neither the size of the polyplexes. The aspect ratio for the non-folate and folate polyplexes was similar (3.25±0.1 and 3.12±0.3 respectively).

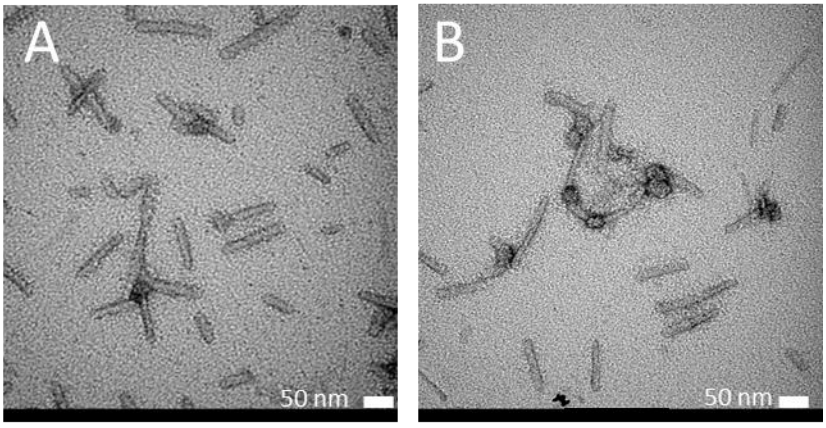

Figure 26. TEM images of (**A**) Agm_6-M-PEG/dsDNA polyplexes and (**B**) 75:25 Agm_6-M-PEG: Agm_6-M-PEG-FA/dsDNA. Both formulations were prepared in PBS buffer, pH 7.4 at 3 N/P ratio.

Gel electrophoresis was performed on Agm_6-M-PEG polymer to evaluate its ability to complex oligonucleotides. The study was performed using siRac1 oligonucleotides, a 19 pb siRNA. 50 pmoles of siRNA were incubated with increasing concentrations of Agm_6-M-PEG polymer to yield polyplexes ranging from 0.5 to 5 N/P ratios.

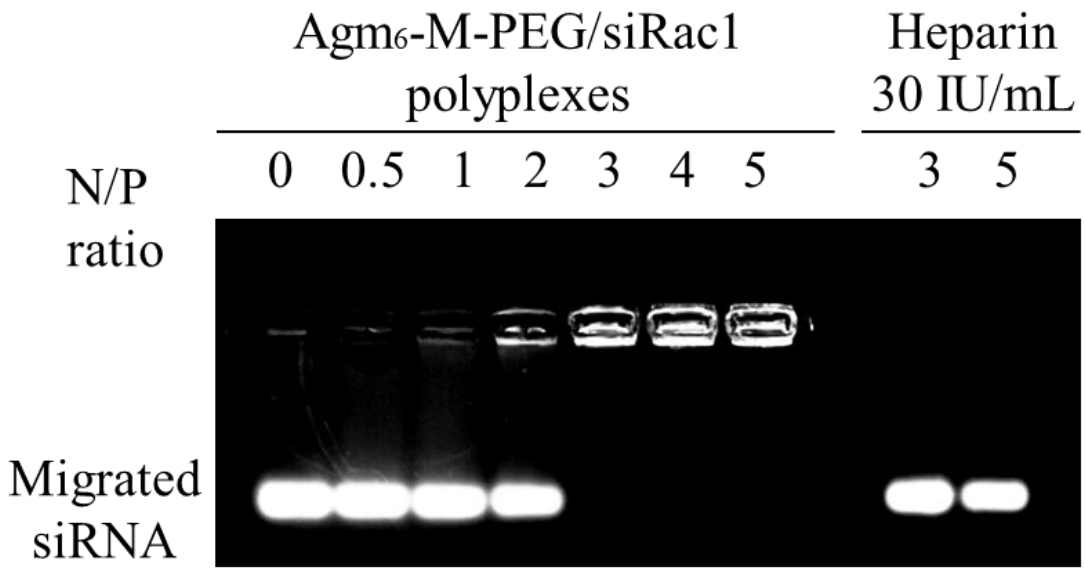

Figure 27. Electrophoresis mobility shift analysis of Agm_6-M-PEG escalating concentrations (0.11-1.1 mg/mL) complexed with siRac1 at fixed concentration (4.16 μM in PBS, pH 7.4) to achieve different nitrogen/phosphorus (N/P) ratios.

The electrophoretic chromatography was performed using 2% agarose gel in TAE running buffer and the siRNA migration was visualized by staining the migrated oligonucleotides with ethidium bromide. Complete retardation of siRNA mobility was observed at N/P ratio of 3:1 and above (Figure 2), suggesting the total complexation of siRNA as indicated by the inhibition of its migration.

3.3.3 Agm_6-M-PEG/siRac1 polyplexes possess good plasma stability and high biocompatibility in ex vivo studies

In order to evaluate the interaction strength between the cationic polymer Agm_6-M-PEG and the oligonucleotides (ONs) for the *in vivo* applicability of the system, Agm_6-M-PEG/siRNA polyplexes at 3 and 5 N/P ratio were incubated in the presence of increasing concentration of heparin (0-15 IU/mL) (Figure 28). The results showed that for both the N/P ratios in analysis, a total siRNA displacement was observed above a heparin concentration of 2.5 UI/mL, which is about 16-times higher with respect to the physiological heparin concentration in the blood.

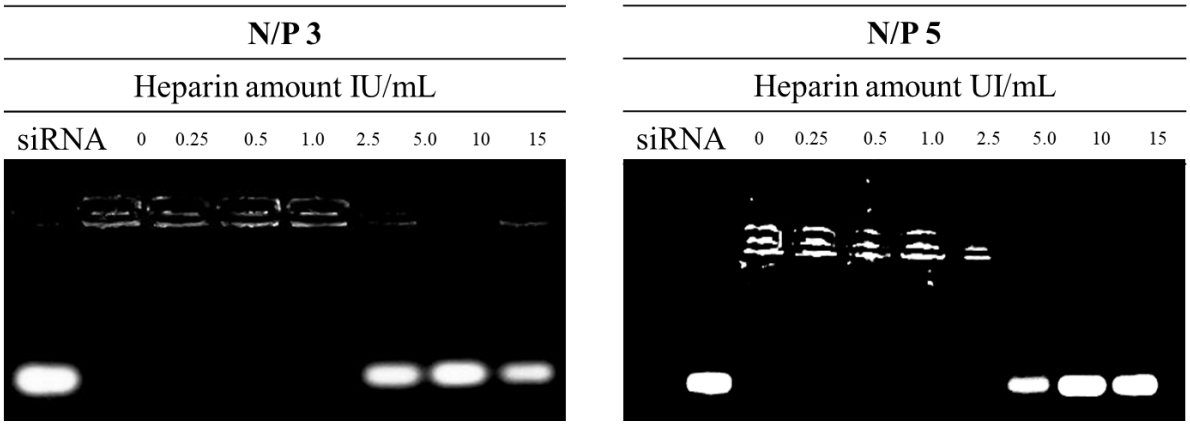

Figure 28. Heparin displacement assay with Agm_6-M-PEG/siRac1polyplexes at 3 and 5 N/P ratios.

Further investigations were performed to test the ability of Agm_6-M-PEG/siRNA polyplexes at 3 and 5 N/P ratios to preserve the degradation of siRNA by RNAses enzyme in 100% mouse serum. Samples at 3 and 5 N/P ratios were incubated at 37°C in plasma and at scheduled time points the ability of the polymer to remain associated with the ONs and the integrity of siRNA was assessed by agarose gel electrophoresis. A good stability for both the formulations up to 8 hours was observed, as shown in Figure 29.

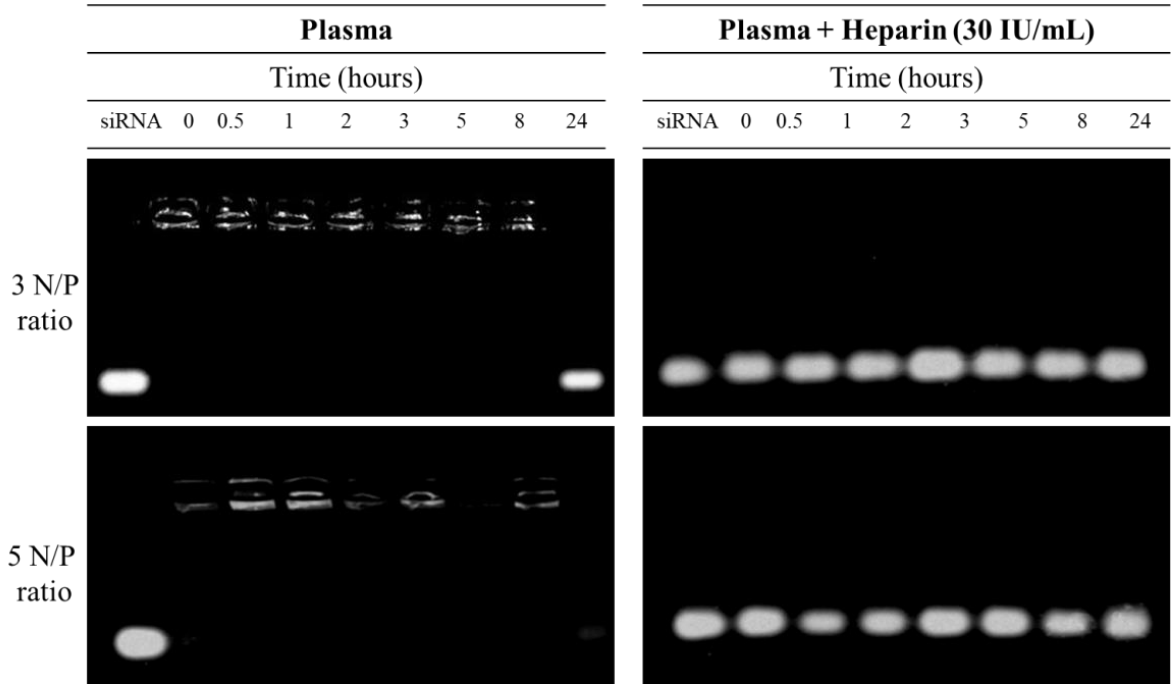

Figure 29. Plasma stability of Agm_6-M-PEG/siRac1 polyplexes at 3 and 5 N/P ratios. The integrity of siRac1 was evaluated by 30 UI/mL heparin addition.

The hemo-toxicity of Agm_6-M-PEG/siRNA polyplexes at 3 and 5 N/P ratios was assessed by measuring red blood cells (RBCs) lysis. The polyplexes concentrations used were the same adopted for the *in vivo* applications, adjusted to dilution in the mouse blood volume. The results reported in Figure 30 show that the extent of hemolysis deriving from the RBCs incubation with polyplexes is negligible and comparable to those of the negative controls – i.e. PBS and Dextran.

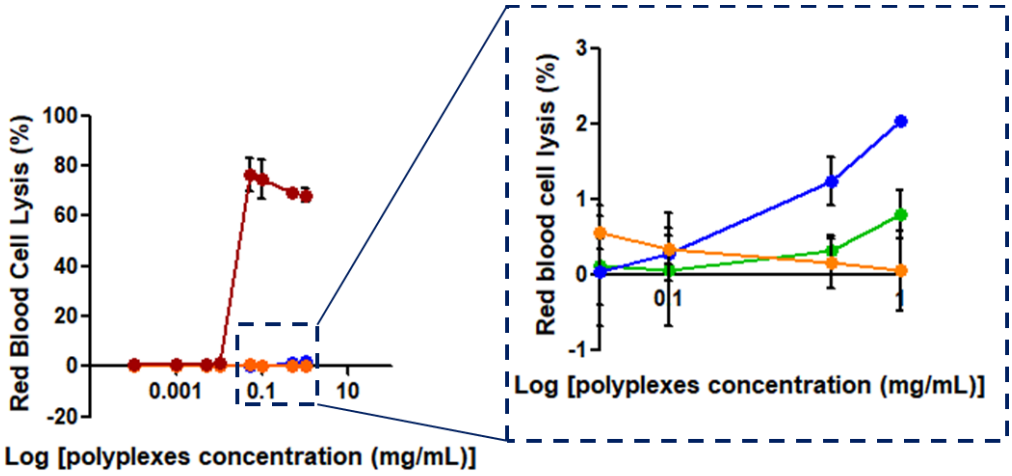

Figure 30. Hemolysis test of Agm_6-M-PEG:siRac1 polyplexes at 3 (green line) and 5 (blu line) N/P ratio tested at increasing concentrations. Dextran (orange line) and Sodium Dodecyl Sulfate (SDS) (brown line) were used as negative and positive control, respectively.

3.3.4 Folate binding receptors studies reveal a high expression of folic acid receptors on MDA-MB-231.

A screening study of the folate receptor (FR) expression on different cell lines was performed to select the best model for *in vitro* and *in vivo* studies. In particular, we focused our attention on two cancer types: melanoma and breast cancer. The FR expression was investigated by competitive studies according to a validated protocol[164]. After 3 hours of incubation with tritiated folic acid ([^{3}H]FA), the cells were lysed in 0.1 M NaOH and the disintegration per minute (DPM) was measured. The study highlighted that MDA-MB-231 cell line highly express the FR (Figure 31) in presence or absence of FA in the growth medium. A significant expression of the receptor was also observed in HeLa cells independently of the growing conditions, while HUVEC, that were found to have a very low expression of the folate receptor, were selected as negative control. For these reasons, MDA-MB-231 were identified as the best model for all the following studies.

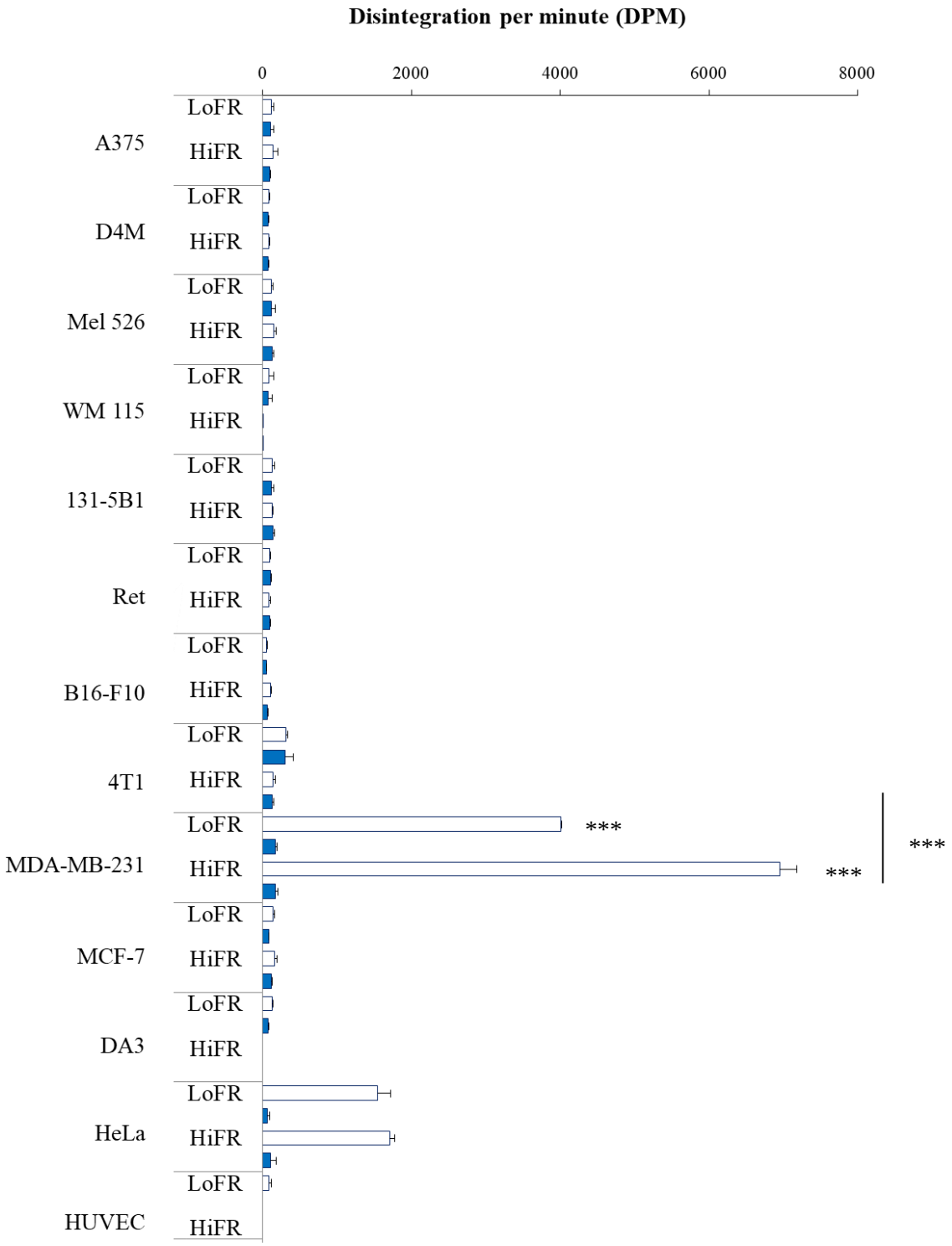

Figure 31. Folic acid receptor expression in melanoma and breast cancer cells. Selected cell lines were growth in presence (LoFR) or absence (HiFR) of folic acid to induce the overexpression on FR. The cells were incubated with 0.2 µM [3H]FA alone ( ) or in competition with non-radiolabelled FA ( ). Among the cell lines in analysis, only the MDA-MB-231 cell lines showed high [3H]FA internalization. The intracellular radioactivity dramatically decreased when the MDA-MB-231 cells were treated with FA, competing on the binding to the FR. HeLa and HUVEC cells were used as positive and negative controls.

3.3.5 Rac1 gene knockdown activity of folate and non-folate polyplexes.

The ability of the folate and non-folate polyplexes to silence selective oncogenes was tested on HeLa and MDA-MB-231 cell lines using siRac1 as therapeutic ON. As described elsewhere, Rac1 gene is involved in migration, invasion and metastatic processes[3]. The *in vitro* silencing of Rac1 gene was performed using PSICHECK method as described by Polyak et al.[167]. A preliminary screening was performed using folate polyplexes with increasing amount of Agm_6-M-PEG-FA content (Figure 32).

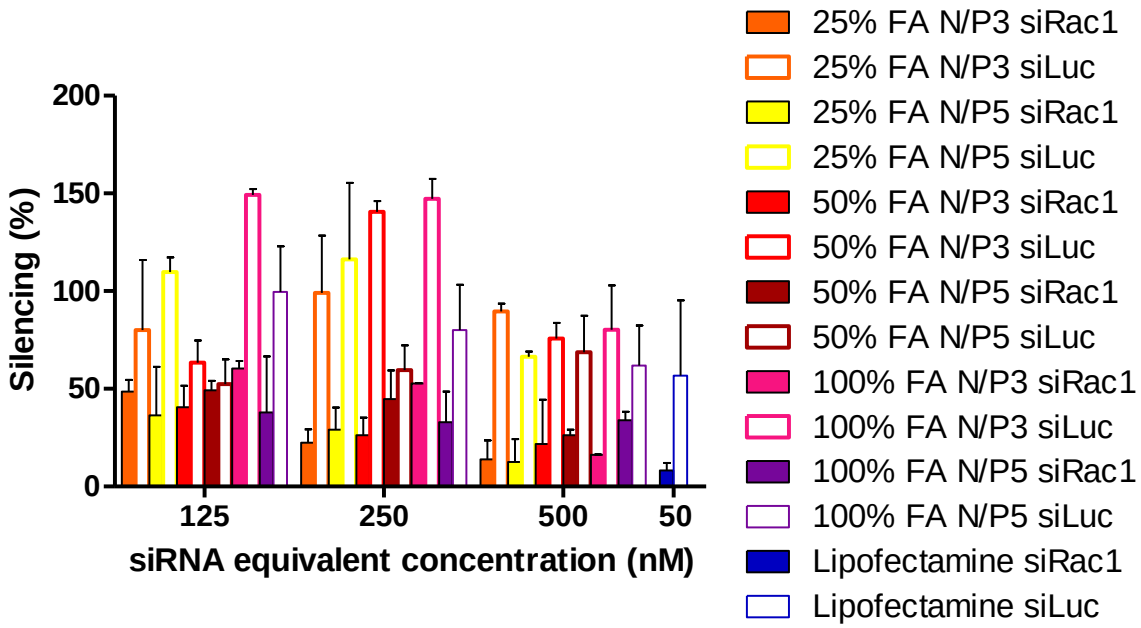

Figure 32. Silencing Rac1 gene study on HeLa cells using polyplexes bearing different percentage of FA.

The better results in terms of Rac1 gene knockdown, silencing specificity and cytotoxicity were obtained using 75:25 %w/w Agm_6-M-PEG:Agm_6-M-PEG-FA/siRac1 formulation that was therefore selected for dose-response studies. siLuc was used as scramble oligonucleotide in order to evaluate the specificity of the oligonucleotide delivery system when incubated with cells at 125, 250 and 500 nM siRNA equivalent doses for 72 hours.
The results displayed in Figure 8 showed that both 75:25 %w/w Agm_6-M-PEG:Agm_6-M-PEG-FA/siRac1 and Agm_6-M-PEG/siRac1 polyplexes showed a dose-dependent Rac1 gene silencing in both the cell lines used. Notably, in HeLa cells 75:25 %w/w Agm_6-M-PEG:Agm_6-M-PEG-FA/siRac1 showed a 86% gene silencing, about two folds higher compared to Agm_6-M-PEG/siRac1 polyplexes (54% gene silencing), as reported in Figure 33A. In a similar manner, the Rac1 silencing on MDA-MB-231 showed a higher silencing with folate in comparison to non-folate polyplexes, with a siRNA dose-dependent response for the folate-targeted system (Figure 33B).

A)

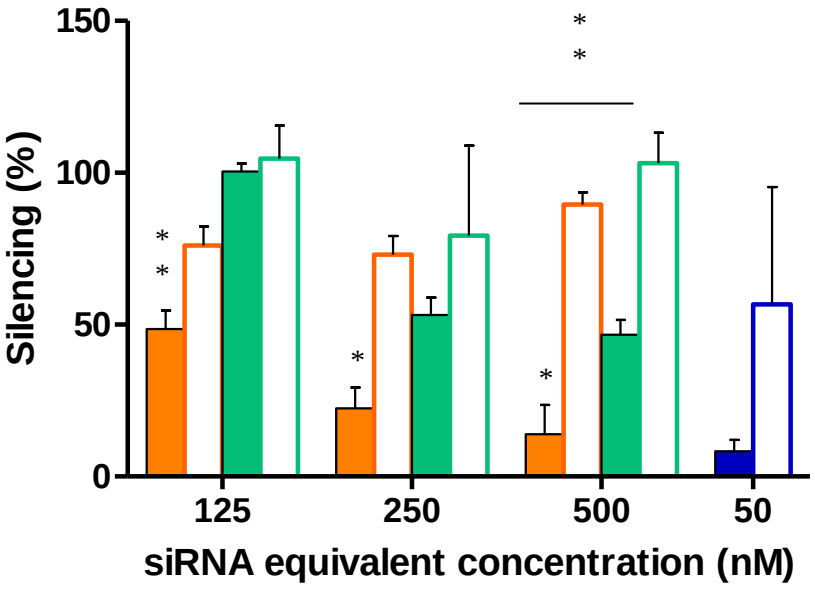

B)

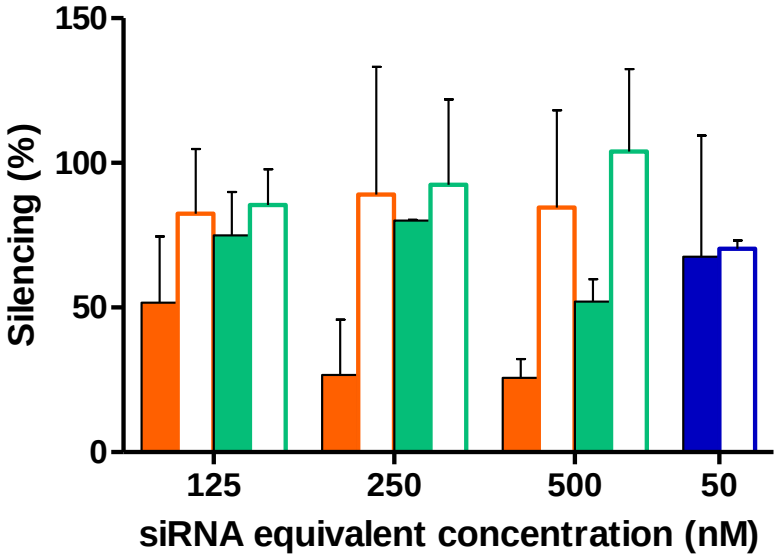

Figure 33. Silencing study of Rac1 in HeLa (A) and MDA-MB-231 (B) cells. 75:25 %w/w Agm_6-M-PEG:Agm_6-M-PEG-FA/siRac1 ( ) and Agm_6-M-PEG/siRac1 ( ) polyplexes were incubated with cells for 72 h and the final gene knockdown was measured. Lipofectamine/siRac1 ( ) was used as commercial standard. 75:25 %w/w Agm_6-M-PEG:Agm_6-M-PEG-FA/siRac1 ( ), Agm_6-M-PEG/siRac1 ( ) polyplexes and Lipofectamine/siLuc ( ) were used as control.

The gene silencing efficiency of 75:25 %w/w Agm_6-M-PEG:Agm_6-M-PEG-FA/siRac1 and Agm_6-M-PEG/siRac1 polyplexes was also evaluated by wound healing assay on MDA-

MB-231 cell line. In this study the ability to inhibit the cell migration was assessed. A scratch was apply after complete confluence of the MDA-MB-231 cells in wells was achieved and the gap closure of MDA-MB-231 cell line was observed after treatment with 75:25 Agm_6-M-PEG-FA:Agm_6-M-PEG:siRac1 polyplexes at 3 N/P ratio. The toxicity of both formulations was performed after 72 hours of incubation of targeted and non-targeted polyplexes on HeLa and MDA-MB-231 cells. The results indicated a good biocompatibility of the polyplexes.

A)

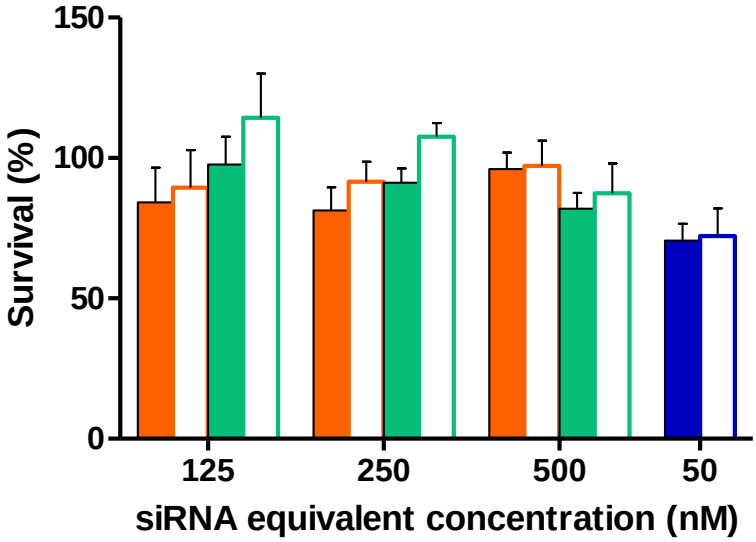

B)

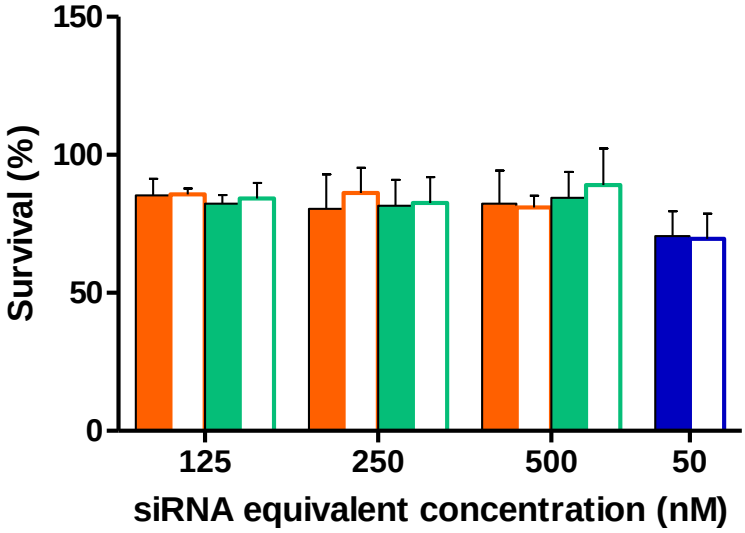

Figure 34. MTT study on HeLa (**A**) and MDA-MB-231 (**B**) cells. 75:25 %w/w Agm_6-M-PEG: Agm_6-M-PEG-FA/siRac1 ( ) and Agm_6-M-PEG/siRac1 ( ) polyplexes were incubated with cells for 72 h and the cell

viability was assessed. Lipofectamine/siRac1 ( ) was used as commercial standard. 75:25 %w/w Agm_6-M-PEG: Agm_6-M-PEG-FA/siRac1 ( ) and Agm_6-M-PEG/siRac1 ( ) polyplexes and Lipofectamine/siLuc ( ) were used as control.

Figure 35 shows a 40% inhibition of the cell migration after 12 hours using a 500 nM of siRNA equivalent dose. On the contrary, the inhibition of cell migration obtained with Agm_6-M-PEG:siRac1 polyplexes at 3 N/P ratio was less than 10%.

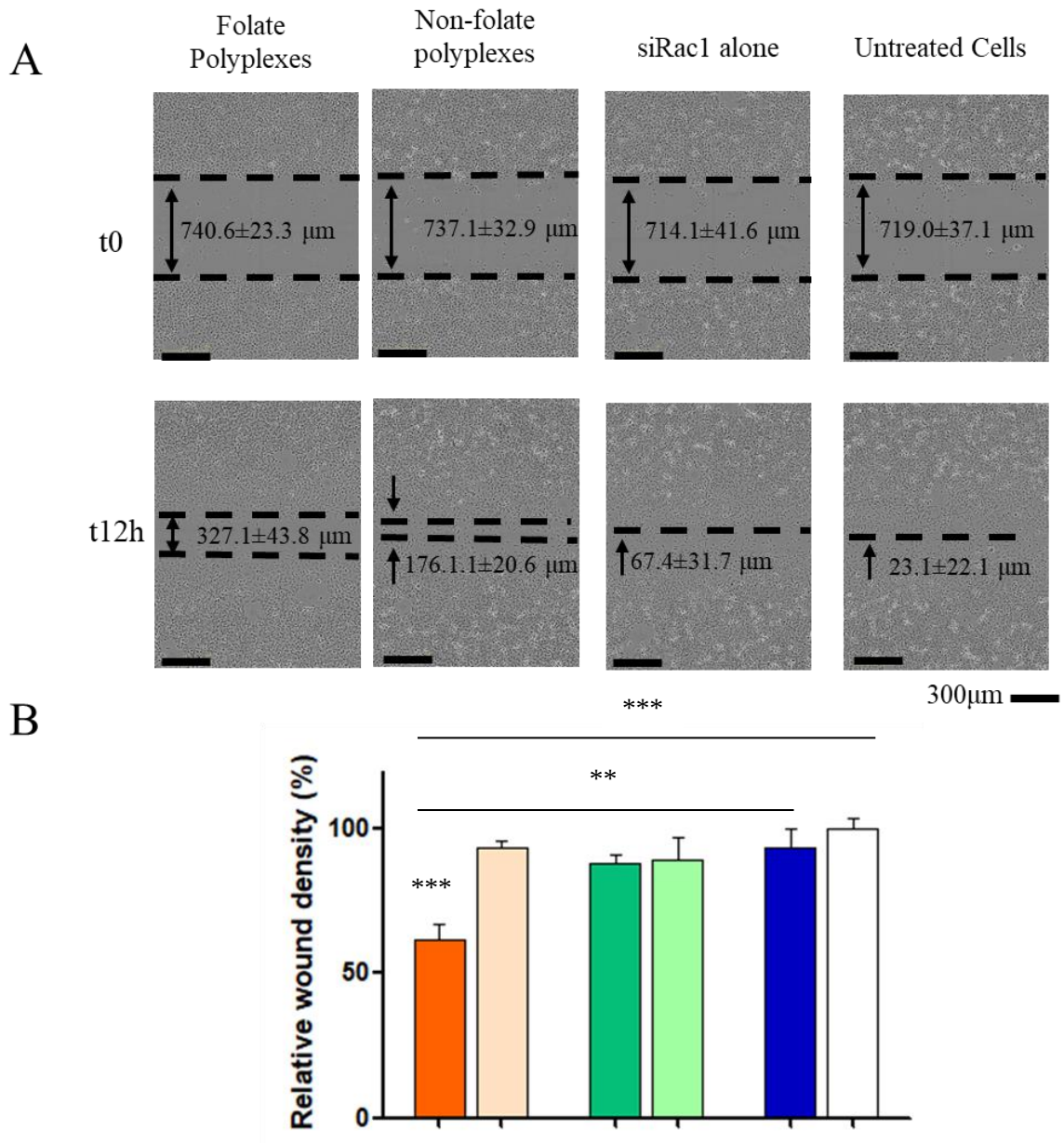

Figure 35. Wound healing closure of MDA-MB-231 cells treated with various polyplexes. In figure A, representative images of wound closure and in figure B, relative wound density quantification after 12 hours cells treatment with 75:25 %w/w Agm_6-M-PEG:Agm_6-M-PEG-FA/siRac1 ( ), 75:25 %w/w Agm_6-M-PEG:Agm_6-M-PEG-FA:siLuc ( ), Agm_6-M-PEG/siRac1 ( ) and Agm_6-M-PEG/siLuc ( ) polyplexes. siRac1 alone ( ) and untreated cells ( ) were used as controls.

3.3.6 Folate and non-folate polyplexes show the same cell uptake but different intracellular fate and low competition between free folic acid and folate polyplexes.

Cell uptake of Agm_6-M-PEG/siRac1and 75:25 %w/w Agm_6-M-PEG:Agm_6-M-PEG-FA/siRac1 polyplexes was evaluate by Imagestream analysis and confocal microscopy observation through the addition to the formulation of the labelled polymer Agm_6-M-PEG-Cy3. 99:1 w/w% Agm_6-M-PEG:Agm_6-M-PEG-Cy3/siRac1and 74:25:1 %w/w Agm_6-M-PEG:Agm_6-M-PEG-FA:Agm_6-M-PEG-Cy3/siRac1 polyplexes were incubated with MDA-MB-231 cells and the uptake was measured at scheduled time points. The Imagestream graph (Figure 36) showed a progressive uptake of folate and non-folate polyplexes, with the global fluorescence exponentially increasing from 5 min to 6 h and 24 h of incubation. No significant differences were observed between folate and non-folate polyplexes.

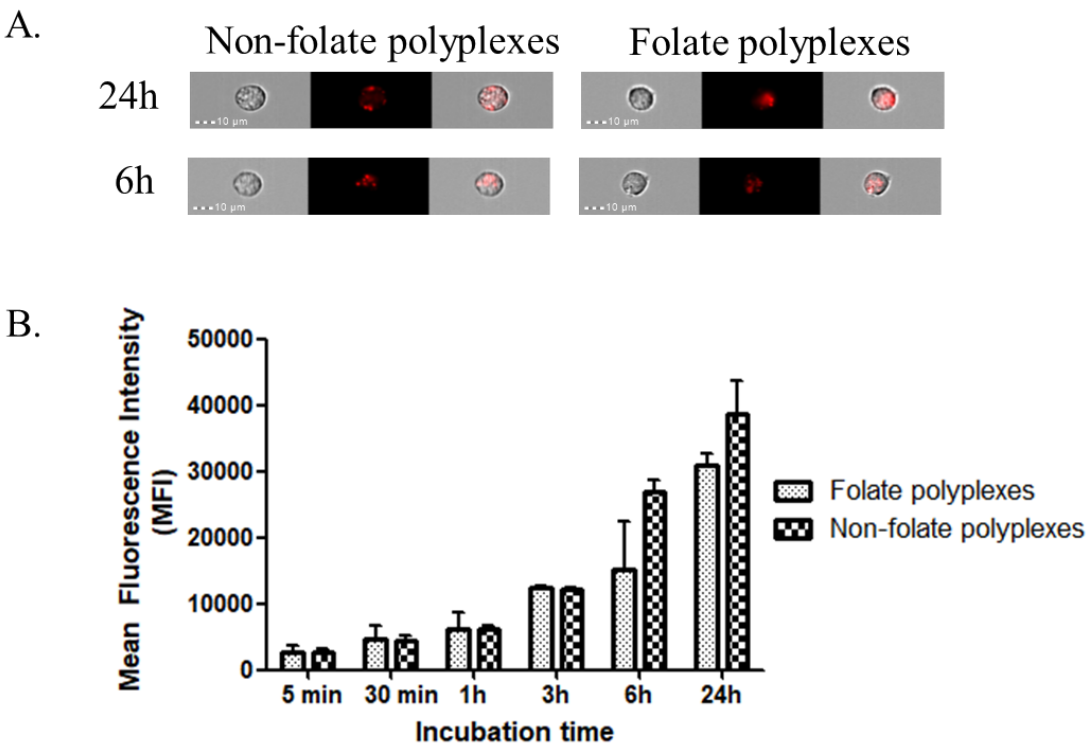

Figure 36. Imagestream analysis of 99:1 w/w% Agm_6-M-PEG:Agm_6-M-PEG-Cy3/siRac1 (non-folate polyplexes) and 74:25:1 %w/w Agm_6-M-PEG:Agm_6-M-PEG-FA:Agm_6-M-PEG-Cy3/siRac1 polyplexes (folate polyplexes). In panel A. representative images of non-folate and folate polyplexes uptake are reported. In panel B. the MDA-MB-231 intracellular uptake quantification at different time points for non-folate and folate polyplexes is shown.

99:1 w/w% Agm_6-M-PEG:Agm_6-M-PEG-Cy3/siRac1 and 74:25:1 %w/w Agm_6-M-PEG:Agm_6-M-PEG-FA:Agm_6-M-PEG-Cy3/siRac1 polyplexes uptake was also evaluated

by confocal microscopy performed on MDA-MB-231 cells by incubation with folate and non-folate polyplexes for 6 and 24 hours (Figure 37).

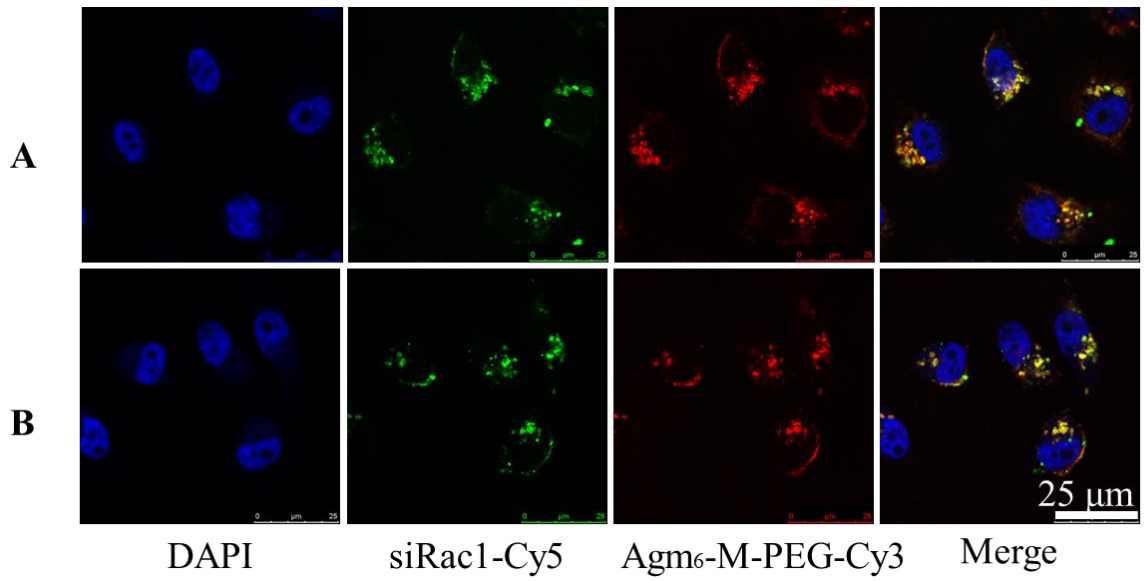

Figure 37. Confocal analysis of MDA-MB-231 cells incubated with 74:25:1 %w/w Agm_6-M-PEG:Agm_6-M-PEG-FA:Agm_6-M-PEG-Cy3/siRac1 polyplexes (A) and 99:1 %w/w Agm_6-M-PEG:Agm_6-M-PEG-Cy3/siRac1 polyplexes (B). Single XY plane imaging of Agm_6-M-PEG-Cy3 (■), Cy5-siRac1 (■) and DAPI (■) nuclei staining showed cytoplasmatic accumulation of the polyplexes after 24 h of incubation. Merged images showed a good co-localization of the polymer and siRNA. Scale bar is 25 µm.

A relevant intracellular uptake was detected corresponding to a significant fluorescence signal observed in the cytoplasm. For both formulations, the images showed an increasing overlap of Agm_6-M-PEG-Cy3 and siRac1-Cy5 signals over time. Despite the presence of the targeting agent, folate polyplexes revealed a very similar uptake to the non-folate ones.
The ability of folate-polyplexes to bind FR on MDA-MB-231 cell membrane surface was assessed by free folic acid competition assay. Folate-polyplexes prepared with increasing concentration of Agm_6-M-PEG-FA in the range of 0-100% were tested. The result showed that no receptor occupation was found for all the polyplexes studied (Figure 38).

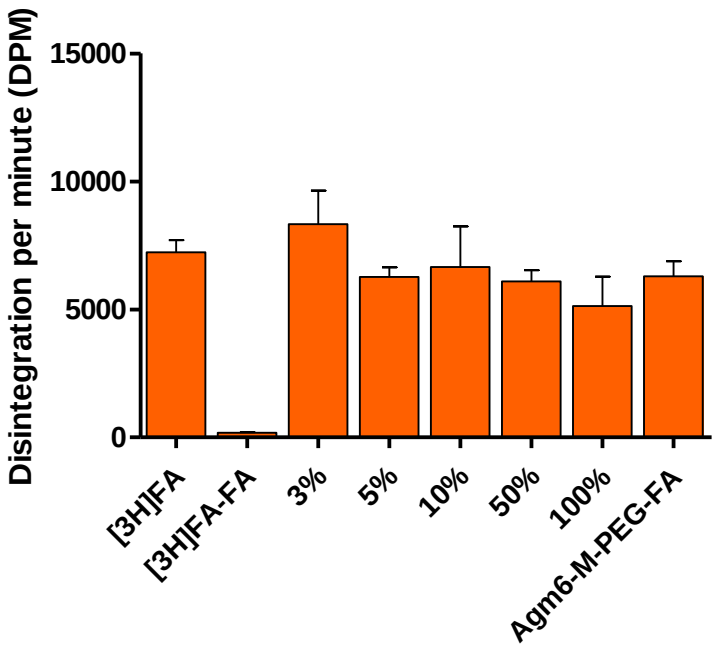

Figure 38. Polyplexes bearing folic acid ability to bind folic acid receptor displayed on MDA-MB-231 cell surface. Polyplexes decorated with 3%, 5%, 10%, 50%, 100% of Agm6-M-PEG-FA or Agm6-M-PEG-FA alone were incubated for 3 hours with MDA-MB-231 cells in FF-RPMI. Afterwards, tritiated FA was added and the radioactivity was measured. MDA-MB-231 incubated only with tritiated folic acid ([3H]FA) or with non-radioactive folic acid ([3H]FA-FA) were used as control.

3.3.7 Different endocytotic portal and intracellular fate was observed for folate and non-folate polyplexes

The intracellular trafficking of Agm_6-M-PEG/siRac1-Cy5 and 75:25 %w/w Agm_6-M-PEG:Agm_6-M-PEG-FA/siRac1-Cy5 polyplexes in MDA-MB-231 cells was assessed by immunofluorescence analysis. Early endosomes were stained with anti-EEA1 (Early Endosomes Antigen-1) using a secondary antibody labelled with rhodamine. At the same time, lysosomes were stained with rabbit anti-LAMP-1 (Lysosomal-associated membrane protein-1) and a secondary antibody labelled with Alexa Fluor®488. Folate and non-folate polyplexes localization was observed after 3 and 24 hours of incubation. The images in Figure 39 show a high internalization of non-folate polyplexes into the early endosomes (EEA-1) after 3 hours of incubation. After 24 hours, full colocalization of Agm_6-M-PEG/siRac1-Cy5 in lysosomes (LAMP-1) was detected.

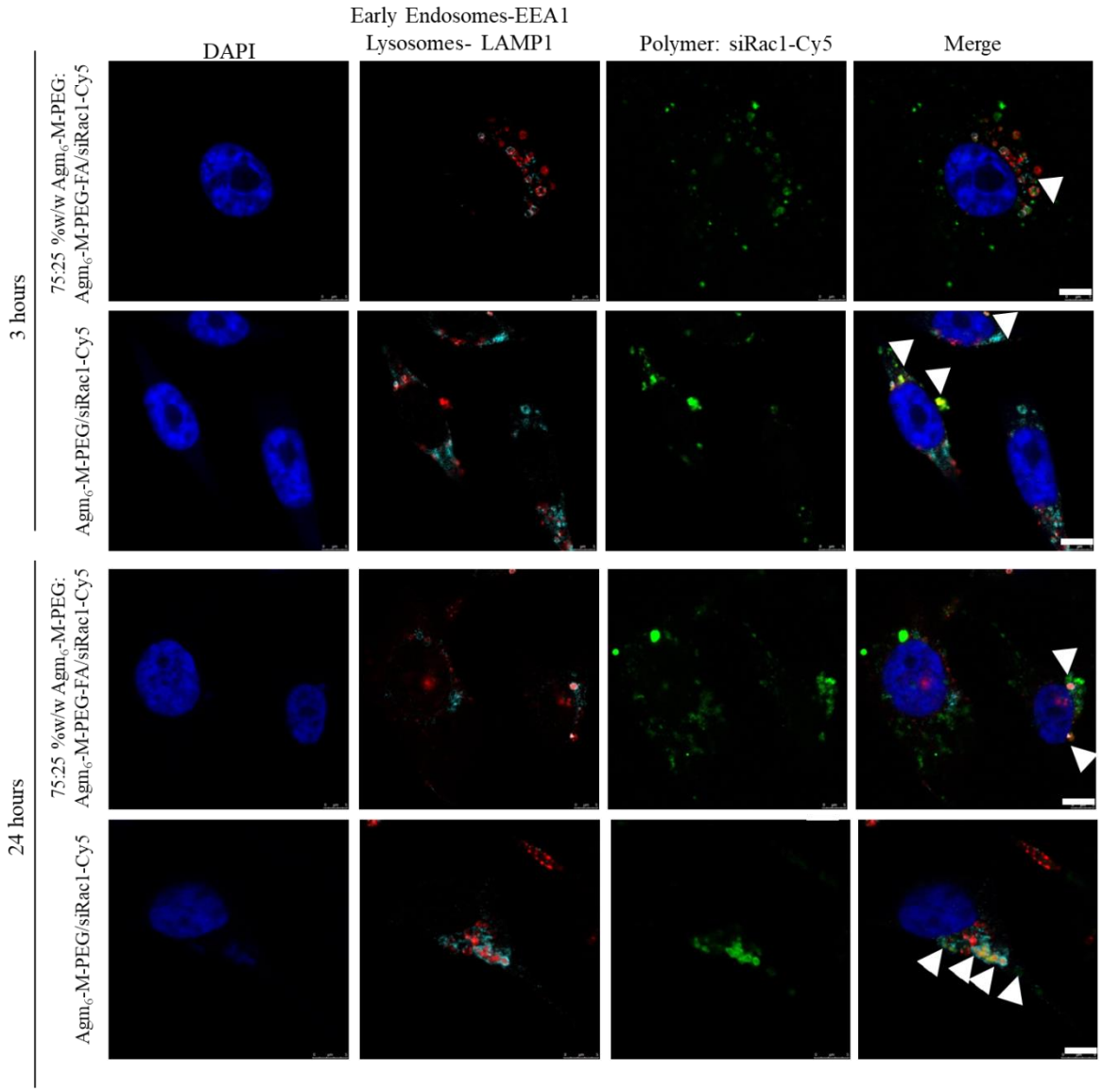

Figure 39. Co-localization studies of Agm_6-M-PEG/siRac1-Cy5 and 75:25 %w/w Agm_6-M-PEG:Agm_6-M-PEG-FA/siRac1-Cy5 polyplexes in MDA-MB-231 cells after 3 and 24 hours of incubation. Cells were stained for early endosomes ( ) and lysosomes ( ). Polyplexes were labelled using siRac1-Cy5 ( ). Nuclei were stained with DAPI ( ). The scale bar is 5 μm.

Most of the signal related to non-folate polyplexes was found to be similarly associated with the early endosomes or lysosomes at all the time points analyzed. Conversely, after 3 hours of incubation folate-polyplexes showed a lower association with the endosomes and only limited traces of lysosomes colocalization. After 24 hours, a negligible colocalization of 75:25 %w/w Agm_6-M-PEG:Agm_6-M-PEG-FA/siRac1-Cy5 polyplexes into lysosomes or endosomes was observed. Most of the fluorescent signal related to 75:25 %w/w Agm_6-M-PEG:Agm_6-M-PEG-FA/siRac1-Cy5 polyplexes appeared into the cytosol after 24 hours of incubation.

To further investigate the intracellular pathway of folate and non-folate polyplexes, MDA-MB- 231 cells were incubated with Agm_6-M-PEG/siRac1-Cy5 or 75:25 %w/w Agm_6-M-PEG:Agm_6-M-PEG-FA/siRac1-Cy5 polyplexes for 3 hours and cells were stained for caveolae and clathrin. Caveolae were detected with mouse anti caveolin-1 (anti Cav-1) and clathrin with rabbit anti clathrin heavy chain antibody (anti-CHC) marked with rhodamine and Alexa Fluor® 488, respectively. Agm_6-M-PEG/siRac1-Cy5 co-localized mainly with clathrin suggesting that non-targeted polyplexes were internalized by a clathrin-mediated process. Conversely, 75:25 %w/w Agm_6-M-PEG:Agm_6-M-PEG-FA/siRac1-Cy5 polyplexes showed a good colocalization in caveolae suggesting an endocytosis predominately caveolae-mediated (Figure 40). FA-PEG-Cy5.5 was also tested as control and it showed a significant colocalization with clathrin indicating that the folate targeted polymer is likely to enter the cells through a clathrin-mediated pathway These results, suggest an effect of cationic moiety on the internalization in cells.

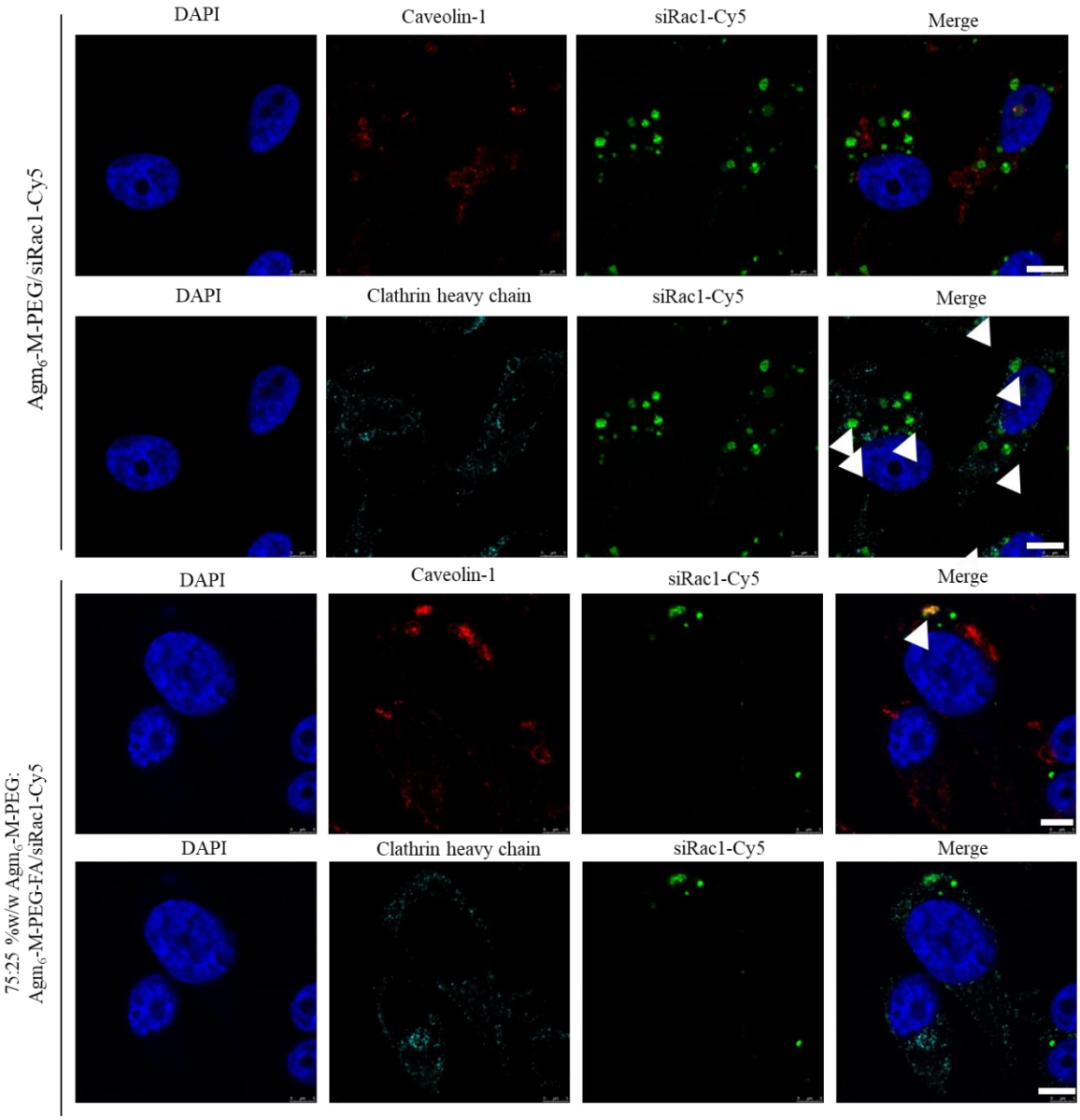

Figure 40. Intracellular trafficking study of Agm_6-M-PEG/siRac1-Cy5 and 75:25 %w/w Agm_6-M-PEG:Agm_6-M-PEG-FA/siRac1-Cy5 polyplexes in MDA-MB-231 cells. Cells were treated with polyplexes at the N/P ratio of 3 using 200 nM concentration of siRac1-Cy5 (■). Colocalization with caveolin-1 (■) and clathrin heavy chain (■) was observed after 3 hours of incubation. Nuclei were stained with DAPI (■). The scale bar is 5 μm.

3.3.8 Folate and non-folate polyplexes do not induce immuno-stimulation.

TNF-α release from PBMCs was evaluated by incubation of Agm_6-M-PEG/siRac1 or 75:25 %w/w Agm_6-M-PEG:Agm_6-M-PEG-FA/siRac1 polyplexes prepared at 3 N/P ratio, Agm_6-M-PEG or 75:25 %w/w Agm_6-M-PEG:Agm_6-M-PEG-FA polymers or siRac1 alone with isolated PBMCs (Figure 41). This assay was performed in collaboration with Dr. Anna Scomparin from Tel Aviv University. The cells were treated with 125 or 250 nM

siRNA equivalent doses. Results showed a dose dependent response of Agm_6-M-PEG/siRac1 or 75:25 %w/w Agm_6-M-PEG:Agm_6-M-PEG-FA/siRac1 polyplexes. Low TNF-α release was detected for both polymers alone. These evidences confirm the polyplexes safety and makes them suitable candidates for the i.v. administration route.

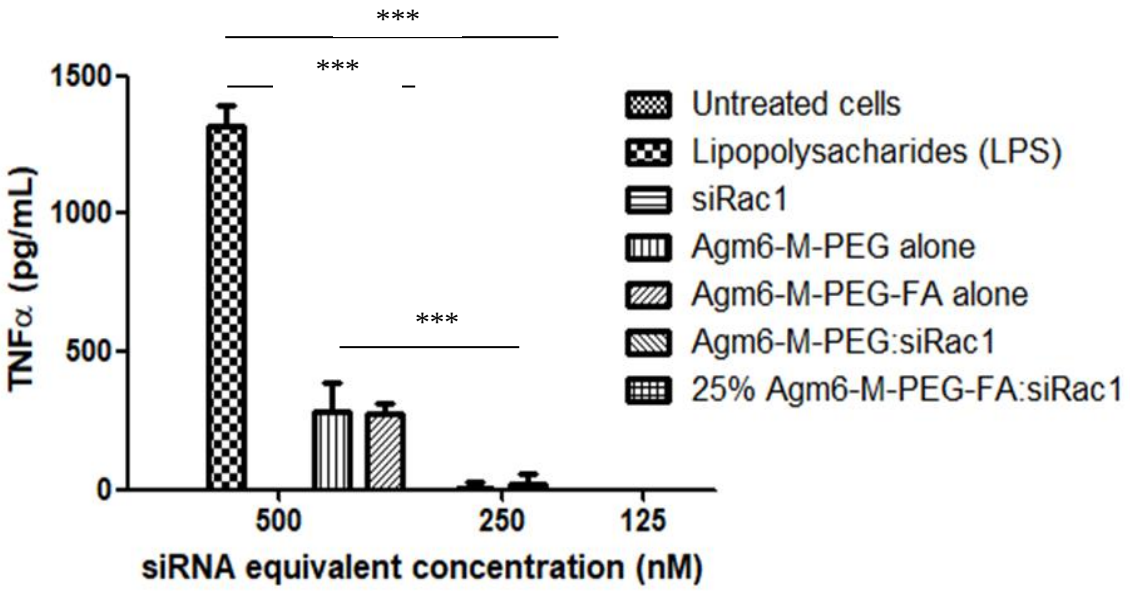

Figure 41. TNF-α cytokine secretion from human peripheral blood mononuclear cells following 12 h incubation with Agm_6-M-PEG or 75:25 %w/w Agm_6-M-PEG:Agm_6-M-PEG-FA polymers alone or complexed with siRNA. Cells were treated with 125 nM or 250 nM of siRNA equivalent dose. TNF-α cytokine secretion related to oligonucleotide sequence was also tested.

3.3.9 *In vivo* administration of 75:25 %w/w Agm_6-M-PEG:Agm_6-M-PEG-FA/siRac1 polyplexes show no toxicity and high siRac1 tumor accumulation.

The intravenous toxicity of Agm_6-M-PEG/siRac1 and 75:25 %w/w Agm_6-M-PEG:Agm_6-M-PEG-FA/siRac1 polyplexes at 3 N/P ratio and siRNA concentration ranging from 1 to 6 mg/kg was evaluated on Nu/Nu female mice (dosing volume of 100 μL/mouse). Mice were monitored for up to 7 days post injection. A stepwise escalation dose was performed consisting on a single administration in order to establish a Maximum Tolerated Dose (MTD) in the short-term. No toxicity was found for all the doses used for both the formulations (Table 1).

Table 1. Determination of maximum tolerated dose (MTD). Nu/nu mice were administered with single i.v. injection of Agm_6-M-PEG/siRac1 and 75:25 %w/w Agm_6-M-PEG:Agm_6-M-PEG-FA/siRac1 polyplexes at 3 N/P ratio, at siRNA-equivalent concentration of 1-6 mg/kg, and monitored during 7 days post injection.

siRNA dose (mg/Kg)	75:25 %w/w Agm_6-M-PEG:Agm_6-M-PEG-FA/siRac1 survival	Agm_6-M-PEG/siRac1 survival
1	+	+
2	+	+
4	+	+
6	+	+

On the basis of the *in vitro* results, showing that non-folate polyplexes possess low gene knockdown efficacy, all the *in vivo* studies were performed using only the targeted formulation by intravenous administration in nude female mice bearing an orthotopic MDA-MB-231 human adenocarcinoma. The tumor accumulation of the 75:25 %w/w Agm_6-M-PEG:Agm_6-M-PEG-FA/siRac1 polyplexes (4 mg/kg siRac1 equivalent dose) was performed by 3 sequential i.v. administration (24 hours interval) in Nu/Nu mice bearing intra-mammary tumors. Mice were euthanized 24 hours following the last injection and the tumors were collected for analysis. siRac1 levels were measured by RT-PCR and results indicated ~500-fold and ~65-fold increase in Rac1 siRNA tumor accumulation following treatment with 75:25 %w/w Agm_6-M-PEG:Agm_6-M-PEG-FA/siRac1 polyplexes with respect to saline or scramble siRNA (siEGFP) treatments, respectively.

The biodistribution of folate-polyplexes was performed by labelling polyplexes with 15% w/w Agm_6-M-PEG-Cy3. 60:25:15 %w/w Agm_6-M-PEG:Agm_6-M-PEG-FA:Agm_6-M-PEG-Cy3/siRac1 polyplexes were i.v. administered and at scheduled times (30 min, 3 hours and 6 hours) Nu/Nu mice bearing MDA-MB-231 tumors were sacrificed.

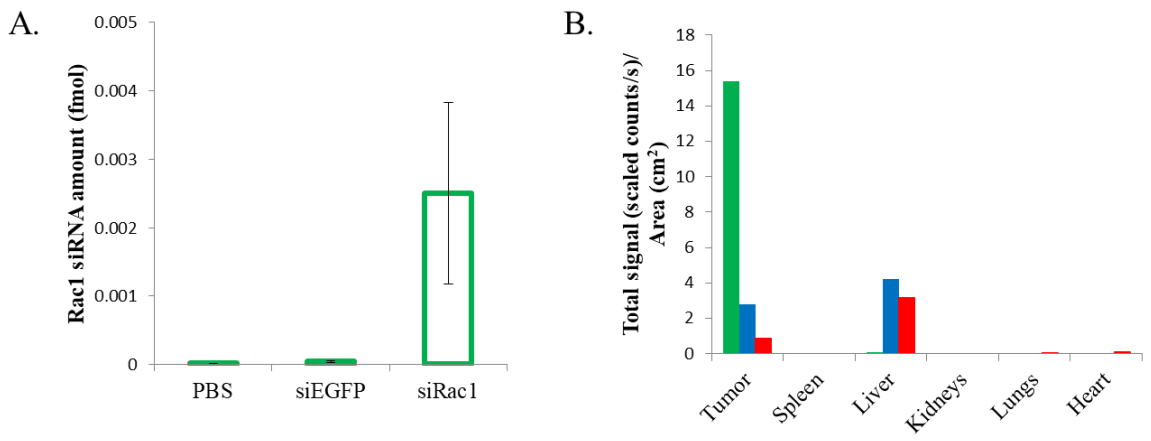

Figure 42. A. 75:25 %w/w Agm_6-M-PEG:Agm_6-M-PEG-FA/siRac1 polyplexes (4 mg/kg siRac1 equivalent dose) showed high tumor accumulation following systemic administration into orthotopic MDA-MB-231 tumor bearing mice; PBS and 75:25 %w/w Agm_6-M-PEG:Agm_6-M-PEG-FA/siEGFP polyplexes were used as control. B. Biodistribution of 60:25:15 %w/w Agm_6-M-PEG:Agm_6-M-PEG-FA:Agm_6-M-PEG-Cy3/siEGFP polyplexes following systemic administration. Quantification of the fluorescent signal obtained from organs collected at 0.5 ( ), 3 ( ) and 6( ) hours post-injection (i.v.).

The results showed high accumulation of polyplexes into the tumor at 30 min after administration. The signal is still quite significant at 3 and 6 hours post-injection, thus suggesting the permanence of the polyplexes in the tumor tissue. Polyplexes were also found in the liver at 3 and 6 hours after the administration with a peak of concentration at the 3 hours. No relevant fluorescence signals due to the polyplexes were detected in the heart, lungs, spleen and kidneys. These results indicate a good biodistribution profile for the folate-polyplexes and a significant accumulation into the tumor tissue which is maintained over time.

Tumor analyzed for biodistibution purposes, were exported and a histological investigations was performed. This study, was done in collaboration with Dr. Sabina Pozzi from Tel Aviv University. Slides were stained with DAPI (nuclei) and CD31-FITC (vessels). Histological studies display a good intratumor polymer accumulation over time.

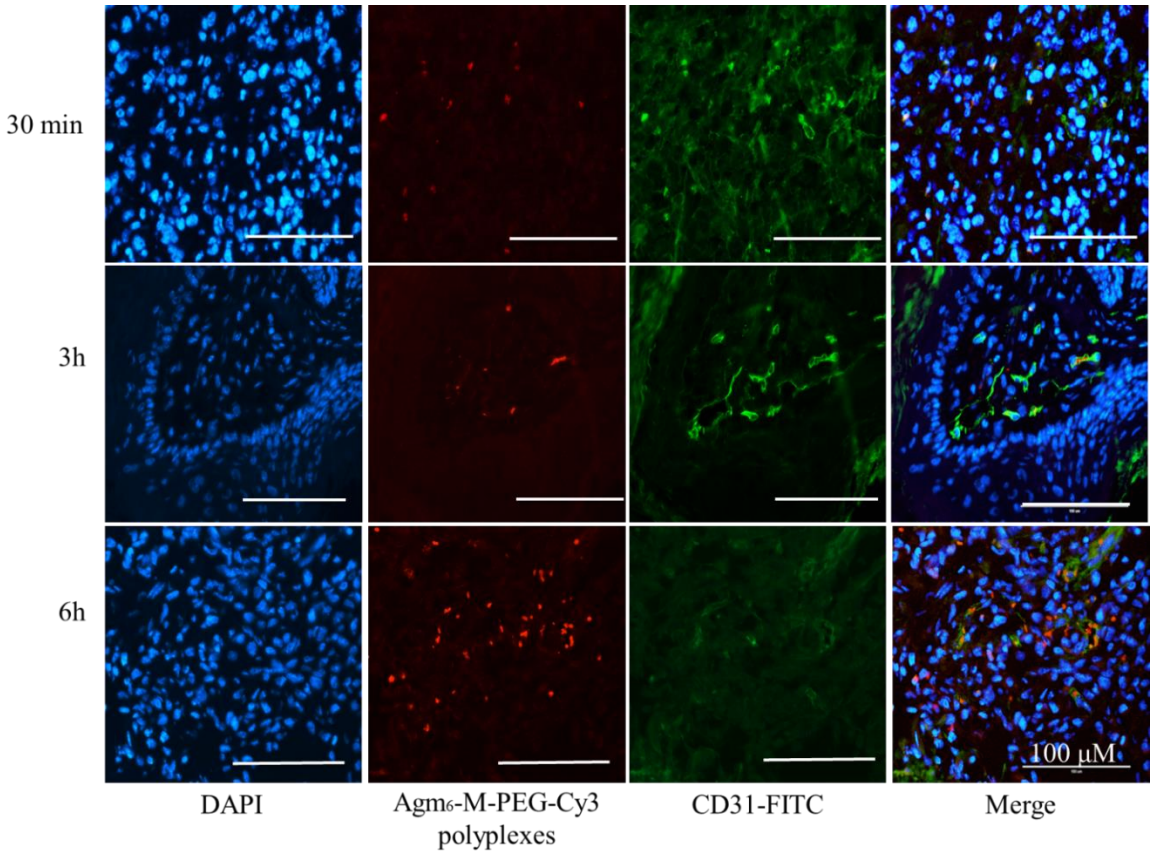

Figure 43: Histological analysis on polyplexes accumulation in tumor tissue. At 30 min, 3 and 6 hours the accumulation of polymer in tumor was evaluated. Tumor tissues were stained with DAPI ( ) and CD31-FITC ( ). Polyplexes were stained with Cyanine 3 ( ). Scale bar is 100 µm.

3.4 Discussion

The new bioconjugates presented in this work were specifically designed to complex oligonucleotides (ONs). In particular, we focused our attention on siRNA engineered polyplexes able to protect it from degradation by nucleases while achieving an efficient ONs delivery into the tumor cells. The colloidal nature of these nanocarriers was thought to have suitable properties for passive accumulation into the tumor tissue thanks to the "Enhanced Permeability and Retention" (EPR) effect.

To this aim, we decided to functionalize maltotriose with molecules displaying a guanidine-group, and specifically we selected acryloyl agmatine. Several attempts of maltotriose modification using various coupling reagents, such as p-nitrophenylchloroformiate, lead to unsuccessful degree of substitution (less than 1 out of 10 hydroxyl groups available). We finally set up an optimized multi-step procedure involving (I) the oligoscaccharide derivatization with ε-aminocaproic acid, (II) the generation of a macroinitiator by reacting the product of step (I) with 2-isobutyryl bromide and (III) the multicationic functionalization of the macroinitiator by reaction with acryloyl agmatine using the Atom Transfer Radical Polymerization (ATRP) technique, as described in the previous section.

Finally, the $(agmatinyl)_6$-maltotriosyl-N-acetyl-amino-hexanoic acid (Agm_6-M-COOH) star-like cationic molecule was conjugate to a 5 kDa α-methoxy-ω-amino-polyethylene glycol ($mPEG_{5kDa}$-NH_2) using standard coupling procedure with DCC/NHS and obtaining a very good conjugation yield.

In view of generating a tumor targeted system with increased site-specificity and recognition properties, we decided to further modified the obtained Agm_6-M-PEG polymer by conjugating it with folic acid (FA)[146]. It has been already described that the folate receptor (FR) is overexpressed in several cancer cell line[168-170]. For this reason, FA represents a good candidate when designing a targeted delivery system for anticancer drugs, and in this specific case for ONs. Moreover, FA is well known to be non-toxic, it is available in the market at competitive prices and it improves the nanocarriers internalization by FR expressing cells[114]. The generation of folate polymer (Agm_6-M-PEG-FA) was performed in a two steps procedure which involves (I) the conjugation of FA to the PEG through the use of NHS and DCC coupling agents and (II) the conjugation of the obtained PEG-FA to Agm_6-M-COOH. Initially, to purify the crude product and remove the excess of FA, a dialysis against water supplemented of 0.05% v/v NH_3 was performed. The

analysis of the purified polymer still showed traces of free FA, probably due to the low solubility of FA in water that makes the dialysis purification method inefficient. For these reason, an additional purification step via gel filtration chromatography was required.

After the polymers were fully characterized from a physico-chemical point of view, we started to investigate their ability to condense ON and form polyplexes. Agm_6-M-PEG/ siRNA complexation efficiency was evaluated by gel electrophoresis. Polymers showed a complete ON complexation at 3 N/P ratio, thus suggesting that FA do not alter the polymer electrostatic interaction with siRNA. No significant differences were observed neither by DLS or TEM analysis regarding the size and shape of the obtained Agm_6-M-PEG and Agm_6-M-PEG-FA polyplexes at 3 N/P ratio. These results indicate that the targeting ligand do not affect the interaction of the polymer cationic heads with the negatively charged ONs. It is important to highlight that low N/P ratios of complexation are normally favored as this is an important feature that dictate the gene delivery system efficiency. Indeed, as confirmed by several publications, the presence of free polymer chains non-complexed with siRNA, which are more likely to be there at high N/P ratios, could elicits toxicity and influence the biodistribution (*vide infra*)[171].

The plasma stability data of Agm_6-M-PEG:siRac1 prepared at the 3 and 5 N/P ratio showed a strong complexation polymer-siRNA that protects the ONs after systemic administration as confirmed by the *in vivo* studies where a high siRac1 accumulation in MDA-MB-231 intramammary tumor was observed.

Another important thing to consider when designing ON delivery system is that polyplexes may interact with anionic components of the extracellular matrix of different cell type or anionic components circulating in the blood stream. The presence of these negatively charged molecules, which are polyanionic polymers (i.e. heparin or chondroitin sulfate), could affect the positive/negative charge stability of the polyplexes resulting in a nanocarrier destabilization. The investigation of the interaction between these polyanions and the polyplexes can give interesting information about the uses of this system for *in vitro* transfection and *in vivo* application. Heparin is a component of the human serum and the heparin level in human plasma is 0.15 IU/mL [4]. We therefore tested the stability of our polyplexes in the presence of increasing concentration of heparin. Importantly, we found that the resistance of polyplexes to siRNA displacement by heparin was very high. Indeed, siRNA release could be achieved only when using a heparin concentration 16 times higher than the physiological levels.

A key point when testing targeted and non-targeted system *in vitro* is the selection of suitable cells line for the assays. To identify an adequate *in vitro* model for the comparison of folate and non-folate polyplexes performances, the folate receptor expression of several cell lines was investigated by binding of tritiated FA ([^{3}H]FA). The screening was performed on different melanoma and breast cancer derived cells cultured in regular or folate free medium. Among all the cell lines analyzed, human adenocarcinoma MDA-MB-231 cells displayed the highest internalization of radioactive FA both in folate depleted medium and in regular RPMI. On the contrary, melanoma cell lines showed a low tritiated folic acid internalization, which was corresponding to a low FR expression. Taken these results together, MDA-MB-231 and HeLa cell lines, showing the highest FR expression, were selected for polyplexes investigations.

Another important parameter to look at is the density of the targeting agent required to improve the carrier performances. In view of that, dedicated gene knockdown studies were carried out on HeLa cells incubated with polyplexes prepared at 3 and 5 N/P ratios and containing different percentages of folic acid decoration. The polymer compositions analyzed were Agm_6-M-PEG:Agm_6-M-PEG-FA 75:25, 50:50 and 0:100 weight ratios. In the assay siRac1 was used as a model therapeutic siRNA for its ability to inhibit cell migration, metastatization and cell invasion of cancer cells. As a matter of fact, Rac1 proteins seems be overexpressed in many cancer cells and represent an interesting molecular target[3]. siRac1 was also used as model oligonucleotide to evaluate the ability of the nanocarrier to silence defined gene without eliciting cell killing. All the formulations tested showed to different extent gene knockdown capacity and a certain level of silencing specificity. However, preliminary cytotoxicity test did show a slight decrease of the polyplexes biocompatibility that was inversely proportional to the folate density. In addition to that, the 25% w/w folate end-derivatized Agm_6-M-PEG cationic polymer in the final composition and at the N/P ratio of 3 showed a nice dose response correlation and the best silencing performances. Therefore, the 75:25 %w/w Agm_6-M-PEG:Agm_6-M-PEG-FA/siRac1 polyplexes 3 N/P ratio was identified as the best formulation for the next studies. Agm_6-M-PEG/siRac1 polyplexes at the same N/P ratio were always used as non-targeted reference system.

Comparison between folate and non-folate polyplexes was performed on both HeLa and MDA-MB-231 cells. Transfection data of gene Rac1 showed how 75:25 %w/w Agm_6-M-PEG:Agm_6-M-PEG-FA/siRac1 polyplexes possess higher gene knockdown efficiency than Agm_6-M-PEG/siRac1 polyplexes, and that the silencing effect is dose-dependent. This data

were also confirmed by wound healing assay performed on MDA-MB-231 cells where it was observed that after 12 hours of cells incubation with 75:25 %w/w Agm_6-M-PEG:Agm_6-M-PEG-FA/siRac1 only the 60% of the gap was healed. The better silencing profile of 75:25 %w/w Agm_6-M-PEG:Agm_6-M-PEG-FA/siRac1 polyplexes cannot be explained only with the amount of polyplexes internalized. Indeed, when the folate and non-folate polyplexes were tested for their internalization in MDA-MB-231 FR expressing cells, the same cell uptake profiles were observed at all the scheduled time investigated. Taken these results together, we considered that clarifying FA role in the polyplexes uptake was a crucial step to understand the differences observed in the gene silencing assay. The binding capacity of polyplexes bearing folic acid to the specific receptor was therefore assessed by simultaneous incubation with Agm_6-M-PEG:Agm_6-M-PEG-FA/siRNA at different wt% (from 100:0 to 0:100% w/w) with radioactive folic acid. Surprisingly, none of the polyplexes decorated with increasing amount of folic acid showed any reduction in terms of cell associated radioactivity, suggesting that folate polyplexes do not actually compete with tritiated FA for the internalization process. These results are similar to what has been recently described by Jones et al.[172] and may be ascribed to the synergistic effect of the dimerization of folic acid on the surface (which inhibits the FR binding). The low binding capacity of folate polyplexes is in agreement with the evidences obtained by other groups which independently observed that the transfection obtained from nanocarriers bearing folic acid is not mediated by FR[173-175]. The non-targeting role of FA could imply an internalization by a non-specific receptor of folate polyplexes.

The intracellular fate of the nanosystems was then studied by confocal microscopy aiming at evaluating if the non-FR mediated uptake of folate and non-folate polyplexes could be eventually correlated with different internalization pathway and therefore with the different silencing efficacy. Agm_6-M-PEG/siRac1 polyplexes showed high internalization within the endosomes and lysosomes. On the other hand, folate polyplexes showed a low colocalization with endosomes and lysosomes while a diffused signal was detected in the cells cytoplasm that may be related to endosomal-escape properties of the polymeric carrier. Indeed, as described in the works done by Duarte et al.[21] and Reddy et al.[176,177], folic acid covalently and electrostatically associated on the polyplex surface could lead to endosomal escape and polyplexes destabilization. Therefore, folate-polyplexes may exhibit a more efficient gene silencing because they facilitate siRNA endosomal escape from the endosomes into the cytosol. Non-folate polyplexes do not possess any “destabilizing”

capacity, resulting in a lower transfection efficiency when compared to the folate counterpart.

Moreover, mammalian cells offer several distinct endocytic pathways and, as a result, different nanocarriers sorting and intracellular trafficking[120]. Over the past years, it has been extensively demonstrated that the endocytic process strongly affect the success of gene delivery in different cell types[178-180]. Among all the endocytic routes, caveolae and clathrin-mediated uptake represent the most probable internalization pathway of drug nanocarriers[120]. Caveolae are small cell membrane invaginations of 60-80 nm originated from lipids rafts while clathrin-coated pits are of 120 nm in size[120]. Despite the fact that the size of folate and non-folate polyplexes is similar (75 and 82 nm respectively) and therefore cannot affect the cell internalization, we decided to investigate whether folate and non-folate polyplexes could be internalized by different endocytic pathways. For this purpose, caveolin-1 and clathrin heavy chains, which play a key role in caveolae and clathrin-coated pits formation, respectively[181,182], were immunostained after MDA-MB-231 cells incubation with folate and non-folate polyplexes. The results showed that Agm_6-M-PEG/siRac1 polyplexes were taken up by clathrin-dependent endocytosis, then they are first transported to early endosomes and finally they reach the lysosomes. On the other hand, polyplexes bearing folic acid were internalized by caveolae route thereby bypassing or reducing the endosomal transit and therefore the ON degradation. These results are in good agreement with the work done by Gabrielson et al.[60] where polyetilenimine/pDNA polyplexes bearing folic acid displayed a caveolin-mediated uptake resulting in an efficient gene transfection. In particular, recent works have been focused on the relevance of caveolae-mediated internalization with respect to clathrin-dependent uptake to provide high transfection efficiency.

Taken all the results together, we can claim that the polyplexes presented in this work are biocompatible and display interesting features required for a successful ONs delivery system.

Compared to marketed products, such as Jet-PEI which shows good *in vitro* silencing properties accomplished with an undesirable toxicity, our ONs nanoplatforms display a good silencing profile and they are well tolerated both *in vitro* and *in vivo*. Indeed, one of the major issue for the clinical application of cationic polymers is the red blood cell lysis, which is one of the most frequent causes of polyplexes toxicity. Hence, the safety profile of Agm_6-M-PEG:siRac1 polyplexes prepared at 3 and 5 N/P ratios was investigated also in term of hemocompatibility. Remarkably, polyplexes were found to be highly tolerated at

all the relevant concentrations for *in vivo* studies[183]. Negligible hemolysis was detected in blood samples incubated with the higher concentration of polyplexes (1.0 mg/mL), which is well above the theoretical nanocarriers concentration in the blood. Pro-inflammatory factors secretion and immune stimulation after i.v. administration are others limiting factors for the clinical application of cationic siRNA carriers[184-186]. The immune response is related to the siRNA sequences and the slightly positive charge of the polyplexes, which cause adverse effects and make the therapeutic treatment ineffective. We therefore tested our positively charged materials for their compatibility with the immune system. Polymers alone, both folate and non-folate, did not induce any release of TNF-α (early indicator of inflammatory process) when incubated with PBMCs, demonstrating that the new nanocarriers do not elicit an immune response. The safety of folate and non-folate polyplexes was further confirmed with the *in vivo* studies. Following i.v. administration of 75:25 %w/w Agm_6-M-PEG:Agm_6-M-PEG-FA/siRac1 and Agm_6-M-PEG/siRac1 polyplexes at all the relevant concentrations for therapeutic applications it was not possible to detect any severe side effect and mice were healthy.

The physiological stability of folate-polyplexes were correlate with the size of nanocarriers and the ability of the vehicle to accumulate into the tumor was investigated. Indeed, the data concerning the hydrodynamic diameter and charge surface of the polyplexes revealed interesting features to ensure *in vivo* efficient tumor accumulation of the ONs payload. In a pioneer study Kataoka and co-workers demonstrated how sub-100 nm nanoparticles could highly penetrate and accumulate into tumors with low level of vascularization[187]. The polyplexes in this study possesses relatively low hydrodynamic diameter (75 nm) which allows to easily extravasate and accumulate into tumors. This was proved by ex-vivo imaging and siRac1 level quantification following i.v. administration of fluorescently labelled folate-polyplexes which showed a significant polyplexes accumulation into tumor over time. The tissue data distribution of folate polyplexes in 30 min, 3 and 6 hours after i.v administration in tumor bearing mice, shows a good accumulation in tumor in the early time. After 3 hours, folate polyplexes were observed accumulate in liver. This behavior is ascribable to the Kupffer cells in the liver are mainly responsible for capture of (opsonized) polyplexes, in good agreement with other work[188,189]. However, only traces of polyplexes were found in lungs suggesting that polyplex do not induce eritrocytes aggregation subsequent trapping of the aggregates in the lung vasculature. In addition, folate polyplexes display an apparent low retention in the spleen avoiding the interaction

macrophages or splenocytes with further demonstrates the advantages of this nanoplatform for siRNA delivery.

Cryo-sections of tumors were collected after 30 min, 3 and 6 hours of i.v. folate polyplexes administration in tumor bearing mice to validate the in vivo and ex-vivo polyplex accumulation results. Histological analysis displayed a good Cy3 signal in the analyzed section which increase in time-dependent manner. Indeed, a correlation between the tumor vessels and polyplexes signal was observed. These results suggest a good accumulation of folate polyplexes in tumor tissue. However, further investigations are needed to better understand the mechanisms behind the tumor accumulation of the polyplexes.

General conclusions

RNA interference (RNAi) is a regulatory process involved in gene silencing in many eukaryotic cells. This endogenous pathway concern the gene silencing by triggered by double stranded RNA (dsRNA) such as short interfering RNA (siRNA). siRNA can activate this pathway resulting in high efficiently and specificity of gene expression silencing. Due to the intrinsic mechanism, these therapeutics could be used to treat several disease such as infective, cardiovascular and neurodegenerative disorders or cancer targeting unconventional pathways traditionally considered to be "undruggable"[190]. However, the therapeutic potential of these molecules is far to reach. Indeed, due to the nature of these molecules, they suffers of structural fragility, possess high molecular weight and negative charge which preclude the passages though the physiological barriers. Nevertheless siRNA are substrate of serum endonucleases and can elicit immuno-response. To date, many efforts and large amount of capital have been invested in bringing siRNA therapeutics to the market. A key challenge to realizing the broad potential of siRNA-based therapeutics is the need for safe and effective delivery methods.

In this contest a novel biocompatible siRNA delivery system was synthesized.

This study on this new fascinating nanoplatform was splitted in two moment.

In the first part of the study, the supramolecular bioconjugate (Agm_6-M-PEG) was obtained by a multi-step chemical protocol that included the conjugation of agmatine moieties to a maltotriose scaffold. This cationic molecule was designed to further functionalized with polymers, lipids or proteins with the aim to develop new nanocarriers able to deliver oligonulceotides. In this thesis the oligocationic structure was functionalized with polyethylene glycol that can also be further derivatized with a targeting agent as demonstrated in the second part of the work. The synthesis was properly set-up to reproducibly produce the desired nanoplatform with high yield and purity. The intermediates and the final bioconjugates were extensively characterized by different analysis. Association studies were carried out using a 19pb dsDNA as model oligonucleotide. Gel electrophoresis studies displayed that complete dsDNA association with Agm_6-M-PEG was achieved with 3 N/P ratio. Further investigations on the dsDNA association with the carrier were performed by isothermal titration calorimetry which show that the interaction occurs according to a combination of mechanisms depending on the N/P ratio. Accordingly, different structures and compositions were observed by ζ-potential analysis, which showed that the charge of the polyplexes changes with the composition.

The polyplexes displayed a size in the range of 50-75 nm that was stable in the buffer while slightly increased in the presence of serum proteins. The novel Agm_6-M-PEG/dsDNA polyplexes possess a rod-shaped structure, even though the aspect ratio depends on the composition of the polyplexes as confirmed by Transmission electron microscopy (TEM). Cell culture studies showed that the polyplexes were devoid of cytotoxicity. Compared to commercial products which show high gene silencing, namely Lipofectamine, Jet-PEI, or other materials described in the literature, Agm_6-M-PEG the good silencing ability is accomplished by an high biocompatibility.

The polyplexes were efficiently taken up by MCF7 and KB cells while the cell up-take of MC3T3-E1 was significantly lower than the other cells, suggesting a cell specific mechanism for the internalization of these polyplexes. The different composition and structure of the polyplexes was also found to affect the cell up-take: polyplexes with smaller aspect ratio were taken up more efficiently than polyplexes with larger aspect ratio. Preliminary gene silencing studies showed that polyplexes with 3 N/P ratio possess greater ability to reduce the Rac1.

The second part of the work was carried out in collaboration with the Sackler School of Medicine, Department of Physiology and Pharmacology at Tel Aviv University in the Prof. Ronit Satchi-Fainaro's Laboratory.

Polyplexes were prepared with siRac1, an oligonucleotide suitable for inhibit the angiogenesis and metastatization of cell cancer. Polyplexes with 3 and 5 N/P ratio display good stability in plasma serum up to 8 hours highlighting the shield properties of this nanocarrier from RNA degradation. The interaction between the siRNA and the cationic carrier is higher than the heparin level in the blood. Indeed, the novel polyplexes are avoided of the common issue of poly-cationic carrier such as the lysis of the red blood cells.

Taking advantage on the tumor features, different targeting ligand could be coupled to the vehicle. Exploiting the terminal group, the PEG side chain was functionalized with targeting agent namely, folic acid (FA). As well known, folic acid is an excellent targeting ligand due to the features of tumor cells to overexpress folic acid receptor (FR) on their surface. A preliminary screening on different cell lines was performed and MDA-MB-231 showed the higher expression of FR. Folic acid was coupled with the polymer by easy conjugation. The new bioconjugate (Agm_6-M-PEG-FA) was characterized and the percentage of decoration was defined on the silencing activity. Among the formulation tested, 25% w/w Agm_6-M-PEG-FA displayed the better gene silencing results (86% gene

inhibition) on HeLa cells. Compared to the non-folate polyplexes, polyplexes bearing folic acid showed similar size and aspect ratio but the latter display a better silencing profiles than the former. In a similar manner, the Rac1 silencing on MDA-MB-231 cells showed an higher silencing for folate polyplexes in comparison with non-folate polyplexes. Indeed, on both the cell line, a siRNA dose response was observed. The silencing properties of these new nanosystems were confirmed by the wound healing assay.

Despite the silencing results, the comparative cell-uptake study between folate and non-folate polyplexes do not displayed differences. In particular, studies focused on the ability of folate-polyplexes to bind FR on MDA-MB-231 cell membrane surface highlighted that no receptor occupation was found for all the polyplexes formulation. These results meanings that the silencing is not related to the cell uptake and FR do not participate to the polyplexes internalization. The intracellular fate of polyplexes, showed two different route of internalization for the folate and non-folate polyplexes. As a matter of fact, an high accumulation of non-folate polyplexes was observed in endo-lysosomal compartment. On the contrary, polyplexes bearing folic acid displayed low colocalization in endosomes and lysosomes. With the aim to explain the differences in the intracellular trafficking, the endocytotic routes of folate and non-folate polyplexes were studied. 75:25 %w/w Agm_6-M-PEG: Agm_6-M-PEG-FA/siRac1 polyplexes showed an internalization mediated by caveolae while an clathrin-mediate endocytosis was observed for the non folated polyplexes. As reported in literature, the internalization caveolae-mediated is preferred to the others for an efficient silencing. However, both the formulation do not lead the immunosystem activation and are well tolerated in vivo.

A good nanocarrier could exploit the leaky vasculature of the tumor tissue and accumulate in the region of interest. As mentioned above, the polyplexes in this study possesses suitable features such as the low hydrodynamic diameter (82 nm) and charge surface polyplexes displayed interesting features for efficiently ONs in vivo tumor accumulation. Cyanine-3 labelled polyplexes were found accumulate in orthotopic tumor in mice in the time and a high Rac1 accumuation were founded. These results were confirmed also by the histological analysis.

In the present thesis work, the versatile nanocarrier developed provided consistent positive results about the oligonucleotide delivery. Using this nanoplatform, siRNA can be efficiently protect from the degradation of the blood component and targeted to cancer cell. Due to the unexpected uptake mechanism, the endocytotic pathways of polyplexes need further investigations. Although all the encouraging results on the biocompatibility of these

new materials more detailed information on the nanotoxicology of the carrier will be undertaken. Future studies have be to focused on deeper evaluation of in vivo tumor accumulation and toxicity. Optimization for a better in vivo performance can be done by using different targeted systems or by optimizing the polymer architecture.

Owing the observed characteristics, the application of this innovative vehicle could be extended to specifically silence therapeutically relevant intracellular proteins for cancer therapy.

References

1 Pack, D. W., Hoffman, A. S., Pun, S. & Stayton, P. S. Design and development of polymers for gene delivery. *Nature reviews. Drug discovery* **4**, 581 (2005).

2 Geary, R. S., Norris, D., Yu, R. & Bennett, C. F. Pharmacokinetics, biodistribution and cell uptake of antisense oligonucleotides. *Advanced drug delivery reviews* **87**, 46-51 (2015).

3 Bid, H. K., Roberts, R. D., Manchanda, P. K. & Houghton, P. J. RAC1: an emerging therapeutic option for targeting cancer angiogenesis and metastasis. *Molecular cancer therapeutics* **12**, 1925-1934 (2013).

4 Engelberg, H. & Dudley, A. Plasma heparin levels in normal man. *Circulation* **23**, 578-581 (1961).

5 Shi, J., Votruba, A. R., Farokhzad, O. C. & Langer, R. Nanotechnology in drug delivery and tissue engineering: from discovery to applications. *Nano letters* **10**, 3223-3230 (2010).

6 Barenholz, Y. C. Doxil®—the first FDA-approved nano-drug: lessons learned. *Journal of controlled release* **160**, 117-134 (2012).

7 Ma, P. & Mumper, R. J. Paclitaxel nano-delivery systems: a comprehensive review. *Journal of nanomedicine & nanotechnology* **4**, 1000164 (2013).

8 Sun, S.-B., Liu, P., Shao, F.-M. & Miao, Q.-L. Formulation and evaluation of PLGA nanoparticles loaded capecitabine for prostate cancer. *International journal of clinical and experimental medicine* **8**, 19670 (2015).

9 Landeros-Martínez, L.-L., Chavez-Flores, D., Orrantia-Borunda, E. & Flores-Holguin, N. Construction of a Nanodiamond–Tamoxifen Complex as a Breast Cancer Drug Delivery Vehicle. *Journal of Nanomaterials* **2016**, 6 (2016).

10 Hanahan, D. Rethinking the war on cancer. *The Lancet* **383**, 558-563 (2014).

11 Dreaden, E. C., Austin, L. A., Mackey, M. A. & El-Sayed, M. A. Size matters: gold nanoparticles in targeted cancer drug delivery. (2012).

12 Health, U. N. I. o. National Cancer Institute. *Dictionary of cancer terms. Retrieved on January* **19** (2007).

13 Hanahan, D. & Weinberg, R. A. The hallmarks of cancer. *cell* **100**, 57-70 (2000).

14 Douglas, H. & Weinberg, R. A. Hallmarks of cancer: the next generation. *Cell* **144**, 646-674 (2011).

15 Pavlova, N. N. & Thompson, C. B. The emerging hallmarks of cancer metabolism. *Cell metabolism* **23**, 27-47 (2016).

16 Marei, H. & Malliri, A. Rac1 in human diseases: the therapeutic potential of targeting Rac1 signaling regulatory mechanisms. *Small GTPases* **8**, 139-163 (2017).

17 Saci, A., Cantley, L. C. & Carpenter, C. L. Rac1 regulates the activity of mTORC1 and mTORC2 and controls cellular size. *Molecular cell* **42**, 50-61 (2011).

18 Ehrlich, J. S., Hansen, M. D. & Nelson, W. J. Spatio-temporal regulation of Rac1 localization and lamellipodia dynamics during epithelial cell-cell adhesion. *Developmental cell* **3**, 259-270 (2002).

19 Bustelo, X. R., Sauzeau, V. & Berenjeno, I. M. GTP-binding proteins of the Rho/Rac family: Regulation, effectors and functions in vivo. *Bioessays* **29**, 356-370 (2007).

20 Heasman, S. J. & Ridley, A. J. Mammalian Rho GTPases: new insights into their functions from in vivo studies. *Nature reviews. Molecular cell biology* **9**, 690 (2008).

21 Gao, Y., Dickerson, J. B., Guo, F., Zheng, J. & Zheng, Y. Rational design and characterization of a Rac GTPase-specific small molecule inhibitor. *Proceedings of the National Academy of Sciences of the United States of America* **101**, 7618-7623 (2004).
22 Pillai, G. Nanomedicines for cancer therapy: an update of FDA approved and those under various stages of development. *SOJ Pharm Pharm Sci* **1**, 13 (2014).
23 Arcamone, F., Franceschi, G., Penco, S. & Selva, A. Adriamycin (14-hydroxydaunomycin), a novel antitumor antibiotic. *Tetrahedron Letters* **10**, 1007-1010 (1969).
24 Yang, F., Teves, S. S., Kemp, C. J. & Henikoff, S. Doxorubicin, DNA torsion, and chromatin dynamics. *Biochimica et Biophysica Acta (BBA)-Reviews on Cancer* **1845**, 84-89 (2014).
25 Myers, C. E. *et al.* Adriamycin: the role of lipid peroxidation in cardiac toxicity and tumor response. *Science* **197**, 165-167 (1977).
26 Gabizon, A., Goren, D. & Barenholz, Y. Investigations on the antitumor efficacy of liposome-associated doxorubicin in murine tumor models. *Israel journal of medical sciences* **24**, 512-517 (1987).
27 Choy, H. Taxanes in combined modality therapy for solid tumors. *Critical reviews in oncology/hematology* **37**, 237-247 (2001).
28 Khanna, C., Rosenberg, M. & Vail, D. A review of paclitaxel and novel formulations including those suitable for use in dogs. *Journal of veterinary internal medicine* **29**, 1006-1012 (2015).
29 Wani, M. C., Taylor, H. L., Wall, M. E., Coggon, P. & McPhail, A. T. Plant antitumor agents. VI. Isolation and structure of taxol, a novel antileukemic and antitumor agent from Taxus brevifolia. *Journal of the American Chemical Society* **93**, 2325-2327 (1971).
30 Miele, E., Spinelli, G. P., Miele, E., Tomao, F. & Tomao, S. Albumin-bound formulation of paclitaxel (Abraxane® ABI-007) in the treatment of breast cancer. *International journal of nanomedicine* **4**, 99 (2009).
31 Northfelt, D. W. *et al.* Phase 2 trial of paclitaxel polyglumex with capecitabine for metastatic breast cancer. *American journal of clinical oncology* **37**, 167 (2014).
32 Stathopoulos, G. & Boulikas, T. Lipoplatin formulation review article. *Journal of drug delivery* **2012** (2011).
33 Boulikas, T. Clinical overview on Lipoplatin™: a successful liposomal formulation of cisplatin. *Expert opinion on investigational drugs* **18**, 1197-1218 (2009).
34 Fire, A., Xu, S., Montgomery, M. K. & Kostas, S. A. Potent and specific genetic interference by double-stranded RNA in Caenorhabditis elegans. *nature* **391**, 806 (1998).
35 McClorey, G. & Wood, M. J. An overview of the clinical application of antisense oligonucleotides for RNA-targeting therapies. *Current opinion in pharmacology* **24**, 52-58 (2015).
36 Frank-Kamenetsky, M. *et al.* Therapeutic RNAi targeting PCSK9 acutely lowers plasma cholesterol in rodents and LDL cholesterol in nonhuman primates. *Proceedings of the National Academy of Sciences* **105**, 11915-11920 (2008).
37 Halder, J. *et al.* Focal adhesion kinase targeting using in vivo short interfering RNA delivery in neutral liposomes for ovarian carcinoma therapy. *Clinical Cancer Research* **12**, 4916-4924 (2006).
38 Bernstein, E., Caudy, A. A., Hammond, S. M. & Hannon, G. J. Role for a bidentate ribonuclease in the initiation step of RNA interference. *Nature* **409**, 363 (2001).
39 Rand, T. A., Ginalski, K., Grishin, N. V. & Wang, X. Biochemical identification of Argonaute 2 as the sole protein required for RNA-induced silencing complex

activity. *Proceedings of the National Academy of Sciences of the United States of America* **101**, 14385-14389 (2004).
40 Whitehead, K. A., Langer, R. & Anderson, D. G. Knocking down barriers: advances in siRNA delivery. *Nature reviews. Drug discovery* **8**, 129 (2009).
41 Reischl, D. & Zimmer, A. Drug delivery of siRNA therapeutics: potentials and limits of nanosystems. *Nanomedicine: Nanotechnology, Biology and Medicine* **5**, 8-20 (2009).
42 Judge, A. & Maclachlan, I. Overcoming the innate immune response to small interfering RNA. *Human gene therapy* **19**, 111-124 (2008).
43 Nayerossadat, N., Maedeh, T. & Ali, P. A. Viral and nonviral delivery systems for gene delivery. *Advanced biomedical research* **1** (2012).
44 De Paula, D., Bentley, M. V. L. & Mahato, R. I. Hydrophobization and bioconjugation for enhanced siRNA delivery and targeting. *Rna* **13**, 431-456 (2007).
45 Parhofer, K. G. Mipomersen: evidence-based review of its potential in the treatment of homozygous and severe heterozygous familial hypercholesterolemia. *Core evidence* **7**, 29 (2012).
46 Deleavey, G. F., Watts, J. K. & Damha, M. J. Chemical modification of siRNA. *Current Protocols in Nucleic Acid Chemistry*, 16.13. 11-16.13. 22 (2009).
47 Amer, M. H. Gene therapy for cancer: present status and future perspective. *Molecular and cellular therapies* **2**, 27 (2014).
48 Ramamoorth, M. & Narvekar, A. Non viral vectors in gene therapy-an overview. *Journal of clinical and diagnostic research: JCDR* **9**, GE01 (2015).
49 Heller, R., Shirley, S., Guo, S., Donate, A. & Heller, L. in *Engineering in Medicine and Biology Society, EMBC, 2011 Annual International Conference of the IEEE*. 736-738 (IEEE).
50 Newman, C. & Bettinger, T. Gene therapy progress and prospects: ultrasound for gene transfer. *Gene therapy* **14**, 465 (2007).
51 Al-Dosari, M. S. & Gao, X. Nonviral gene delivery: principle, limitations, and recent progress. *The AAPS journal* **11**, 671 (2009).
52 Herweijer, H. & Wolff, J. Progress and prospects: naked DNA gene transfer and therapy. *Gene therapy* **10**, 453 (2003).
53 Ginn, S. L., Alexander, I. E., Edelstein, M. L., Abedi, M. R. & Wixon, J. Gene therapy clinical trials worldwide to 2012–an update. *The journal of gene medicine* **15**, 65-77 (2013).
54 Thomas, C. E., Ehrhardt, A. & Kay, M. A. Progress and problems with the use of viral vectors for gene therapy. *Nature Reviews Genetics* **4**, 346-358 (2003).
55 Schnell, M. A. *et al.* Activation of innate immunity in nonhuman primates following intraportal administration of adenoviral vectors. *Molecular Therapy* **3**, 708-722 (2001).
56 Midoux, P., Breuzard, G., Gomez, J. P. & Pichon, C. Polymer-based gene delivery: a current review on the uptake and intracellular trafficking of polyplexes. *Current gene therapy* **8**, 335-352 (2008).
57 Behr, J.-P. The proton sponge: a trick to enter cells the viruses did not exploit. *CHIMIA International Journal for Chemistry* **51**, 34-36 (1997).
58 Boussif, O. *et al.* A versatile vector for gene and oligonucleotide transfer into cells in culture and in vivo: polyethylenimine. *Proceedings of the National Academy of Sciences* **92**, 7297-7301 (1995).
59 Wojda, U. & Miller, J. L. Targeted transfer of polyethylenimine–avidin–DNA bioconjugates to hematopoietic cells using biotinylated monoclonal antibodies. *Journal of pharmaceutical sciences* **89**, 674-681 (2000).

60 Gabrielson, N. P. & Pack, D. W. Efficient polyethylenimine-mediated gene delivery proceeds via a caveolar pathway in HeLa cells. *Journal of Controlled Release* **136**, 54-61 (2009).
61 Lei, Y., Rahim, M., Ng, Q. & Segura, T. Hyaluronic acid and fibrin hydrogels with concentrated DNA/PEI polyplexes for local gene delivery. *Journal of controlled release* **153**, 255-261 (2011).
62 Zauner, W., Ogris, M. & Wagner, E. Polylysine-based transfection systems utilizing receptor-mediated delivery. *Advanced drug delivery reviews* **30**, 97-113 (1998).
63 Wu, G. Y. & Wu, C. H. Receptor-mediated in vitro gene transformation by a soluble DNA carrier system. *Journal of Biological Chemistry* **262**, 4429-4432 (1987).
64 Wu, G. Y. & Wu, C. H. Receptor-mediated gene delivery and expression in vivo. *Journal of Biological Chemistry* **263**, 14621-14624 (1988).
65 Putnam, D., Gentry, C. A., Pack, D. W. & Langer, R. Polymer-based gene delivery with low cytotoxicity by a unique balance of side-chain termini. *Proceedings of the National Academy of Sciences* **98**, 1200-1205 (2001).
66 Haensler, J. & Szoka Jr, F. C. Polyamidoamine cascade polymers mediate efficient transfection of cells in culture. *Bioconjugate chemistry* **4**, 372-379 (1993).
67 Yin, H. *et al.* Non-viral vectors for gene-based therapy. *Nature Reviews Genetics* **15**, 541-555 (2014).
68 Davis, M. E. & Brewster, M. E. Cyclodextrin-based pharmaceutics: past, present and future. *Nature reviews. Drug discovery* **3**, 1023 (2004).
69 Seu, K. J., Cambrea, L. R., Everly, R. M. & Hovis, J. S. Influence of lipid chemistry on membrane fluidity: tail and headgroup interactions. *Biophysical journal* **91**, 3727-3735 (2006).
70 Barichello, J. M., Ishida, T. & Kiwada, H. Complexation of siRNA and pDNA with cationic liposomes: the important aspects in lipoplex preparation. *Liposomes: Methods and Protocols, Volume 1: Pharmaceutical Nanocarriers*, 461-472 (2010).
71 Tagami, T. *et al.* Anti-angiogenic therapy via cationic liposome-mediated systemic siRNA delivery. *International journal of pharmaceutics* **422**, 280-289 (2012).
72 Bates, D. & Harper, S. Regulation of vascular permeability by vascular endothelial growth factors. *Vascular pharmacology* **39**, 225-237 (2002).
73 Jain, R. K. The next frontier of molecular medicine: delivery of therapeutics. *Nature medicine* **4**, 655-657 (1998).
74 Jain, R. K. & Stylianopoulos, T. Delivering nanomedicine to solid tumors. *Nature reviews Clinical oncology* **7**, 653-664 (2010).
75 Hobbs, S. K. *et al.* Regulation of transport pathways in tumor vessels: role of tumor type and microenvironment. *Proceedings of the National Academy of Sciences* **95**, 4607-4612 (1998).
76 Matsumura, Y. & Maeda, H. A new concept for macromolecular therapeutics in cancer chemotherapy: mechanism of tumoritropic accumulation of proteins and the antitumor agent smancs. *Cancer research* **46**, 6387-6392 (1986).
77 Maeda, H., Wu, J., Sawa, T., Matsumura, Y. & Hori, K. Tumor vascular permeability and the EPR effect in macromolecular therapeutics: a review. *Journal of controlled release* **65**, 271-284 (2000).
78 Cabral, H. *et al.* Accumulation of sub-100 nm polymeric micelles in poorly permeable tumours depends on size. *Nature nanotechnology* **6**, 815-823 (2011).
79 Blanco, E., Shen, H. & Ferrari, M. Principles of nanoparticle design for overcoming biological barriers to drug delivery. *Nature biotechnology* **33**, 941-951 (2015).

80 Bertrand, N., Wu, J., Xu, X., Kamaly, N. & Farokhzad, O. C. Cancer nanotechnology: the impact of passive and active targeting in the era of modern cancer biology. *Advanced drug delivery reviews* **66**, 2-25 (2014).
81 Noble, G. T., Stefanick, J. F., Ashley, J. D., Kiziltepe, T. & Bilgicer, B. Ligand-targeted liposome design: challenges and fundamental considerations. *Trends in biotechnology* **32**, 32-45 (2014).
82 Mimeault, M., Hauke, R. & Batra, S. Recent advances on the molecular mechanisms involved in the drug resistance of cancer cells and novel targeting therapies. *Clinical Pharmacology & Therapeutics* **83**, 673-691 (2008).
83 Bae, Y. H. & Park, K. Targeted drug delivery to tumors: myths, reality and possibility. *Journal of Controlled Release* **153**, 198 (2011).
84 Lammers, T., Kiessling, F., Hennink, W. E. & Storm, G. Drug targeting to tumors: principles, pitfalls and (pre-) clinical progress. *Journal of controlled release* **161**, 175-187 (2012).
85 Bazak, R., Houri, M., El Achy, S., Kamel, S. & Refaat, T. Cancer active targeting by nanoparticles: a comprehensive review of literature. *Journal of cancer research and clinical oncology* **141**, 769-784 (2015).
86 Srinivasarao, M. & Low, P. S. Ligand-Targeted Drug Delivery. *Chemical Reviews* (2017).
87 Irvine, D. J. Drug delivery: One nanoparticle, one kill. *Nature materials* **10** (2011).
88 Allen, T. M. Ligand-targeted therapeutics in anticancer therapy. *Nature reviews. Cancer* **2**, 750 (2002).
89 Mura, S., Nicolas, J. & Couvreur, P. Stimuli-responsive nanocarriers for drug delivery. *Nature materials* **12**, 991 (2013).
90 Li, J. *et al.* Redox-sensitive micelles self-assembled from amphiphilic hyaluronic acid-deoxycholic acid conjugates for targeted intracellular delivery of paclitaxel. *Biomaterials* **33**, 2310-2320 (2012).
91 Jurcic, J. G. Antibody therapy for residual disease in acute myelogenous leukemia. *Critical reviews in oncology/hematology* **38**, 37-45 (2001).
92 Danhier, F., Feron, O. & Préat, V. To exploit the tumor microenvironment: passive and active tumor targeting of nanocarriers for anti-cancer drug delivery. *Journal of Controlled Release* **148**, 135-146 (2010).
93 Singh, M. Transferrin as a targeting ligand for liposomes and anticancer drugs. *Current pharmaceutical design* **5**, 443-452 (1999).
94 Gatter, K. C., Brown, G., Trowbridge, I., Woolston, R. & Mason, D. Transferrin receptors in human tissues: their distribution and possible clinical relevance. *Journal of clinical pathology* **36**, 539-545 (1983).
95 Head, J. F., Wang, F. & Elliott, R. L. Antineoplastic drugs that interfere with iron metabolism in cancer cells. *Advances in enzyme regulation* **37**, 147-169 (1997).
96 Faulk, W., Taylor, C., Yeh, C. & McIntyre, J. Preliminary clinical study of transferrin-adriamycin conjugate for drug delivery to acute leukemia patients. *Molecular biotherapy* **2**, 57-60 (1990).
97 Byrne, J. D., Betancourt, T. & Brannon-Peppas, L. Active targeting schemes for nanoparticle systems in cancer therapeutics. *Advanced drug delivery reviews* **60**, 1615-1626 (2008).
98 Huttenlocher, A. & Horwitz, A. R. Integrins in cell migration. *Cold Spring Harbor perspectives in biology* **3**, a005074 (2011).
99 Nisato, R. E., Tille, J.-C., Jonczyk, A., Goodman, S. L. & Pepper, M. S. αv β 3 and αv β 5 integrin antagonists inhibit angiogenesis in vitro. *Angiogenesis* **6**, 105-119 (2003).

100 Danhier, F., Le Breton, A. & Préat, V. r. RGD-based strategies to target alpha (v) beta (3) integrin in cancer therapy and diagnosis. *Molecular pharmaceutics* **9**, 2961-2973 (2012).
101 Zhong, Y., Meng, F., Deng, C. & Zhong, Z. Ligand-directed active tumor-targeting polymeric nanoparticles for cancer chemotherapy. *Biomacromolecules* **15**, 1955-1969 (2014).
102 Xiao, Z. & Farokhzad, O. C. Aptamer-functionalized nanoparticles for medical applications: challenges and opportunities. *ACS nano* **6**, 3670-3676 (2012).
103 Gao, H. *et al.* Whole-cell SELEX aptamer-functionalised poly (ethyleneglycol)-poly (ε-caprolactone) nanoparticles for enhanced targeted glioblastoma therapy. *Biomaterials* **33**, 6264-6272 (2012).
104 Gu, F. *et al.* Precise engineering of targeted nanoparticles by using self-assembled biointegrated block copolymers. *Proceedings of the National Academy of Sciences* **105**, 2586-2591 (2008).
105 Drabovich, A. P., Berezovski, M. V., Musheev, M. U. & Krylov, S. N. Selection of smart small-molecule ligands: the proof of principle. *Analytical chemistry* **81**, 490-494 (2008).
106 Arpicco, S., De Rosa, G. & Fattal, E. Lipid-based nanovectors for targeting of CD44-overexpressing tumor cells. *Journal of drug delivery* **2013** (2013).
107 Surace, C. *et al.* Lipoplexes targeting the CD44 hyaluronic acid receptor for efficient transfection of breast cancer cells. *Molecular pharmaceutics* **6**, 1062-1073 (2009).
108 Leuschner, C. *et al.* LHRH-conjugated magnetic iron oxide nanoparticles for detection of breast cancer metastases. *Breast cancer research and treatment* **99**, 163-176 (2006).
109 Steinhauser, I., Spänkuch, B., Strebhardt, K. & Langer, K. Trastuzumab-modified nanoparticles: optimisation of preparation and uptake in cancer cells. *Biomaterials* **27**, 4975-4983 (2006).
110 Tan, W. B., Jiang, S. & Zhang, Y. Quantum-dot based nanoparticles for targeted silencing of HER2/neu gene via RNA interference. *Biomaterials* **28**, 1565-1571 (2007).
111 Chen, H. *et al.* Preparation and characterization of PE38KDEL-loaded anti-HER2 nanoparticles for targeted cancer therapy. *Journal of Controlled Release* **128**, 209-216 (2008).
112 Low, P. S. & Antony, A. C. Folate receptor-targeted drugs for cancer and inflammatory diseases. *Advanced drug delivery reviews* **56**, 1055-1058 (2004).
113 Sudimack, J. & Lee, R. J. Targeted drug delivery via the folate receptor. *Advanced drug delivery reviews* **41**, 147-162 (2000).
114 Hilgenbrink, A. R. & Low, P. S. Folate receptor-mediated drug targeting: From therapeutics to diagnostics. *Journal of pharmaceutical sciences* **94**, 2135-2146 (2005).
115 Chen, C. *et al.* Structural basis for molecular recognition of folic acid by folate receptors. *Nature* **500**, 486 (2013).
116 Gabizon, A. *et al.* Long-circulating liposomes for drug delivery in cancer therapy: a review of biodistribution studies in tumor-bearing animals. *Advanced Drug Delivery Reviews* **24**, 337-344 (1997).
117 Gabizon, A. *et al.* Targeting folate receptor with folate linked to extremities of poly (ethylene glycol)-grafted liposomes: in vitro studies. *Bioconjug. Chem.* **10**, 289-298 (1999).
118 Yoo, H. S. & Park, T. G. Folate receptor targeted biodegradable polymeric doxorubicin micelles. *Journal of Controlled Release* **96**, 273-283 (2004).

119 Besterman, J. M. & Low, R. B. Endocytosis: a review of mechanisms and plasma membrane dynamics. *Biochemical Journal* **210**, 1 (1983).
120 Vercauteren, D. *et al.* On the cellular processing of non-viral nanomedicines for nucleic acid delivery: mechanisms and methods. *Journal of controlled release* **161**, 566-581 (2012).
121 Swanson, J. A. Shaping cups into phagosomes and macropinosomes. *Nature reviews. Molecular cell biology* **9**, 639 (2008).
122 Kopatz, I., Remy, J. S. & Behr, J. P. A model for non-viral gene delivery: Through syndecan adhesion molecules and powered by actin. *The journal of gene medicine* **6**, 769-776 (2004).
123 Vercauteren, D. *et al.* Flotillin-dependent endocytosis and a phagocytosis-like mechanism for cellular internalization of disulfide-based poly (amido amine)/DNA polyplexes. *Biomaterials* **32**, 3072-3084 (2011).
124 Liberali, P. *et al.* The closure of Pak1-dependent macropinosomes requires the phosphorylation of CtBP1/BARS. *The EMBO journal* **27**, 970-981 (2008).
125 Roth, T. F. & Porter, K. R. Yolk protein uptake in the oocyte of the mosquito Aedes aegypti. L. *The Journal of cell biology* **20**, 313-332 (1964).
126 Elkin, S. R., Lakoduk, A. M. & Schmid, S. L. Endocytic pathways and endosomal trafficking: a primer. *Wiener Medizinische Wochenschrift* **166**, 196-204 (2016).
127 Kirchhausen, T., Owen, D. & Harrison, S. C. Molecular structure, function, and dynamics of clathrin-mediated membrane traffic. *Cold Spring Harbor perspectives in biology* **6**, a016725 (2014).
128 Kirchhausen, T. Adaptors for clathrin-mediated traffic. *Annual review of cell and developmental biology* **15**, 705-732 (1999).
129 McMahon, H. T. & Boucrot, E. Molecular mechanism and physiological functions of clathrin-mediated endocytosis. *Nature reviews. Molecular cell biology* **12**, 517 (2011).
130 Traub, L. M. & Bonifacino, J. S. Cargo recognition in clathrin-mediated endocytosis. *Cold Spring Harbor Perspectives in Biology* **5**, a016790 (2013).
131 Doherty, G. J. & McMahon, H. T. Mechanisms of endocytosis. *Annual review of biochemistry* **78**, 857-902 (2009).
132 Hillaireau, H. & Couvreur, P. Nanocarriers' entry into the cell: relevance to drug delivery. *Cellular and Molecular Life Sciences* **66**, 2873-2896 (2009).
133 Harush-Frenkel, O., Debotton, N., Benita, S. & Altschuler, Y. Targeting of nanoparticles to the clathrin-mediated endocytic pathway. *Biochemical and biophysical research communications* **353**, 26-32 (2007).
134 Gratton, S. E. *et al.* The effect of particle design on cellular internalization pathways. *Proceedings of the National Academy of Sciences* **105**, 11613-11618 (2008).
135 Douglas, K. L., Piccirillo, C. A. & Tabrizian, M. Cell line-dependent internalization pathways and intracellular trafficking determine transfection efficiency of nanoparticle vectors. *European Journal of Pharmaceutics and Biopharmaceutics* **68**, 676-687 (2008).
136 Sovadinova, I., Palermo, E. F., Huang, R., Thoma, L. M. & Kuroda, K. Mechanism of polymer-induced hemolysis: nanosized pore formation and osmotic lysis. *Biomacromolecules* **12**, 260-268 (2010).
137 Liu, Y. *et al.* Immunostimulatory properties and enhanced TNF-α mediated cellular immunity for tumor therapy by C60 (OH) 20 nanoparticles. *Nanotechnology* **20**, 415102 (2009).

138 Takae, S. *et al.* PEG-detachable polyplex micelles based on disulfide-linked block catiomers as bioresponsive nonviral gene vectors. *Journal of the American Chemical Society* **130**, 6001-6009 (2008).
139 Matyjaszewski, K. Atom transfer radical polymerization (ATRP): current status and future perspectives. *Macromolecules* **45**, 4015-4039 (2012).
140 Siegwart, D. J., Oh, J. K. & Matyjaszewski, K. ATRP in the design of functional materials for biomedical applications. *Progress in polymer science* **37**, 18-37 (2012).
141 Stenzel-Rosenbaum, M. H., Davis, T. P., Chen, V. & Fane, A. G. Synthesis of poly (styrene) star polymers grown from sucrose, glucose, and cyclodextrin cores via living radical polymerization mediated by a half-metallocene iron carbonyl complex. *Macromolecules* **34**, 5433-5438 (2001).
142 Otiai, M. *et al.* (Google Patents, 2004).
143 Sakaguchi, S. A new color reaction of protein and arginine. *J. Biochem* **5**, 25-31 (1925).
144 Sims, G. E. C. & Snape, T. J. A method for the estimation of polyethylene glycol in plasma protein fractions. *Analytical Biochemistry* **107**, 60-63, doi:http://dx.doi.org/10.1016/0003-2697(80)90492-3 (1980).
145 Polyak, D. *et al.* Systemic delivery of siRNA by aminated poly (α) glutamate for the treatment of solid tumors. *Journal of Controlled Release* **257**, 132-143 (2017).
146 Gallon, E. *et al.* Triblock copolymer nanovesicles for pH-responsive targeted delivery and controlled release of siRNA to cancer cells. *Biomacromolecules* **16**, 1924-1937 (2015).
147 Ma, P. L., Lavertu, M., Winnik, F. M. & Buschmann, M. D. New Insights into chitosan− DNA interactions using isothermal titration microcalorimetry. *Biomacromolecules* **10**, 1490-1499 (2009).
148 Samanta, K., Jana, P., Bäcker, S., Knauer, S. & Schmuck, C. Guanidiniocarbonyl pyrrole (GCP) conjugated PAMAM-G2, a highly efficient vector for gene delivery: the importance of DNA condensation. *Chemical Communications* **52**, 12446-12449 (2016).
149 Pozharski, E. & MacDonald, R. C. Thermodynamics of cationic lipid-DNA complex formation as studied by isothermal titration calorimetry. *Biophysical journal* **83**, 556-565 (2002).
150 Srinivasachari, S., Liu, Y., Prevette, L. E. & Reineke, T. M. Effects of trehalose click polymer length on pDNA complex stability and delivery efficacy. *Biomaterials* **28**, 2885-2898 (2007).
151 Griffiths, M. Z., Alkorta, I. & Popelier, P. L. Predicting pKa values in aqueous solution for the guanidine functional group from gas phase ab initio bond lengths. *Molecular informatics* **32**, 363-376 (2013).
152 Bersani, S. *et al.* Star-like oligo-arginyl-maltotriosyl derivatives as novel cell-penetrating enhancers for the intracellular delivery of colloidal therapeutic systems. *Bioconjugate chemistry* **23**, 1415-1425 (2012).
153 Pozharski, E. & MacDonald, R. C. Lipoplex thermodynamics: determination of DNA-cationic lipoid interaction energies. *Biophysical journal* **85**, 3969-3978 (2003).
154 Nisha, C., Manorama, S. V., Ganguli, M., Maiti, S. & Kizhakkedathu, J. N. Complexes of poly (ethylene glycol)-based cationic random copolymer and calf thymus DNA: a complete biophysical characterization. *Langmuir* **20**, 2386-2396 (2004).
155 Mahmoudi, M. *et al.* Protein− nanoparticle interactions: opportunities and challenges. *Chemical reviews* **111**, 5610-5637 (2011).

156 Liu, X. *et al.* Size dependent cellular uptake of rod-like bionanoparticles with different aspect ratios. *Scientific reports* **6** (2016).
157 Agarwal, R. *et al.* Mammalian cells preferentially internalize hydrogel nanodiscs over nanorods and use shape-specific uptake mechanisms. *Proceedings of the National Academy of Sciences* **110**, 17247-17252 (2013).
158 He, W. *et al.* Rod-Shaped Drug Particles for Cancer Therapy: The Importance of Particle Size and Participation of Caveolae Pathway. *Particle & Particle Systems Characterization* (2017).
159 Qiu, Y. *et al.* Surface chemistry and aspect ratio mediated cellular uptake of Au nanorods. *Biomaterials* **31**, 7606-7619 (2010).
160 Dasgupta, S., Auth, T. & Gompper, G. Shape and orientation matter for the cellular uptake of nonspherical particles. *Nano letters* **14**, 687-693 (2014).
161 Brazzale, C. *et al.* Enhanced selective sonosensitizing efficacy of ultrasound-based anticancer treatment by targeted gold nanoparticles. *Nanomedicine* **12**, 3053-3070 (2016).
162 Berlier, J. E. *et al.* Quantitative comparison of long-wavelength Alexa Fluor dyes to Cy dyes: fluorescence of the dyes and their bioconjugates. *Journal of Histochemistry & Cytochemistry* **51**, 1699-1712 (2003).
163 DEITCH, A. D. An improved Sakaguchi reaction for microspectrophotometric use. *Journal of Histochemistry & Cytochemistry* **9**, 477-483 (1961).
164 Scomparin, A. *et al.* A comparative study of folate receptor-targeted doxorubicin delivery systems: dosing regimens and therapeutic index. *Journal of Controlled Release* **208**, 106-120 (2015).
165 Polyak, D. *et al.* Systemic delivery of siRNA by aminated poly (α) glutamate for the treatment of solid tumors. *Journal of Controlled Release* (2016).
166 Cory, A. H., Owen, T. C., Barltrop, J. A. & Cory, J. G. Use of an aqueous soluble tetrazolium/formazan assay for cell growth assays in culture. *Cancer communications* **3**, 207-212 (1991).
167 Polyak, D. *et al.* Systemic delivery of siRNA by aminated poly (α) glutamate for the treatment of solid tumors. *Journal of controlled release: official journal of the Controlled Release Society* **257**, 132-143 (2017).
168 Zwicke, G. L., Ali Mansoori, G. & Jeffery, C. J. Utilizing the folate receptor for active targeting of cancer nanotherapeutics. *Nano reviews* **3**, 18496 (2012).
169 Shi, H., Guo, J., Li, C. & Wang, Z. A current review of folate receptor alpha as a potential tumor target in non-small-cell lung cancer. *Drug design, development and therapy* **9**, 4989 (2015).
170 Kalli, K. R. *et al.* Folate receptor alpha as a tumor target in epithelial ovarian cancer. *Gynecologic oncology* **108**, 619-626 (2008).
171 Gary, D. J., Min, J., Kim, Y., Park, K. & Won, Y. Y. The effect of N/P ratio on the in vitro and in vivo interaction properties of PEGylated poly [2-(dimethylamino) ethyl methacrylate]-based siRNA complexes. *Macromolecular bioscience* **13**, 1059-1071 (2013).
172 Jones, S. K., Sarkar, A., Feldmann, D. P., Hoffmann, P. & Merkel, O. Revisiting the value of competition assays in folate receptor-mediated drug delivery. *Biomaterials* (2017).
173 Guo, W. & Lee, R. J. Receptor-targeted gene delivery viafolate-conjugated polyethylenimine. *The AAPS Journal* **1**, 20-26 (1999).
174 Duarte, S., Faneca, H. & de Lima, M. C. P. Folate-associated lipoplexes mediate efficient gene delivery and potent antitumoral activity in vitro and in vivo. *International journal of pharmaceutics* **423**, 365-377 (2012).

175 Yang, S. *et al.* Non-covalent complexes of folic acid and oleic acid conjugated polyethylenimine: An efficient vehicle for antisense oligonucleotide delivery. *Colloids and Surfaces B: Biointerfaces* **135**, 274-282 (2015).
176 Duarte, S., Faneca, H. & de Lima, M. C. P. Non-covalent association of folate to lipoplexes: a promising strategy to improve gene delivery in the presence of serum. *Journal of controlled release* **149**, 264-272 (2011).
177 Reddy, J. *et al.* Folate-targeted, cationic liposome-mediated gene transfer into disseminated peritoneal tumors. *Gene therapy* **9**, 1542 (2002).
178 Van der Aa, M. *et al.* Cellular uptake of cationic polymer-DNA complexes via caveolae plays a pivotal role in gene transfection in COS-7 cells. *Pharmaceutical research* **24**, 1590-1598 (2007).
179 Rejman, J., Bragonzi, A. & Conese, M. Role of clathrin-and caveolae-mediated endocytosis in gene transfer mediated by lipo-and polyplexes. *Molecular Therapy* **12**, 468-474 (2005).
180 Von Gersdorff, K. *et al.* The internalization route resulting in successful gene expression depends on both cell line and polyethylenimine polyplex type. *Molecular Therapy* **14**, 745-753 (2006).
181 Boscher, C. & Nabi, I. R. in *Caveolins and Caveolae* 29-50 (Springer, 2012).
182 Kasprowicz, J. *et al.* Inactivation of clathrin heavy chain inhibits synaptic recycling but allows bulk membrane uptake. *The Journal of cell biology* **182**, 1007-1016 (2008).
183 Dai, L. *et al.* Novel multiarm polyethylene glycol-dihydroartemisinin conjugates enhancing therapeutic efficacy in non-small-cell lung cancer. *Scientific reports* **4** (2014).
184 Robbins, M., Judge, A. & MacLachlan, I. siRNA and innate immunity. *Oligonucleotides* **19**, 89-102 (2009).
185 Marques, J. T. & Williams, B. R. Activation of the mammalian immune system by siRNAs. *Nature biotechnology* **23**, 1399 (2005).
186 Chen, X. *et al.* Enhanced humoral and cell-mediated immune responses generated by cationic polymer-coated PLA microspheres with adsorbed HBsAg. *Molecular pharmaceutics* **11**, 1772-1784 (2014).
187 Itaka, K. *et al.* Polyion complex micelles from plasmid DNA and poly (ethylene glycol)–poly (l-lysine) block copolymer as serum-tolerable polyplex system: physicochemical properties of micelles relevant to gene transfection efficiency. *Biomaterials* **24**, 4495-4506 (2003).
188 Fenske, D. B., MacLachlan, I. & Cullis, P. R. Long-circulating vectors for the systemic delivery of genes. *Current opinion in molecular therapeutics* **3**, 153-158 (2001).
189 Dash, P., Read, M., Barrett, L., Wolfert, M. & Seymour, L. Factors affecting blood clearance and in vivo distribution of polyelectrolyte complexes for gene delivery. *Gene therapy* **6** (1999).
190 Kanasty, R., Dorkin, J. R., Vegas, A. & Anderson, D. Delivery materials for siRNA therapeutics. *Nature materials* **12** (2013).